



EVALUATION OF RISK-CONSISTENCY OF FORCE-BASED AND DISPLACEMENT- BASED DESIGN OF RC WALL BUILDINGS

A Dissertation Submitted in Partial Fulfilment of the Requirements
for the Master Degree in

Earthquake Engineering

By

JOSÉ RAFAEL LEONE VILLALBA

Supervisors: Dr. Ricardo Monteiro and Dr. Gerard O'Reilly

February 2019

Istituto Universitario di Studi Superiori di Pavia

The dissertation entitled “Evaluation of Risk Consistency of Force-Based and Displacement-Based Design Methods: RC Walls”, by Jose Rafael Leone Villalba, has been approved in partial fulfilment of the requirements for the Master Degree in Earthquake Engineering.

Dr. Ricardo Monteiro _____

Dr. Gerard O'Reilly 

ABSTRACT

Force-based design (FBD) governs the current state of practice for the seismic design of structures but important drawbacks have been identified over the years in the procedure. Moreover, studying building response during earthquakes has helped recognise the main role that deformations, rather than strength, play in the overall seismic performance of structures. Displacement-based design (DBD) method was born as an alternative design philosophy that addresses the shortcomings of FBD. Performance-based earthquake engineering allows structural performance under seismic actions to be quantified within a probabilistic framework. In the past, several studies have been carried out to assess the collapse risk of structures designed using FBD. However, less research has been carried out for buildings following DBD and no comparison of both methodologies has been performed in terms of collapse risk. With a view to address this, this study evaluates the collapse risk consistency of reinforced concrete (RC) wall buildings designed by FBD and DBD methods and the parameters that influence its calculation; the overall process from seismic hazard estimation, seismic resistant system design to collapse risk assessment was performed. Design of 3-storey, 6-storey and 9-storey buildings was carried out according to ASCE 7-16 force-based design provisions and DBD12 displacement-based model code. A 2D numerical model was built in OpenSees using a multiple vertical line element model to model the RC wall response. A set of hazard-compatible ground motion records were selected through a conditional spectrum approach and non-linear time-history analyses were carried out within an incremental dynamic analysis procedure. The mean annual frequency of exceedance (MAFE) versus maximum peak storey drift ratio (MPSD) curves were computed using the closed-form SAC/FEMA framework, accounting for both ground motion and numerical modelling uncertainties. Collapse risk consistency was evaluated by comparing the mean annual frequency of collapse and the collapse margin ratios of the designed structures. Results showed that there is indeed risk consistency between both methods for one of the studied cases and considerable similarities for the others. Moreover, risk consistency was evaluated within different structures designed by the same method, concluding that no risk consistency is achieved by either method from this point of view, despite MAFE curves spanning a relatively narrow band.

Keywords: Risk-consistency; Force-based design; Displacement-based design; Reinforced concrete; Structural walls.

ACKNOWLEDGEMENTS

I would like to thank the European Union and the MEEES Master Program for depositing their trust in me, and for handing the scholarship that allowed me to pursue this graduate degree, which would have not been possible otherwise.

My deepest gratitude to my thesis advisors Dr. Ricardo Monteiro and Dr. Gerard O'Reilly, who were always helpful and ready to provide guidance since day one. Thanks for their enthusiasm and patience, I am glad I had the opportunity to work with them.

Special thanks to Dr. Francisco Barrios, who during my undergraduate at Universidad Del Magdalena encouraged me to do research in structural engineering and initiated me in the world of numerical modelling and nonlinear response of structures.

To God, that supreme entity that makes everything possible. To my Mother, who has always been my role model, to my brother and sister, to Kelly, Hugo and all my family, who always encouraged me and helped me in everything I have achieved in life. You have always given me support and have fed me with energy and optimism whatever I do and wherever I go.

To the IUSS Pavia staff, who were always kind and provided any assistance that was needed. Moreover, thanks for putting up this programme, the number of things I learned being around such highly qualified and experienced professors has no price.

Finally, to my new friends with which I shared this journey, Andrés, Diana, Nevena, Lana, Deniz, Rafa, Cristina, Subash, Nic, Luke, Beatrice, Daniel, Bryan, and Robin (I hope I did not forget anyone!). Thanks for all the fun and the endless midnight discussions on life affairs, always in company of a nice bottle of wine.

TABLE OF CONTENTS

	Page
ABSTRACT	iii
ACKNOWLEDGEMENTS.....	iv
TABLE OF CONTENTS.....	v
LIST OF FIGURES	viii
LIST OF TABLES.....	xii
1 INTRODUCTION	1
1.1 General	1
1.2 Objective	3
1.3 Outline.....	3
2 LITERATURE REVIEW	5
2.1 Introduction	5
2.2 Force-based design	5
2.3 Issues with force-based design	8
2.3.1 Relationship between strength and stiffness	8
2.3.2 Period calculation.....	10
2.3.3 Force-reduction factors	10
2.3.4 Strength and ductility demand	10
2.4 Displacement-based design	11
2.5 PEER PBEE for collapse assessment.....	13
2.5.1 Previous studies on collapse risk	13
2.5.2 Collapse risk assessment methodology.....	14
3 HAZARD	17
3.1 Introduction	17
3.2 Location.....	17

3.3	PSHA input model.....	18
3.4	PSHA results	21
4	BUILDINGS DESIGN	23
4.1	General considerations	23
4.2	Force-based design	25
4.2.1	Design spectrum definition	25
4.2.2	Force-reduction factors and design coefficients	26
4.2.3	Computational model and structural analysis	27
4.2.4	Reinforcement detailing and final design	31
4.3	Direct displacement-based design	34
4.3.1	Displacement spectrum for design.....	34
4.3.2	Alternative displacement design spectrum.....	36
4.3.3	Material strengths for design.....	39
4.3.4	Desired inelastic mechanism and displacement shapes	39
4.3.5	SDOF substitute structure and structural analysis	42
4.3.6	Special Case: Design displacement exceeds the spectral demand	45
4.3.7	Capacity design considerations	46
4.3.8	Reinforcement detailing and final design	48
4.4	FBD and DDBD	51
5	NUMERICAL MODELLING	57
5.1	Introduction	57
5.2	Modelling strategy: RC wall macro-model selection	58
5.3	Materials constitutive behaviour	59
5.4	Fibre model discretisation	61
5.5	MVLEM discretisation.....	61
5.6	Pushover analysis	62
5.7	Wall model selected for NLTHA	70
6	RISK ASSESSMENT	71
6.1	Introduction	71
6.2	Ground motion record selection	71
6.2.1	Disaggregation	73
6.2.2	Conditional spectrum computation and ground motion record selection.....	75
6.3	Collapse definition	76
6.4	Incremental dynamic analysis	77
6.5	Modelling uncertainty	80

6.6	Mean annual frequency of exceedance.....	81
6.7	Risk-consistency evaluation	87
7	CONCLUSIONS.....	90
7.1	Summary and conclusions	90
7.1.1	Design methods.....	92
7.1.2	Collapse assessment and risk-consistency	94
7.2	Future research	95
8	REFERENCES.....	97
APPENDIX A. FORCE-BASED DESIGN		A1
A.1	General Requirements	A1
A.2	Period Estimation and Base-Shear Calculation	A2
A.3	ELF Vertical Distribution of Seismic Forces and Accidental Torsion Checks	A3
A.4	Modal Analysis Results.....	A5
A.5	MRSA Base Shear Scaling Factors	A7
A.6	Drift and P-Delta Checks	A7
A.7	Structural Design of the Walls	A9
APPENDIX B. DIRECT-DISPLACEMENT BASED DESIGN		B1
B.1	General requirements	B1
B.2	Wall allowable plastic rotations and design displacement profiles.....	B1
B.3	Equivalent SDOF properties	B3
B.4	Equivalent viscous damping and spectrum scaling factor.....	B4
B.5	Effective period, stiffness and design base shear	B4
B.6	Vertical distribution of seismic forces and stability coefficient check.....	B5
B.7	Capacity design envelopes	B8
B.8	Structural design of the walls	B9
APPENDIX C. HAZARD CURVES, RECORDS SELECTION AND MAFE CURVES		C1
C.1	Hazard curves and disaggregation.....	C1
C.2	Conditional spectrum and records selection.....	C5
C.3	Hazard fit and individual MAFE curves	C7

LIST OF FIGURES

	Page
Figure 2.1. Workflow of FBD. (Adapted from Priestley et al., 2007).....	7
Figure 2.2. Relationship between strength, stiffness and yield curvature for RC sections. (Priestley et al. 2007)	9
Figure 2.3. Fundamentals of DDBD. (Priestley et al. 2007).....	11
Figure 3.2. Site Location (Google Earth).....	18
Figure 3.2. PSHA fault model representation. (Adapted from SARA Project).....	20
Figure 3.3. PSHA subduction model representation (Adapted from SARA Project).....	20
Figure 3.4. Mean Hazard Curves for PGA, $Sa(0.5s)$ and $Sa(1.0s)$	21
Figure 3.5. Mean Uniform Hazard Spectra (UHS) 5% damping for two hazard levels.	22
Figure 4.1. Floor plan of the designed buildings.	24
Figure 4.2. Comparison UHS for design vs code-based (ASCE 7-16 and NSR-10) smoothed spectrum.	26
Figure 4.3. Graphic representation computational model for 9-Storeys building. (Autodesk Robot Structural 2019).....	27
Figure 4.4. FBD: Moment (left) and Shear (right) design profiles results, MRSA analysis with scaled spectrum.....	30
Figure 4.5. (FBD) Force-Based Design, 9-Storeys Building. (Rebar size in Imperial System).	32
Figure 4.6. (FBD) Force-Based Design, 6-Storeys Building. (Rebar size in Imperial System).	33
Figure 4.7. (FBD) Force-Based Design, 3-Storeys Building. (Rebar size in Imperial System).	33
Figure 4.8. Design displacement spectra illustration. 5% damping and reduced by equivalent viscous damping ξ_{eq}	34
Figure 4.9. Displacement spectra used for design, bilinear fit of PSHA results.....	35
Figure 4.10. Disaggregation for PGA and 475 years return period.	37
Figure 4.11. Graphical comparison alternative estimates of the design displacement spectra.	39
Figure 4.12. Design displaced shape for RC cantilever walls. Adapted from (Sullivan et al., 2012)....	40

Figure 4.13. Displacement Shapes and Drift Profiles of the three buildings.....	41
Figure 4.14. Effective period T_e calculation procedure.	43
Figure 4.15. DDBD: Moment (left) and Shear (right) design profiles results.	45
Figure 4.16. Typical case in which displacement capacity (Δ_d) exceeds reduced spectral demand ($\Delta_{\xi,eq}$).	45
Figure 4.17. Moment and Shear capacity design envelopes described by DBD12.	47
Figure 4.18. (DDBD) Displacement-Based Design, 3-Storeys Building. (Rebar size in Imperial System).....	49
Figure 4.19. (DDBD) Displacement-Based Design, 6-Storeys Building. (Rebar size in Imperial System).....	50
Figure 4.20. (DDBD) Displacement-Based Design, 9-Storeys Building. (Rebar size in Imperial System).....	50
Figure 4.21. 9-Storeys: Moment and Shear profiles obtained from structural analysis. FBD vs DDBD.	54
Figure 4.22. 6-Storeys: Moment and Shear profiles obtained from structural analysis. FBD vs DDBD.	54
Figure 4.23. 3-Storeys: Moment and Shear profiles obtained from structural analysis. FBD vs DDBD.	55
Figure 5.1. Analytical model used for NLTHA in OpenSees. MVLEM model for RC walls.....	58
Figure 5.2. Confined and unconfined concrete stress-strain curves. FBD 9-Storeys building.	60
Figure 5.3. Steel02 Material - Giuffré-Menegotto-Pinto Model. (Adapted from OpenSees).....	61
Figure 5.4. Illustration of the wall fibre model discretisation.....	61
Figure 5.5 - MVLEM Discretisation 6 m Wall, 9-storeys building. Used in FBD (All floors) and DDBD (Ground Floor to 3rd Floor).....	62
Figure 5.6 - MVLEM Discretisation 6 m Wall, 9-storeys building. Used in DDBD (4th Floor to Roof).	62
Figure 5.7. MVLEM Discretisation 4 m Wall, 3-Storeys and 6-Storeys building. Used in FBD (All Floors) and DDBD (All Floors).	62
Figure 5.8. Pushover curves comparison between FBD and DDBD for both MVLEM and fibre models. 3-storey Building.	63
Figure 5.9. Pushover curves comparison between FBD and DDBD for both MVLEM and fibre models. 6-storey Building.	63
Figure 5.10. Pushover curves comparison between FBD and DDBD for both MVLEM and fibre models. 9-storey building.....	64
Figure 5.11. Pushover curves comparison FBD vs DDBD with MVLEM wall models.	65
Figure 5.12. Pushover curves comparison FBD vs DDBD with fibre wall models.	66

Figure 5.13. Normalised pushover curves for all designs.....	67
Figure 5.14. Overstrength pushover curves for FBD buildings and DDBD buildings, with MVLEM wall model.....	68
Figure 6.1. Disaggregation DDBD-3, $Sa(T_1=1.00s)$. 2475 years return period.....	74
Figure 6.2. Disaggregation FBD-6, $Sa(T_1=1.94s)$. 2475 years return period.....	75
Figure 6.3. FBD-6 Building: Response spectra of selected ground motion records conditioned on $Sa(T_1=1.94s)$	76
Figure 6.4. DDBD-6 Building: Response spectra of selected ground motion records conditioned on $Sa(T_1=1.7s)$	76
Figure 6.5. FBD 3-Story building IDA curves, $Sa(T_1=0.72s)$	78
Figure 6.6. FBD 6-Story building IDA curves, $Sa(T_1=1.94s)$	78
Figure 6.7. FBD 9-Story building IDA curves, $Sa(T_1=2.59s)$	79
Figure 6.8. DDBD 3-Story building IDA curves, $Sa(T_1=1.00s)$	79
Figure 6.9. DDBD 6-Story building IDA curves, $Sa(T_1=1.73s)$	80
Figure 6.10. DDBD 9-Story building IDA curves, $Sa(T_1=1.98s)$	80
Figure 6.11. Maximum peak storey drift ratio MAFE curves for FBD (left) and DDBD (right).....	81
Figure 6.12. CMR comparison for all designs.....	83
Figure 6.13. Normalized pushover curves in terms of roof drift ratio for all designs.....	86
Figure 6.14. Variation of MAFC with CMR for all the studied cases.....	86
Figure 6.15. All designs comparison, maximum peak storey drift MAFE curves. Green line marks the 5% MPSD.....	87
Figure C1. Hazard curves for $Sa(T_1)$ of each building.....	C1
Figure C2. Disaggregation $Sa(0.72s)$ 2475-years return period.....	C2
Figure C3. Disaggregation $Sa(1.00s)$ 2475-years return period.....	C2
Figure C4. Disaggregation $Sa(1.17s)$ 2475-years return period.....	C3
Figure C5. Disaggregation $Sa(1.40s)$ 2475-years return period.....	C3
Figure C6. Disaggregation $Sa(1.73s)$ 2475-years return period.....	C4
Figure C7. Disaggregation $Sa(1.98s)$ 2475-years return period.....	C4
Figure C8. FBD-3: Response spectra of selected ground motion records conditioned on $Sa(T_1=0.72s)$	C5
Figure C9. FBD-6: Response spectra of selected ground motion records conditioned on $Sa(T_1=1.94s)$	C5
Figure C10. FBD-9: Response spectra of selected ground motion records conditioned on $Sa(T_1=2.60s)$	C6
Figure C11. DDBD-3: Response spectra of selected ground motion records conditioned on $Sa(T_1=1.00s)$	C6

Figure C12. DDBD-6: Response spectra of selected ground motion records conditioned on $Sa(T_1=1.73s)$	C7
Figure C13. DDBD-9: Response spectra of selected ground motion records conditioned on $Sa(T_1=1.98s)$	C7
Figure C14. FBD-3 hazard curve polynomial fit	C8
Figure C15. FBD-6 hazard curve polynomial fit	C8
Figure C16. FBD-9 hazard curve polynomial fit	C9
Figure C17. DDBD-3 hazard curve polynomial fit	C9
Figure C18. DDBD-6 hazard curve polynomial fit	C10
Figure C19. DDBD-9 hazard curve polynomial fit	C10
Figure C20. FBD 3-Story building, maximum peak storey drift ratio MAFE curve.....	C11
Figure C21. FBD 6-Story building, maximum peak storey drift ratio MAFE curve.....	C11
Figure C22. FBD 9-Story building, maximum peak storey drift ratio MAFE curve.....	C12
Figure C23. DDBD 3-Story building, maximum peak storey drift ratio MAFE curve.	C12
Figure C24. DDBD 6-Story building, maximum peak storey drift ratio MAFE curve.	C13
Figure C25. DDBD 9-Story building, maximum peak storey drift ratio MAFE curve	C13

LIST OF TABLES

	Page
Table 3.1. GMPEs and corresponding weights included in the PSHA input model's logic tree. (Adapted from SARA Project, GEM)	19
Table 4.1. Load combinations used for FBD and DDBD.....	25
Table 4.2. Comparison of different period definitions results. MRSA vs ASCE 7-16 formulas.....	29
Table 4.3. Scale factors and comparison of base shear (V_b) for MRSA and ELF procedures.....	30
Table 4.4. Summary of flexural design at wall base for FBD cases.....	32
Table 4.5. Summary of FBD design characteristics at wall-base section of all buildings.....	33
Table 4.6. M-R results from disaggregation of PGA and 475 years return period.....	36
Table 4.7. M-R results from disaggregation of Sa(2.0s) and 475 Years Return Period.	36
Table 4.8. Comparison T_c (sec) estimates	37
Table 4.9. Comparison δ_{max} (mm) estimates.....	38
Table 4.10. Initial properties of the SDOF substitute structure for each designed building.....	42
Table 4.11. Properties of the SDOF Substitute Structure after iterative procedure for 6-Storeys and 9- Storeys buildings.....	43
Table 4.12. Summary of flexural design at wall base for DDBD cases.	49
Table 4.13. Summary of DDBD geometry and reinforcement at wall-base section of all buildings.	49
Table 4.14. Comparison FBD vs DDBD design for shear at wall base (2 walls).....	51
Table 4.15. Comparison FBD vs DDBD design for moments at wall base (2 walls).....	52
Table 4.16. FBD vs DDBD comparison of reinforcement steel placed at typical wall base section for all buildings designed.....	53
Table 4.17. Comparison FBD vs DDBD design overstrength values.....	55
Table 4.18. First-mode vibration periods of each building comparison.	56
Table 5.1. Parameters to define concrete material model.....	59
Table 5.2. Parameters to define steel material model.	60

Table 5.3. Base shear coefficients and pushover base shear overstrength for all buildings	67
Table 5.4. Comparison analysis and design moments at wall base FBD.....	68
Table 5.5. Pushover base moment overstrength for all buildings.....	69
Table 6.1. First-mode vibration periods of each building according to pushover results, used for disaggregation and record selection.....	74
Table 6.2. Collapse Margin Ratio (CMR) and Mean Annual Frequency of Collapse (MAFC) calculated for all the designs.....	83
Table 6.3. Summary of parameters involved in collapse performance and collapse risk evaluation for all designs.....	85
Table 6.4. Comparison of parameters involved in CMR and MAFC for FBD-6 and DDBD-9 models.	85
Table 6.5. Comparison of parameters involved in CMR and MAFC for FBD-6, DDBD-6 and DDBD-9 models.	86
Table 6.6. Mean Annual Frequency of Collapse (MAFC) comparison FBD vs DDBD.	87
Table A1. Seismic response parameters for seismic design requirements.....	A1
Table A2. Response modification “R”, overstrength “ Ω_0 ” and deflection amplification coefficients. A2	A2
Table A3. Load combinations used for FBD-3, FBD-6 and FBD-9 designs.....	A2
Table A4. Comparison of different period definitions results. MRSA vs ASCE 7-16 formulas.....	A3
Table A5. ELF base shear and base shear coefficients computed for FBD buildings.	A3
Table A6. (ELF) FBD-3 building, vertical distribution of seismic forces	A4
Table A7. (ELF) FBD-6 building, vertical distribution of seismic forces	A4
Table A8. (ELF) FBD-9 building, vertical distribution of seismic forces	A4
Table A9. (ELF) FBD-9 Computation of forces for accidental torsion checks.	A5
Table A10. (ELF) FBD-9 Torsion irregularity check.	A5
Table A11. FBD-3 Modal response characteristics.	A6
Table A12. FBD-6 Modal response characteristics.	A6
Table A13. FBD-9 Modal response characteristics.	A6
Table A14. Scale factors for 100% ELF requirement and final base shear (Vb) for MRSA procedure.	A7
Table A15. FBD-3 Drift check.	A8
Table A16. FBD-6 Drift check.	A8
Table A17. FBD-9 Drift check.	A8
Table A18. FBD-3 Stability coefficient check for P-Delta verifications.....	A8
Table A19. FBD-6 Stability coefficient check for P-Delta verifications.....	A9
Table A20. FBD-9 Stability coefficient check for P-Delta verifications.....	A9
Table A21. FBD-3 Final loads for wall design (load values for a single wall).	A10

Table A22. FBD-6 Final loads for wall design (load values for a single wall).....	A10
Table A23. FBD-9 Final loads for wall design (load values for a single wall).....	A10
Table A24. FBD-3 Web horizontal reinforcement verification.....	A11
Table A25. FBD-6 Web horizontal reinforcement verification.....	A11
Table A26. FBD-9 Web horizontal reinforcement verification.....	A11
Table A27. FBD-3 Web vertical reinforcement verification.....	A12
Table A28. FBD-6 Web vertical reinforcement verification.....	A12
Table A29. FBD-9 Web vertical reinforcement verification.....	A12
Table A30. FBD-3 Summary design for flexure.	A12
Table A31. FBD-6 Summary design for flexure.	A13
Table A32. FBD-9 Summary design for flexure.	A13
Table A33. FBD-3 Boundary element vertical reinforcement verification.	A13
Table A34. FBD-6 Boundary element vertical reinforcement verification.	A13
Table A35. FBD-9 Boundary element vertical reinforcement verification.	A14
Table A36. FBD-6 Boundary element requirement check.	A14
Table A37. FBD-3 Boundary element transversal reinforcement spacing verification.	A14
Table A38. FBD-6 Boundary element transversal reinforcement spacing verification.	A14
Table A39. FBD-9 Boundary element transversal reinforcement spacing verification.	A15
Table B1. DDBD-3 Wall allowable plastic rotations.	B1
Table B2. DDBD-6 Wall allowable plastic rotations.	B2
Table B3. DDBD-9 Wall allowable plastic rotations.	B2
Table B4. DDBD-3 Design displacement profile calculation.....	B2
Table B5. DDBD-6 Design displacement profile calculation.....	B2
Table B6. DDBD-9 Design displacement profile calculation.....	B3
Table B7. DDBD-3 Equivalent SDOF properties.....	B3
Table B8. DDBD-6 Equivalent SDOF properties.....	B3
Table B9. DDBD-9 Equivalent SDOF properties.....	B4
Table B10. Equivalent viscous damping and spectrum scaling factor computation.....	B4
Table B11. Final design properties and effective period calculation for all buildings.	B5
Table B12. Base shear and overturning moment calculation for all designs.	B5
Table B13. DDBD-3 Vertical distribution of shear and moments (values for 2 walls)....	B6
Table B14. DDBD-6 Vertical distribution of shear and moments (values for 2 walls)....	B6
Table B15. DDBD-9 Vertical distribution of shear and moments (values for two walls)....	B6
Table B16. DDBD-3 Stability coefficient verification.	B7
Table B17. DDBD-6 Stability coefficient verification	B7
Table B18. DDBD-9 Stability coefficient verification.	B7

Table B19. DDBD-3 Capacity design shear and moments (single wall) used for design.	B8
Table B20. DDBD-6 Capacity design shear and moments (single wall) used for design.	B8
Table B21. DDBD-9 Capacity design shear and moments (single wall) used for design.	B8
Table B22. DDBD-3 Web horizontal reinforcement verification.....	B9
Table B23. DDBD-6 Web horizontal reinforcement verification.....	B9
Table B24. DDBD-9 Web horizontal reinforcement verification.....	B10
Table B25. DDBD-3 Web vertical reinforcement verification.....	B10
Table B26. DDBD-6 Web vertical reinforcement verification.....	B10
Table B27. DDBD-9 Web vertical reinforcement verification.....	B10
Table B28. DDBD-3 Summary design for flexure.	B11
Table B29. DDBD-6 Summary design for flexure.	B11
Table B30. DDBD-9 Summary design for flexure.	B11
Table B31. DDBD-3 Boundary element vertical reinforcement verification.....	B12
Table B32. DDBD-6 Boundary element vertical reinforcement verification.....	B12
Table B33. DDBD-9 Boundary element vertical reinforcement verification.....	B12
Table B34. DDBD-6 Boundary element requirement check.	B12
Table B35. DDBD-3 Boundary element transversal reinforcement spacing verification.	B12
Table B36. DDBD-6 Boundary element transversal reinforcement spacing verification.	B13
Table B37. DDBD-9 Boundary element transversal reinforcement spacing verification.	B13

1 INTRODUCTION

1.1 General

Seismic design methods set a framework to estimate the demands and expected response of structures subjected to earthquake-generated ground motions. When coupled with building design codes, they provide rules and recommendations regarding the geometrical and mechanical properties required by the different elements of a structure in order to sustain the actions imposed by earthquakes. Ideally, structures conceived by such methodologies could handle the demands without any kind of damage (elastic response), but in most of the cases this would result in economically unfeasible structures. Instead, structural engineers design buildings allowing for inelastic deformations to occur by relying on the ductile properties of the structural system and considering the fact that design-level earthquakes are very rare events, which then paves the way for more economical designs. Hence, a degree of damage is accepted for the design-level earthquake and it is implicit that buildings designed following this set of design rules will comply with the acceptance criteria while allowing for a certain probability of exceeding such damage. Although it is not quantified during the design process, the acceptance criteria is still a matter of discussion and is usually defined according to the needs of the society. The formulation of design methods and building codes foresees that all resulting designs provide a minimum and somewhat comparable level of safety in theory. Consistent performance of different buildings designed with the same set of rules may be thus expected, however, the practice and experience following past earthquakes around the world shows that this consistency is not always achieved.

Seismic design methods can be separated in two main categories: force-based design (FBD) and displacement-based design (DBD) methods. FBD is the more traditional approach and it is the methodology upon which most international building codes are based (e.g. USA, Colombia,

Europe, New Zealand). It is likely to be the most common design philosophy used throughout the world and has been subject of numerous modifications and improvements over the years. On the other hand, DBD was born as an alternative to overcome fundamental issues identified in FBD, described by Priestley (2003), and has been developed in more recent years. As such, it has not yet fully found its way into national building codes. It is worth mentioning that DBD is further divided in two categories (SEAOC, 1996) as direct DBD (DDBD) and the equal displacement-based design (EBD) procedures. In this study, displacement-based design will refer to DDBD as described by Priestley et al. (2007).

Among many others, the main difference between both design philosophies is self-explanatory by their names: in FBD, the forces are the driving quantity in the process that designers must seek to establish; whereas in DBD, it is the displacements that govern the design process with structures sized to achieve certain level of displacements under earthquake shaking. The reader is referred to Chapter 2 where the differences between both methodologies are discussed in more detail.

Performance-based earthquake engineering (PBEE) (Cornell & Krawinkler, 2000) relies on probabilistic theory to quantify and evaluate the expected performance (thus the expected level of damage) of the designed building when subjected to a given level of ground shaking, which can be compared against performance goals or levels that have been previously defined. These performance levels provide useful information for communities and stakeholders as they measure the level of safety that a structure can provide during an earthquake, which integrated into a risk assessment framework helps to estimate expected economic losses or fatalities to be estimated. Collapse prevention is typically the main objective contemplated in PBEE and seismic design in general, as it is directly related with life safety and is highly important for structures built in zones of moderate/high seismicity.

Risk can be defined as the convolution between hazard, vulnerability and exposure (UNESCO, 1972). There are several methods to quantify collapse risk, most of them involving the development of a computational model of the structure and performing a series of non-linear time history analyses (NLTHA), where structural response to ground motion records is evaluated up to the side-sway collapse of the structure. Then, results are processed to obtain a collapse fragility function of the building, which is integrated with the seismic hazard curve at

the site to get an estimate of the collapse risk. Different methodologies (i.e. FBD vs DBD) lead to different designs and consequently different performance for the same building. Thus, when taking life safety as the main aim of seismic design, it is important to quantify the differences in terms of collapse risk between both methods and understand the reasons if and why such differences are observed.

Reinforced concrete (RC) walls are one of the most commonly used seismic resisting systems for buildings, as this type of members can provide high levels of stiffness, strength and reasonable displacement capacity when subjected to lateral loads coming from earthquakes or wind. In this study, the overall process from seismic hazard estimation, seismic resisting system design to collapse risk assessment was performed for a set of buildings designed following both FBD and DDBD.

1.2 Objective

This study aimed to evaluate the collapse risk consistency of RC wall buildings designed according to FBD and DDBD and analyse the reasons behind such differences and/or similarities. For this purpose, a set of multi-storey buildings were designed following the corresponding design codes for each methodology and collapse risk was assessed via the mean annual frequency of exceedance (MAFE) of a collapse capacity defined in terms of inter-storey drift. Additionally, focus was made on the differences between both design philosophies, and the conclusions focused on the identification and understanding of the parameters that have major influence in the outcome. The main objectives of this research can be listed as follows:

- Evaluate collapse risk consistency of RC wall buildings designed with FBD and DDBD methods, comparing both designs produced using either method and designs of different structures using the same method;
- Provide insight on the fundamental differences between FBD and DDBD, the flaws in FBD and how they are addressed in DDBD;
- Identify the parameters that influence the collapse risk within each method and across both methods.

1.3 Outline

Chapter 2 reviews the principles and assumptions of FBD and DDBD methods. Also, a few issues with FBD are addressed and the collapse risk assessment is introduced by analysis of

previous studies. Emphasis is given to the explanation of DDBD as it may be unfamiliar to readers. This chapter also summarises the main aspects of the methodology used to assess the collapse risk of the structures and a step-by-step outline of the procedure is provided.

Chapter 3 deals with the quantification of the seismic hazard at the site; the assumptions and limitations of the seismic hazard model used are described and the results are presented.

In Chapter 4, the main characteristics of the studied buildings are described. The design of the buildings is carried out, starting with the description of the general aspects that are independent of the design method. Afterwards, design is carried out following FBD and DDBD principles. The design choices are highlighted and discussed with respect to fundamental characteristics of each procedure. The DDBD process is carefully explained. The final wall cross-sections designed by each method are shown at the end of Sections 4.2 and 4.3. Finally, the designs obtained are compared whereas the complete extension of the computations performed for the designs is shown in Appendix A and Appendix B for FBD and DDBD, respectively.

Chapter 5 presents the modelling strategy used to simulate the non-linear response of the buildings. Modelling assumptions and adopted material models are described and a comparison between two different strategies is made in terms of pushover curves. Additionally, normalised pushover curves for the final wall model are plotted and a short description of the final model is given.

Chapter 6 describes in detail the collapse risk assessment methodology reviewed in Section 2.5.2. Matters regarding ground motion record selection and the definition of collapse are discussed. In the remainder of the Chapter, the non-linear time history analyses of all the structures are carried out and the results are shown. Calculation of the MAFE curves is performed and modelling uncertainties are accounted for. Finally, the collapse risk consistency of FBD and DDBD is evaluated and the parameters that influence the results are explained.

In Chapter 7, a summary of the work is presented along with conclusions and recommendations for future research.

2 LITERATURE REVIEW

2.1 Introduction

Seismic design aims to conceive structures that safeguard the lives of its occupants, i.e. designing structures to achieve a given performance level for certain levels of seismic shaking. For life safety purposes, the question of how good or bad a structure performs may be answered within a probabilistic framework, using collapse risk as metric, quantified via its MAFE. With the development of DBD as an alternative methodology to the traditional FBD, it has become important to provide a comparison of the collapse risk of structures designed by both procedures, as well as the identification of the factors that influence this outcome. Here such comparison is expressed in terms of collapse risk consistency.

To embark on this discussion, it is then necessary to give a short summary of the main aspects of both design methodologies, as well as the reasons that led to the development of the DBD method as an alternative to FBD. Furthermore, it is important to discuss previous studies on collapse risk assessment of code-conforming structures, particularly RC walls structures. Mention shall also be made to the concepts of “uniform risk” and “risk consistency” and to which extend they have been addressed in literature.

2.2 Force-based design

Current state of practice in seismic design of structures is focused on the well-known FBD approach. This approach goes back to the beginnings of earthquake engineering where it was noted that buildings designed for lateral wind forces performed better when subjected to earthquake actions than those that did not incorporate any lateral force-resisting system. Then, the idea of seismic design in terms of forces or strength was initially related to the way buildings are designed to stand other actions such as self-weight and live loads, for which structural

members are simply required to have higher strength than the imposed loads to avoid failure. However, with the increasing knowledge of structural dynamics and the development of advanced analysis techniques, it was noted that structural response is more linked to the dynamic properties of the structure (e.g. distribution of mass and stiffness). Ductility also appeared as an important concept for describing the additional deformation capacity that structures undergo. This additional deformation capacity is achieved at expense of allowing the structure to experience inelastic deformations within acceptable levels of damage.

Ductility is understood as the ratio of maximum (or ultimate) to effective yield deformation that can be achieved by the system, as shown in Equation 2.1. With increased understanding of inelastic response, the expected level of ductility that different structural systems could develop was assessed and FBD focused on producing a set of force-reduction or “R” factors that enable the computation of design loads by relating the elastic and inelastic responses of the buildings; giving birth to concepts like “equal displacement rule” and “equal energy rule” (to be discussed later). At this point, it can be noted that ductile deformation of members acquired a major role in seismic design. The introduction of ductility also allowed developing “capacity design” (Park & Paulay, 1975) in which strength of structural members was set to favour the development of ductile failure mechanisms. Thus, higher strength is provided in locations where inelastic deformations, intended to form mechanisms, are to be prevented.

$$\mu = \Delta_{max} / \Delta_y \quad (2.1)$$

Despite increasing improvements in FBD, the process still revolved around strength, while displacement demand was indirectly computed and only considered as an additional check once the design has been finished. Figure 2.1 provides a summary of the FBD process.

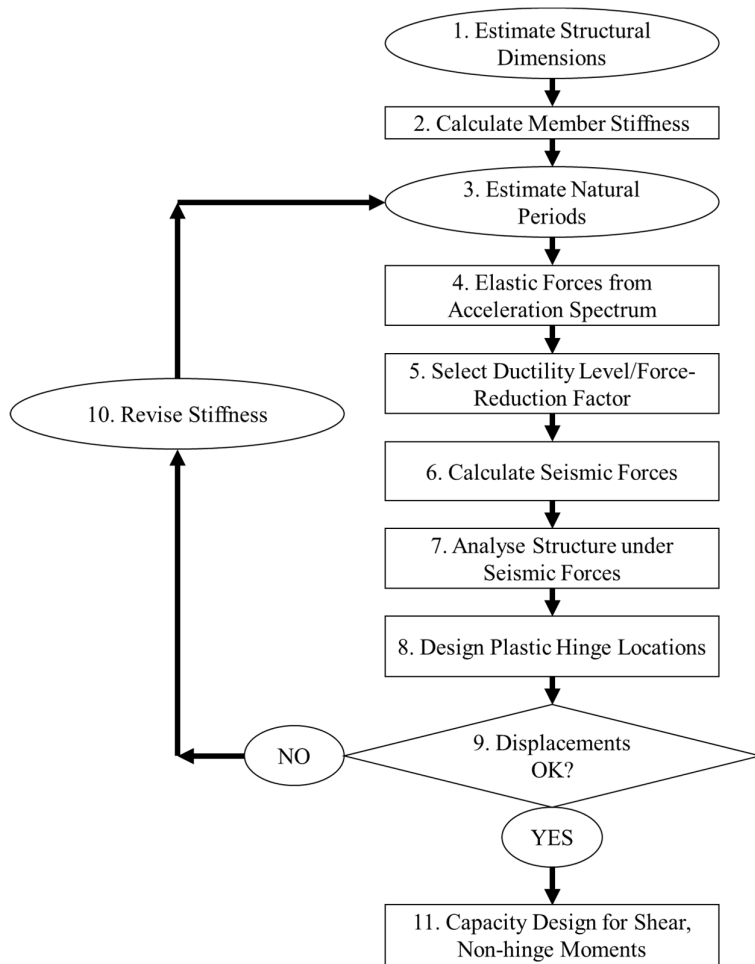


Figure 2.1. Workflow of FBD. (Adapted from Priestley et al., 2007)

The design process begins with an initial estimation of the structural geometry, then elastic stiffness of structural members is estimated based on the size of members. Elastic stiffness may be calculated based on gross section properties or reduced section properties in case of RC members to account for cracking effects. Once the lateral structural stiffness has been defined, the periods of vibration of the structure are estimated based on the distribution of mass and stiffness (modal analysis). Some building codes provide formulas for fundamental period estimation that are based in the height or number of storeys of the building without any consideration of its dynamic properties. The US design code ASCE 7-16 (ASCE, 2016), for example, sets a limit to which periods calculated through modal analysis may deviate from the ones obtained by the height-dependent formula, as discussed in detail later.

Elastic base shear is determined from the design response spectrum, which depends on the estimated vibration period and includes factors to account for building importance and soil conditions at the site. Then, a force-reduction factor “ R ” is chosen according to the assumed ductility capacity of the structural system and material being used. These factors are code-specified and are the result of numerous analyses and experimental campaigns completed in the past. The design seismic base shear is the result of the elastic base shear divided by the force-reduction factor. This base shear is distributed through the building such that a vector of seismic forces is generated, which are then distributed to structural members proportionally to their elastic stiffness.

Finally, the building is analysed under the applied forces combined with gravity loads and the design of the members is carried out. At this point, if no changes of member sizes are required, displacements are checked against the acceptance criteria; if the displacements are not satisfactory or if the design process requires a change in member sizes, then iteration is needed: the stiffness of the structure is revised, the fundamental periods are calculated again and the whole process is repeated. Once displacements are within the code prescribed limits, the final step is to perform capacity design to protect members where no inelastic deformations are desired so as to avoid non-ductile failure modes.

As a result of continued research over past years, several issues and fallacies in FBD have been identified, especially for its application to RC or masonry structures, which will be discussed in the next section. These fundamental flaws and the high importance of ductility suggest that more consideration should be given to displacements in the design process or, rather, that the current design practice should completely move to a displacement-based formulation.

2.3 Issues with force-based design

In this section, a summary of the main issues in FBD is provided, for a deeper discussion on the topic the reader should refer to Priestley et al. (2007) and Priestley (2003).

2.3.1 Relationship between strength and stiffness

As mentioned in the previous section, the first step of the FBD procedure involves an initial estimation of the member sizes and structural geometry, meaning that stiffness is defined prior to seismic forces estimation. An incorrect estimation of the stiffness leads to inaccurate vibration periods and incorrect distribution of lateral forces along the structure. This might be

a frequent case for RC and masonry structures, where initial cracking develops, making the elastic stiffness invalid from an early stage. To account for this, some codes suggest the use of reduced stiffness for the calculation of the vibration periods, through stiffness reduction factors that vary according the type of structural members and from code to code. As seismic forces are calculated from the acceleration spectra, using the structural vibration periods, any small change in the latter results in changes on the demand, which might be particularly large if the periods are in the so-called “constant-velocity” range of the response spectrum.

Nevertheless, the main flaw comes from the fact that stiffness is assumed to be independent of strength, which has been proved to be invalid as stiffness is essentially proportional to strength. As shown in Figure 2.2, a bilinear idealisation of the moment-curvature curve compares the design assumptions (a) versus the realistic behaviour (b) obtained from detailed analyses and experimental evidence. It has been proven (Priestley, 2003; Priestley et al., 1996) that the yield curvature is the one independent of strength rather than stiffness.

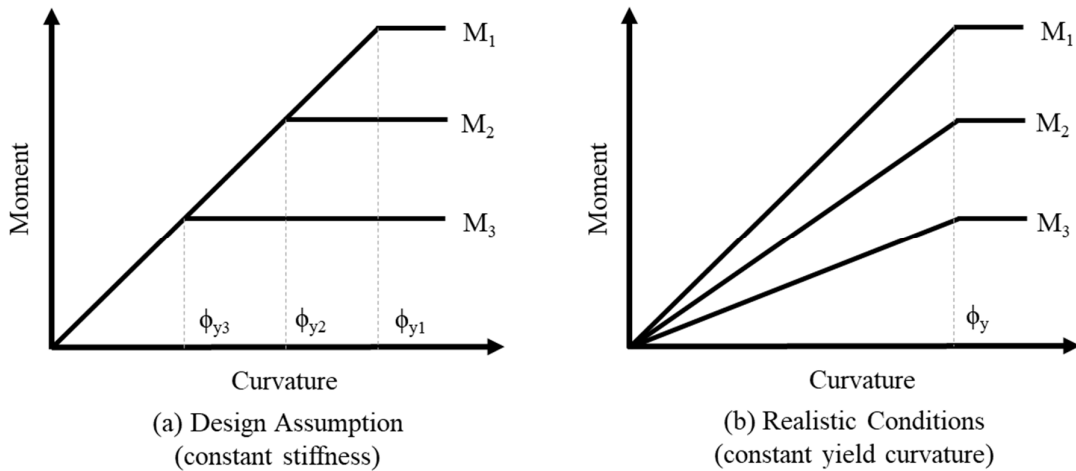


Figure 2.2. Relationship between strength, stiffness and yield curvature for RC sections. (Priestley et al. 2007)

The above implies that for an accurate estimation of stiffness (and consequently, vibration periods and lateral forces distribution), the strength must be known. As member strength is the final product of FBD, iteration is required, which makes the design method somewhat inefficient.

2.3.2 *Period calculation*

Correct estimation of structural vibration periods is a matter of continued research in structural dynamics, as period calculation is strictly tied to the calculation of stiffness. Furthermore, height-dependent equations for period estimation prescribed by building codes produce different results (Priestley & Amaris, 2002). The application of such equations or application of modal analysis based in code-specified stiffness-reduction coefficients, tends to produce low vibration periods. Within FBD, this is considered conservative as low periods are related to higher accelerations in the acceleration spectrum, producing stronger structures. Yet, as it has been previously stated, it is the combination of ductility (thus deformation capacity) and strength that have a major influence on the ability of a structure to survive earthquake actions. This is because displacements are directly related to structural damage and overall building stability.

2.3.3 *Force-reduction factors*

FBD procedure relies on a set of force-reduction factors “R” that are based on ductility considerations, with a unique factor specified for each type of structural system. As extensively explained by Priestley et al. (2007), assigning a uniform force-reduction factor (i.e. uniform ductility capacity) to all structures of the same type is found to be inappropriate as the ductility capacity is influenced by several factors: geometry, elastic flexibility of capacity-designed members, foundation flexibility, among others. Additionally, no clear consensus about the appropriate values of force-reduction factors has been achieved and building codes of different countries provide different values for the same type of structural system. This issue is in close relation with the varied definitions of yield displacement and ultimate displacement (and, consequently, ductility), used by earthquake engineering community nowadays.

2.3.4 *Strength and ductility demand*

The three issues previously described challenge the assumption that more strength equals more safety. It has already been stated that deformation capacity is equally, if not more, important than strength, as displacements are better related to expected damage and building stability during earthquakes. If the proportionality between stiffness and strength is acknowledged, it is noted that, at least for RC sections, the displacement and ductility capacities are reduced with increasing strength (i.e. same section with increased reinforcement ratio). Displacement demand is also reduced, as increased elastic stiffness means low vibration periods, which translates to lower demand from the displacement response spectrum. The above was

numerically examined by Priestley et al. (2007), who concluded that the displacement demand/capacity ratio is insensitive to the strength.

2.4 Displacement-based design

As previously stated in this research, here the term DBD refers to the direct DBD (“direct” because no iteration is required in the design process) methodology proposed by Priestley et al. (2007). It is a rather simple procedure, based in a substitute structure approach (Gulkan & Sozen, 1974; Shibata & Sozen, 1976) and its workflow is opposite to the one performed in FBD. In DDBD, a target displacement is first set, then the base-shear force is determined. The strength is distributed in the structure in order to achieve that displacement for that level of shaking. The DDBD procedure is summarised in Figure 2.3.

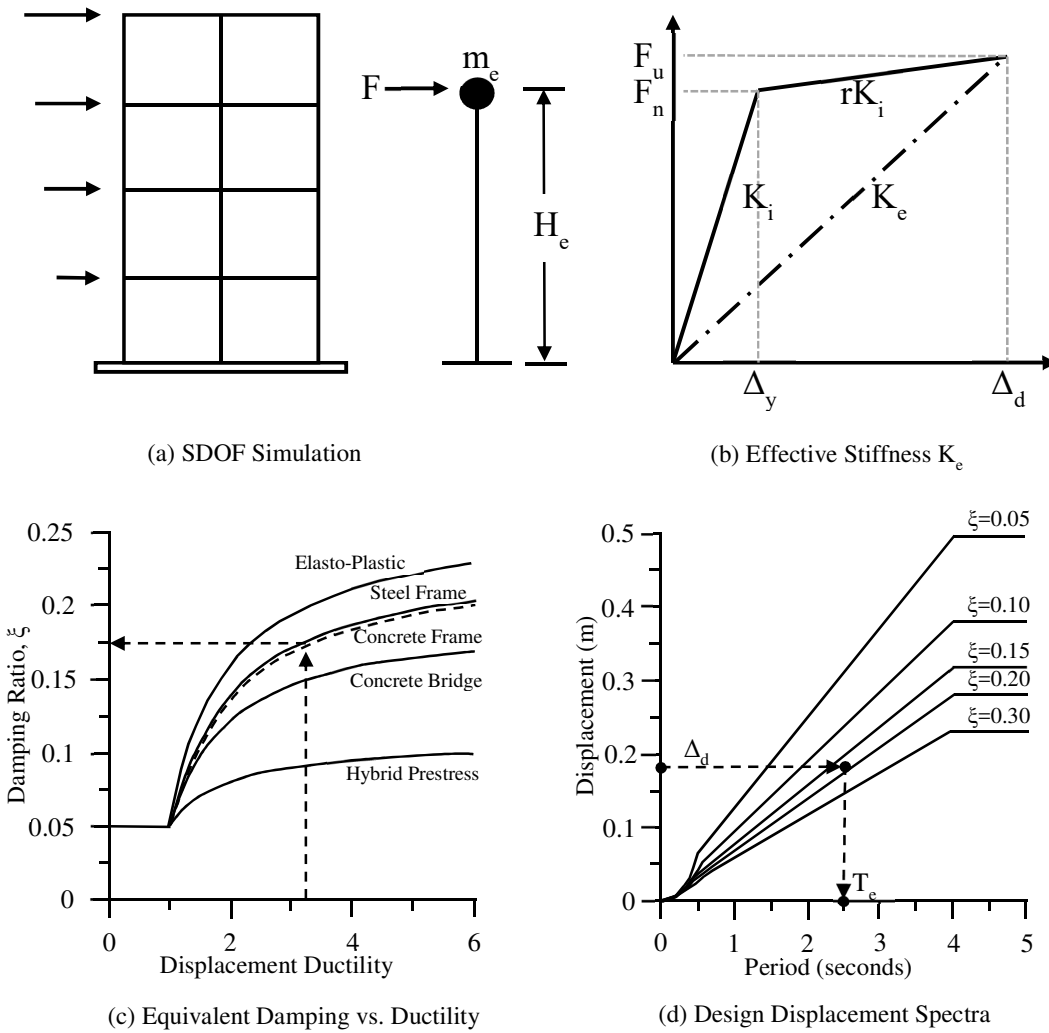


Figure 2.3. Fundamentals of DDBD. (Priestley et al. 2007).

The first step for DDBD of a MDOF structure involves an initial estimation of seismic mass and member sizes, followed by the choice of the desired plastic mechanism to be developed (e.g. plastic hinge at the critical section of an RC cantilever wall). Also, a target displacement or drift must be set (e.g. 2% inter-storey drift) according to the desired performance level. Then, the building must be idealised as an equivalent SDOF structure, which results in the determination of an equivalent mass, design displacement and effective damping. The SDOF design displacement is determined based on an assumption of the displacement shape and the target displacement profile selected for the real structure; the displacement shape is the one corresponding to the inelastic first-mode under the design level excitation and is the outcome of several inelastic time-history analyses developed for each structural type. Considering the relationship between strength and stiffness, the next step involves the calculation of the yield displacement based on the yield strain of the steel and the geometry of the structural members.

Knowing the yield displacement and the design displacement, the expected displacement ductility demand is computed and is related to a level of equivalent viscous damping (which combines elastic and hysteretic damping of the structural system), as shown in Figure 2.3 (c). The elastic displacement response spectrum is then reduced by the appropriate damping ratio and the designer uses the design displacement to get the effective period of vibration for the equivalent SDOF system. Once the effective period and mass have been defined, the effective stiffness K_e is computed from Equation 2.2, which is then multiplied by the design displacement to obtain the design base shear, according to Equation 2.3. Afterwards, the base shear is distributed in the real structure in proportion to mass and displacement at the discretized mass locations, the displacement used for design force distribution is the one corresponding to the design inelastic displacement profile. Finally, capacity design rules are applied to quantify design strength of structural members guaranteeing the development of the desired plastic mechanism.

$$K_e = 4\pi^2 m_e / T_e^2 \quad (2.2)$$

$$V_{base} = K_e \Delta_d \quad (2.3)$$

From the above, it is seen that DDBD relies on the structural properties at maximum response (Δ_d), namely the use of secant (K_e) instead of initial stiffness. It is also noted that while FBD

requires an estimation of the vibration period (T) to read an acceleration from the design spectrum, the inverse procedure is done in DDBD, where the target displacement is used to get the effective period (T_e) from the design spectrum. Overall, it can be concluded that the general process of DDBD is much more simple and easier to implement as many of the issues, or required assumptions discussed in Section 2.3 in relation to FBD, have been largely mitigated.

2.5 PEER PBEE for collapse risk assessment

2.5.1 Previous studies on collapse risk

There are several studies (Galanis & Moehle, 2015; Noh & Tesfamariam, 2018; Zareian & Krawinkler, 2007) in existing literature on the collapse risk of structures designed using FBD. Most of these studies were conducted in the scheme of performance-based earthquake engineering developed by the Pacific Earthquake Engineering Research (PEER) Centre and the application of the so-called PEER integral (see Section 2.5.2). Notable examples are the SAC/FEMA project for steel moment-resisting frames, the ATC-63 (2007) guidelines, the FEMA 273/356 and the HAZUS project.

Haselton et al. (2007) conducted a study to assess the seismic performance of a code-conforming RC moment-resisting frame building, applying the previously mentioned PEER PBEE methodology to calculate collapse risk and loss estimation. Uncertainties in ground motion and structural modelling were included and sensitivity to some variables was assessed. For comparison, the benchmark structure had eight different configurations or designs (perimeter and space frames) all according to IBC2003 and it was a 4-storey office building located in a high seismicity zone. Aspects regarding hazard analysis, ground motion record selection and scaling, numerical modelling, collapse definition, risk calculation and modelling uncertainty were extensively discussed.

For the case of RC wall buildings, there are significantly fewer collapse risk studies in the literature, where most of them focused on the computation of collapse fragility curves and seismic response with varied modelling approaches but did not carry on with the computation of MAPE for collapse. For example, Kolozvari et al. (2018) computed fragility curves and loss analysis for a 5-storey RC shear wall building with three different modelling methods. Also, Dabaghi et al. (2019) studied the collapse performance of RC wall buildings designed following the ASCE 7-10 and ACI 318-14 codes, and focused on analysing the effect of varying number

of stories and reinforcement layout. Others, like Araya-Letelier et al. (2019) computed MAPE for collapse for a dual wall-frame RC building under two different assumed hazard models and two different fragility fitting functions (Lognormal and Gamma).

These studies emphasised the influence that ground motion record selection criteria and inclusion of modelling uncertainties have on the mean annual frequency of collapse, which may differ on various orders of magnitude. Also, it is observed that the collapse risk varies from structure to structure, as code-conforming buildings with distinct number of stories and/or reinforcement ratios produce different results, raising the issue of non-uniform risk when following the FBD methodology.

Fox et al. (2014) performed a comparative study between RC coupled-wall building designed with FBD and DDBD methods, focusing on the comparison of the inter-storey drift design predictions to the ones obtained with non-linear time history analyses. The authors further investigated the effects of P-Delta considerations and showed that DDBD provides accurate prediction of the drift, while there appears to be compensating errors inside the FBD formulation as accuracy is reached as a result of the code-prescribed P-Delta effect considerations.

To the author's knowledge, there are presently no comparative studies on the collapse risk of RC wall buildings designed according to FBD and DDBD available in the literature. Furthermore, no comparison has been performed regarding the "uniform risk" or "risk-consistency" assumption that both methods try to provide. Thus, at a time where the structural design state-of-practice moves towards performance-based approaches, it becomes of great importance to provide insight on these issues and encourage the research community to explore them.

2.5.2 Collapse risk assessment methodology

As mentioned in Chapter 1, PBEE relies on probabilistic theory to quantify and evaluate the expected performance (e.g. the expected level of damage) of the designed building when subjected to a given level of seismic hazard, which can be compared against performance goals or levels that have been previously defined. The reader is referred to (Haselton et al., 2008; Moehle & Deierlein, 2004; Porter, 2009), for example, for a complete description of the methodology.

The basic steps of the procedure involve hazard analysis of the site in terms of a predefined intensity measure (IM), e.g. $Sa(T_1)$, from which a set of hazard-compatible ground motion records are selected. Next, a series of non-linear time history analyses (NLTHA) of the structure are run using a numerical model and the response is characterised using an engineering demand parameter (EDP), e.g. roof displacement, peak inter-storey drift ratio, peak floor acceleration. By carrying out statistics on the EDP vs IM results and convolution with hazard, the mean rate of exceeding an EDP value conditioned on IM can be calculated. This process is analytically described by the equation known as the “PEER integral” (Cornell & Krawinkler, 2000).

This investigation focuses on the computation of collapse risk of newly designed structures. As such, the PEER PBEE methodology is carried out up to the point where the MAPE of an EDP can be calculated, using Equation 2.4. Both epistemic and aleatory uncertainties are considered in the process to account for record-to-record variability (aleatory) and modelling uncertainty (epistemic), for example.

$$\lambda(EDP) = \int G(EDP|IM) d\lambda(IM) \quad (2.4)$$

In Equation (2.4) $G(EDP|IM)$ represents the probability that an EDP is exceeded given a particular value of IM and $\lambda(IM)$ is the mean annual frequency of exceedance for IM level of shaking.

The steps followed in this study for the collapse risk assessment of a set of newly designed buildings were as follows:

- i) Ground motion records are selected from a database, assuring consistency with the hazard at the site conditioned on a specified IM, which was considered here as the spectral acceleration at the fundamental period, $Sa(T_1)$. The set should be comprised of a large enough number of accelerograms to provide statistically meaningful results;
- ii) Numerical models of the buildings are constructed. Choices regarding type of modelling approach for structural members and constitutive model of materials, should be carefully made to guarantee that the non-linear behaviour of the structure

- is represented as faithfully as possible, while also maintaining computational efficiency;
- iii) The method to assess the seismic collapse capacity of the buildings was the incremental dynamic analysis (IDA) (Vamvatsikos & Cornell, 2002). At this point, analyses were carried out and structural response was characterised using an EDP;
 - iv) The collapse capacity point was defined and statistics were performed on the results to compute the median capacity curve of each building;
 - v) The MAFE of the EDP is computed by considering the relationship between IM, EDP, and the rate of exceedance of the IM; which was obtained by second-order fitting of the site hazard curve. At this point, modelling uncertainties were included.

The quantification and description of the choices made at each step of the proposed collapse assessment methodology is presented in Chapter 6.

3 HAZARD

3.1 Introduction

The seismic hazard at the site was estimated by probabilistic seismic hazard analysis (PSHA) (Cornell, 1968; Esteva, 1968; McGuire, 1995) using the OpenQuake software (Silva et al., 2014) developed by the Global Earthquake Model (GEM) Foundation.

PSHA estimates levels of ground motion shaking for different return periods while accounting for the epistemic and aleatory uncertainties involved in the earthquake rupture and ground motion propagation processes. As the collapse risk methodology used in this study utilised ground motion records and considered the propagation of uncertainties along each step of the PBEE procedure, it was then preferred to use a site-specific hazard analysis rather than using prescribed hazard values available at the *Servicio Geologico Colombiano* (SGC)¹ or in the Colombian seismic design building code *NSR-10* (AIS, 2009), which might not have provided this required detailed information.

3.2 Location

The site chosen for the buildings design is the city of Cali, Colombia at 3.450°N, -76.531°W. It is the third largest city in the country and it is classified as high seismic hazard zone by the Colombian Association of Seismic Engineering (AIS-300, 2010). It corresponds to a Seismic Design Category D site according to ASCE 7-16 scale, as shown in Chapter 4.

The city is located in southwest Colombia (Figure 3.2), very close to the Pacific Ocean coast and the well-known “Ring of fire”, which is around 200-300 km away from the subduction

¹ <https://www.sgc.gov.co/>

zone at the boundary between the Nazca Plate and the South American Plate. It is surrounded by active faults such as the “Cauca” and “Junín” systems, which are within 30-50 km of the city. Not surprisingly, strong earthquakes have struck the city in the past (Popayan/Cali, 1566; Cali/Buga, 1766; Tuluá, 1925; Cali, 1995). A special mention is given to the Popayan/Cali earthquake in 1566, as it is the oldest earthquake in the Colombian catalogue and also to the “Colombia-Ecuador” earthquake in 1906, which is the strongest recorded event with Mw 8.8 (Kanamori & McNally, 1982).



Figure 3.2. Site Location (Google Earth).

3.3 PSHA input model

The PSHA model used for hazard estimation was developed by the GEM Foundation as part of the South America Risk Assessment (SARA) Project (Garcia et al., 2017). Two main final products of the PSHA were used in the project: the hazard curves and the uniform hazard spectra (UHS), which is a response spectrum with equal probability of exceedance across all periods for a given site and it is derived from the computation of the individual hazard curves for several periods.

The PSHA input model contained a set of 11 ground motion prediction equations (GMPE) for a total of 11 branches of the logic tree. The GMPEs and their corresponding weights are shown in Table 3.1. A shear-wave velocity on the soil upper 30 m ($V_{s,30}$) of 360 m/s was assumed, corresponding to a Soil Site Class C according to the classification provided by both the Colombian building code (NSR-10) and the ASCE 7-16 code.

Table 3.1. GMPEs and corresponding weights included in the PSHA input model's logic tree. (Adapted from SARA Project, GEM)

Ground Motion Prediction Equation	Weight
Active Shallow Crust	
Akkar et al. (2014)	0.3333
Bindi et al. (2014)	0.3333
Boore et al. (2014)	0.3334
Stable Shallow Crust	
Atkinson and Boore (2006)	0.25
Tavakoli and Pezeshk (2005)	0.5
Drouet (2015) - Brazil with depth version	0.25
Subduction interface	
Zhao et al. (2006)	0.3333
Abrahamson et al. (2015)	0.3333
Montalva et al. (2016)	0.3334
Subduction in-slab	
Abrahamson et al. (2015)	0.5
Montalva et al. (2016)	0.5

The seismicity of the site is influenced by three main tectonic region types, namely subduction interface, subduction intra-slab and active shallow crust regions. Figure 3.2 shows the active faults considered by the PSHA source model, where the two faults that flank the city on both sides are noted. Additionally, Figure 3.3 shows a graphical representation of the 3D model considered for the subduction interface and subduction intra-slab sources. For further information about the PSHA input model, the reader is referred to the SARA Project webpage².

² https://sara.openquake.org/hazard_rt7

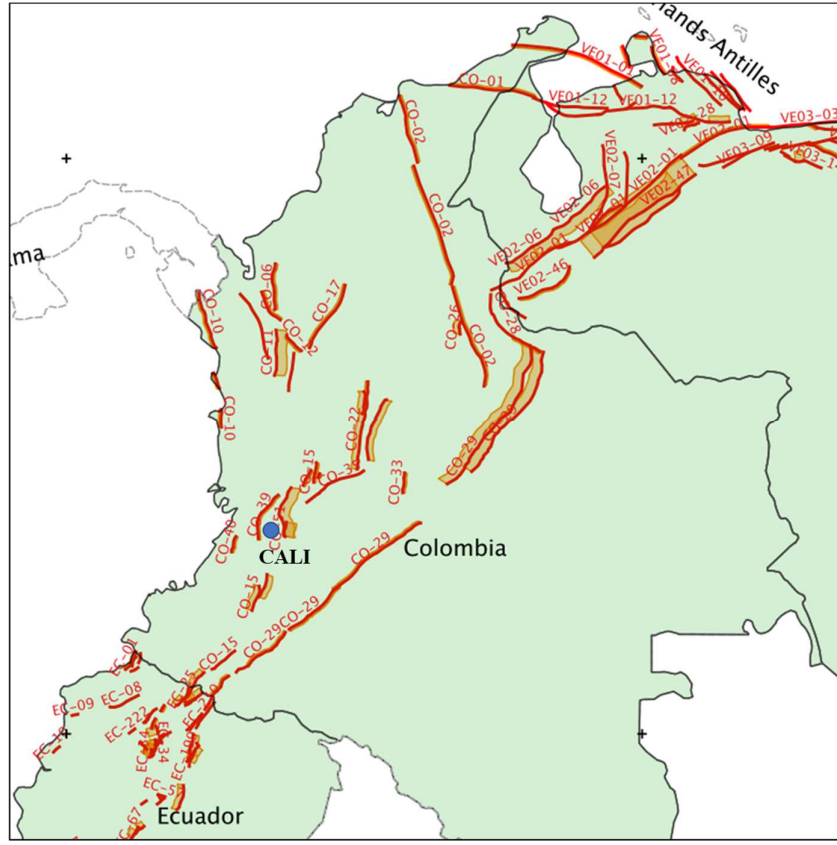


Figure 3.2. PSHA fault model representation. (Adapted from SARA Project).

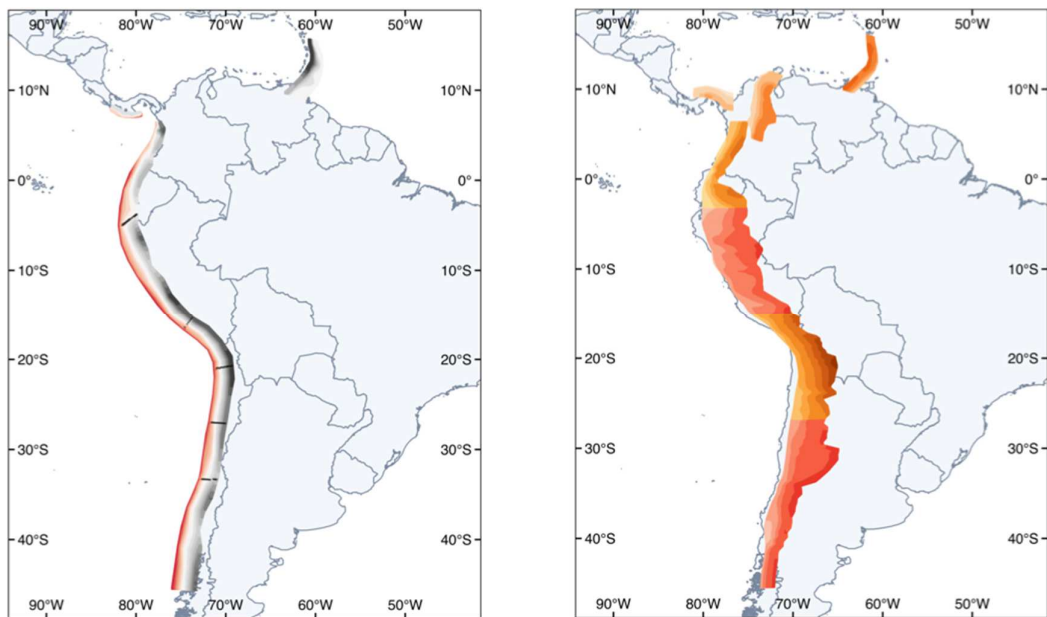


Figure 3.3. PSHA subduction model representation (Adapted from SARA Project).

3.4 PSHA results

Hazard curves for several spectral periods were computed for illustration, whereas more building-specific curves will be characterised later. The mean curves for PGA, $Sa(0.5s)$ and $Sa(1.0s)$ are shown in Figure 3.4. It is worth mentioning that for relatively small values, the probability of exceedance and the rate of exceedance of a certain intensity are approximately equal. Thus, the results of hazard curves can also be interpreted in terms of mean frequency of exceedance vs intensity.

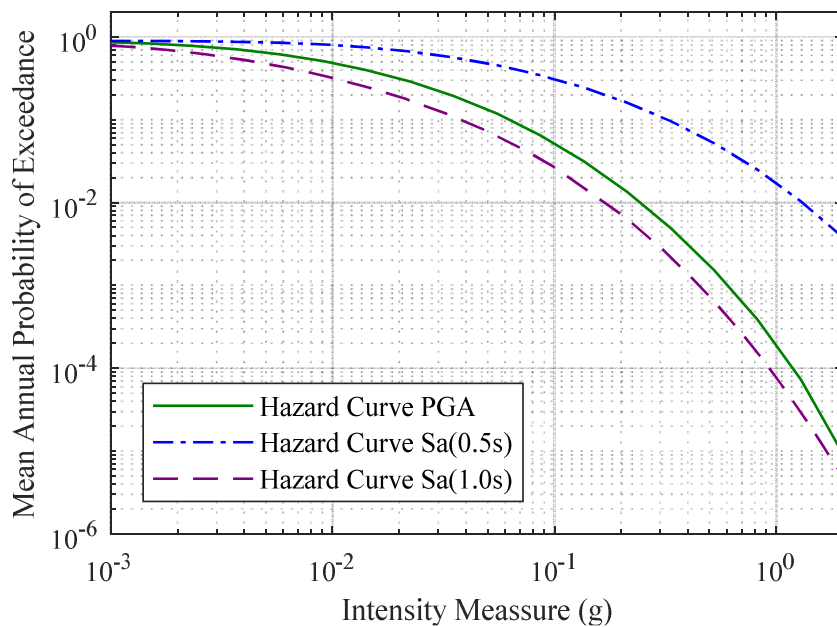


Figure 3.4. Mean Hazard Curves for PGA, $Sa(0.5s)$ and $Sa(1.0s)$.

Two return periods were considered for the UHS computations, 475-years and 2475-years, which correspond to a 10% probability of exceedance and 2% probability of exceedance in 50 years, respectively. These hazard levels are consistent with the levels required by most building codes. Figure 3.5 shows the UHS for both return periods.

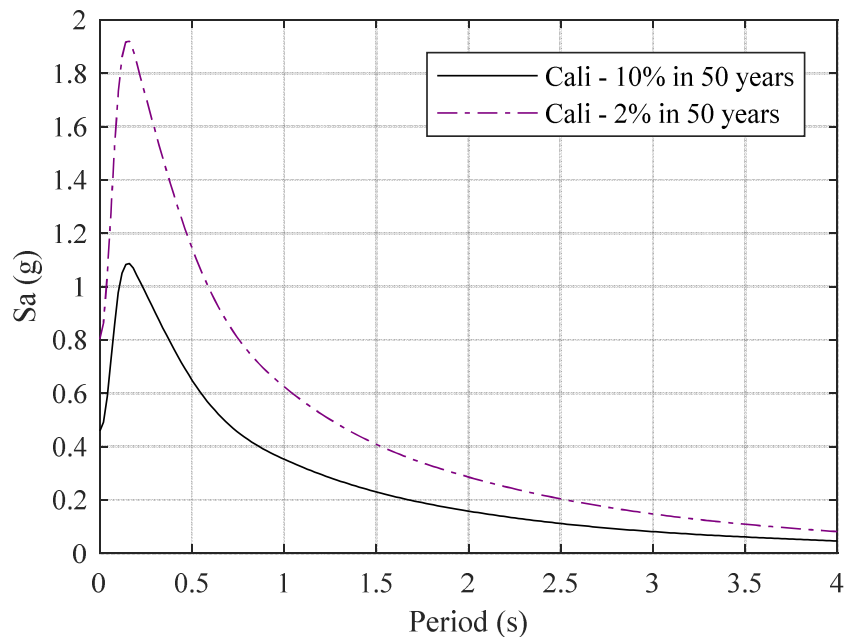


Figure 3.5. Mean Uniform Hazard Spectra (UHS) 5% damping for two hazard levels.

The computed UHS indicate that significant shaking is expected to occur in structures with vibration periods between 0.1 and 0.75 seconds under the design earthquake. This is, not surprisingly, exacerbated for the 2475-years spectrum, which would produce ground motions larger than 0.5g for structural periods up to 1.25s. The UHS and the hazard curve values corresponding to 2% in 50 years may be used as reference for ground motion record selection for collapse assessment as this intensity level is close to the collapse capacity of the structures. Furthermore, it corresponds to the maximum considered earthquake (MCE) level to compute the collapse margin ratio (CMR) of the buildings, as explained in Chapter 6.

4 BUILDINGS DESIGN

4.1 General considerations

Once the hazard at the site was defined, it was possible to proceed and design the buildings. A total of six buildings were designed: three following FBD and three following DDBD. For FBD, the seismic design was carried out following the American Society of Civil Engineers 2016 Standard (ASCE 7-16, 2016) since the seismic design rules are quite similar to those adopted in the Colombian building code NSR-10 (AIS, 2009). For the DDBD procedure, the design was carried out following the 2012 model code (DBD12) developed by Sullivan et al. (2012) as well as the complete DDBD theoretical framework present in Priestley et al. (2007).

The buildings are symmetric in plan and in height, so as to avoid additional complexities deemed to be irrelevant for the present study. All buildings comprise two RC rectangular flexural-dominated walls with boundary elements, as the main seismic resisting system in both orthogonal directions. Gravity-load carrying capacity was given by a combination of flat-slab and columns system (“gravity-columns”). The storey height is 3m, and the floor-plan dimensions and imposed loads (dead and live loads, excluding self-weight) were kept equal for all buildings, as explained below. Wall dimensions were equal for the 3- and 6-storey buildings, but the wall length was increased in the 9-storey building. Figure 4.1 shows the typical floor plan of the buildings. The walls were placed in the perimeter of the building for convenience, given that placing in the centre would require them to be designed as core-walls (as is typically done in practice), which is beyond the scope of this research.

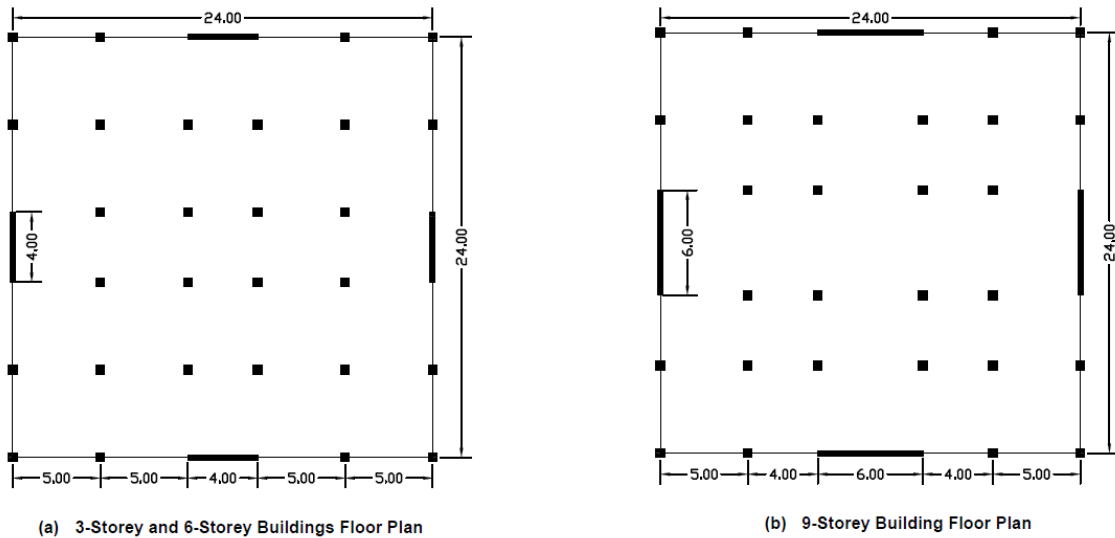


Figure 4.1. Floor plan of the designed buildings.

In order to make a fair comparison, the building's characteristics, such as typical floor plan, storey height, member sizes (where possible) and imposed dead and live loads, were kept equal for both methods. As such, the differences in design were only a result of the way each procedure handles the calculation of seismic actions and how the strength is distributed in the structure, which means, essentially, comparing the seismic design procedures.

For simplicity, superimposed dead load was uniformly distributed, with a value of 1.8 kN/m² assumed for floors and 0.5 kN/m² for the roof. The same distribution was assumed for live loads, with a value of 2.5 kN/m² (roof inclusive), consistent with the guidelines provided in the ASCE 7-16 and NSR-10 standards. Regarding member sizes, gravity columns were 0.5x0.5 m and flat-slab thickness was 0.15 m. Concrete compressive strength (f_c') of 28 MPa and steel yield strength (f_y) of 420 MPa were used for all buildings. Load combinations rules of ASCE 7-16 were used to combine gravity and seismic actions for both methods, wind and snow loads were not considered. The load combinations that governed the design are shown in Table 4.1 whilst the calculation of the load coefficients is presented in Appendix A.

Table 4.1. Load combinations used for FBD and DDBD.

Load Combinations
1.39D + 0.5L +1Qe
1.39D + 0.5L -1Qe
0.71D + 1Qe
0.71D - 1Qe

For both methods, once the seismic design forces were identified, the reinforcement detailing rules of the American Concrete Institute 2014 (ACI 318M-14) Standard (ACI, 2014) were applied, with some exceptions regarding material properties for plastic hinge regions described in the DDBD Code, which are discussed later. Concerning the building category, all the designs are assumed to be office buildings, with seismic importance factor equal to unity.

The full extent of the calculations performed for the designs can be found in Appendix A and B for FBD and DDBD, respectively. Here only the main aspects, decisions and results of the design process are shown. More emphasis is made on the DDBD design process as the reader may be more unfamiliar with it, unlike the traditional FBD procedures.

4.2 Force-based design

4.2.1 Design spectrum definition

Chapter 11 of ASCE 7-16 defines the seismic demands to be used for design in terms of a design acceleration spectrum computed from a couple of parameters, namely $Sa(0.2s)$ and $Sa(1.0s)$, that have been mapped for each site. A slight change was made in this study, as the acceleration spectrum used for design was the UHS computed from PSHA. There are two main reasons behind this decision: the first is because it was not possible to compute the smoothed code spectrum as the mapped acceleration parameters required are only mapped for sites in the United States; and the second, and probably the most important, because it was desired to use a consistent hazard model for both design and assessment. Alternatively, one could have used the mapped acceleration values of the Colombian seismic code (NSR-10) but these values were derived from a different hazard model, meaning the hazard consistency would also have been lost. An additional advantage of using the UHS for design was that it already accounts for the soil conditions at the site and therefore, no site coefficients needed to be applied to modify the design spectrum.

A final comment with respect to seismic demand definition concerns the hazard level used for design. ASCE 7-16 uses risk-targeted mapped acceleration parameters corresponding to 1% in 50 years risk of collapse using a generic fragility function (the so-called Risk-Targeted Maximum Considered Earthquake, MCE_R), which are then reduced by 2/3 to compute the design spectrum. In older versions of the code, mapped acceleration parameters were based on the 2% in 50 years ground motion, which were also reduced by 2/3. This procedure results in a design spectrum that is approximately equal to the one computed for 10% in 50 years probability of exceedance (the 2% in 50 years hazard values are still used in ASCE 7-16 Chapter 21, related to site-specific procedures). In Figure 4.2, the UHS for 10% in 50 years is plotted along with a smoothed spectrum computed following ASCE 7-16 shape using as input the $Sa(0.2s)$ and $Sa(1.0s)$ values of the 2% in 50 years PSHA results. The design spectrum according to the Colombian code NSR-10 is also plotted. Seismic Design Category D was used for the design calculations. It can be seen that there is a good agreement between each of the approaches to construct the design spectrum, hence it was deemed suitable to use the UHS in design.

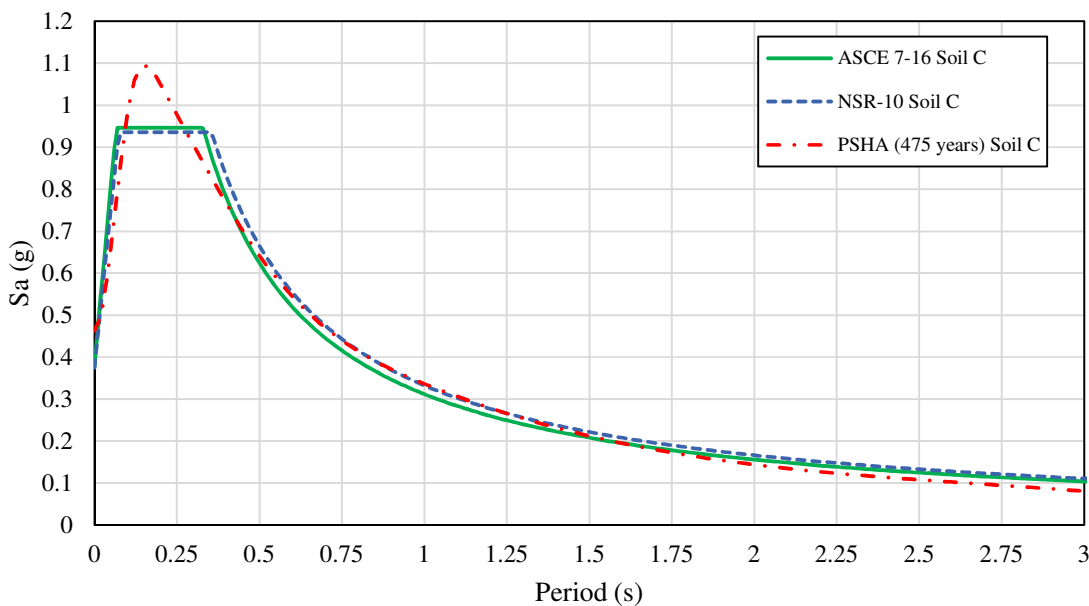


Figure 4.2. Comparison UHS for design vs code-based (ASCE 7-16 and NSR-10) smoothed spectrum.

4.2.2 Force-reduction factors and design coefficients

A fundamental step of FBD is the definition of the force-reduction factor, R , which is tabulated for different structural types in Chapter 12 of ASCE 7-16. All the buildings designed in this

research fall in the category of building frame system with special reinforced concrete shear walls, since the vertical load bearing capacity is given by the combined action of gravity columns and flat-slab and the RC walls act only as the seismic-force resistance system, thus they cannot be considered as bearing walls. Three design coefficients are obtained as a result: the response modification coefficient (i.e. force reduction factor), R, equal to 6; an overstrength factor of 2.5 and a deflection amplification factor, C_d , of 5. The same values were used for the three buildings, as these coefficients depend only on the structural type.

4.2.3 Computational model and structural analysis

A 3D computational model was built using Autodesk Robot Structural 2019³, structural analysis software. The structure was assumed to be fixed at the supports, the floor-slabs were considered as rigid diaphragms and the walls were modelled with shell elements formulation. A preview of the models is shown in Figure 4.3.

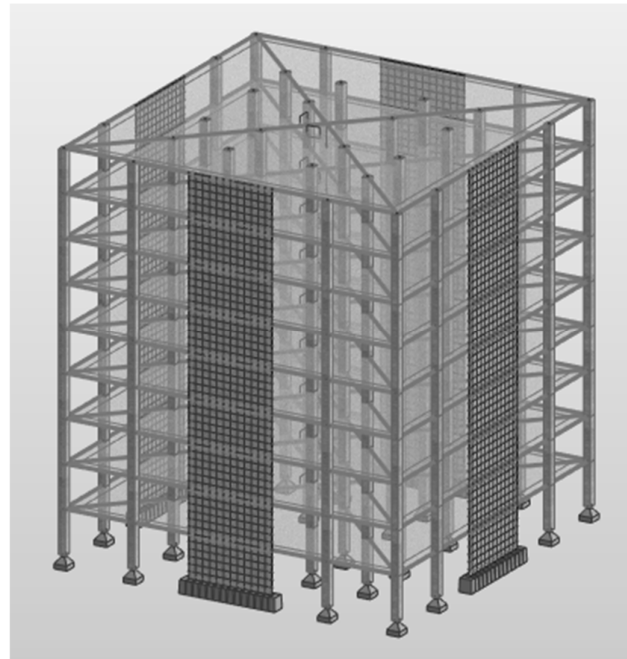


Figure 4.3. Graphic representation computational model for 9-Storeys building. (Autodesk Robot Structural 2019).

The ASCE 7-16 calculation of seismic loads accounts for the combination of both vertical and horizontal effects (Equation 4.1), the calculation of horizontal effects involves the computation of a structural redundancy factor which might amplify the seismic actions for structures

³ <https://www.autodesk.com/products/robot-structural-analysis/>

assigned to Seismic Category D. Following the code regulations for structural wall buildings, this reduction factor would be equal to 1.0 for the 9-Storey building and 1.3 for both the 3-Storey and 6-Storey buildings. However, to keep consistency across all designs and to keep a fair comparison with DDBD method, this factor was taken as 1.0 for all the designs, as no modifications of the seismic load different than the ones inherent to FBD methodology were desired.

$$E = E_h \pm E_v \quad (4.1)$$

No vertical or horizontal structural irregularities were expected as the buildings are fully symmetric, however, the accidental eccentricity checks were carried out. The effective seismic weight considered for calculations was obtained by adding the building's self-weight and the unfactored dead loads. The same effective seismic weight was used for both FBD and DDBD.

Different analysis procedures are allowed, namely equivalent lateral force (ELF) procedure, modal response spectrum analysis (MRSA), linear response history analysis, and non-linear response history analysis. The MRSA method, as applied in the design code, also requires partial results of ELF procedure. Given the simplicity of the ELF method, both analyses were carried out and the MRSA results were used for structural design. The code requires that cracked section properties be used for modelling of RC members. Hence, a stiffness-reduction factor of 0.5 was applied, according to the values stated in ACI 318-14 code.

Two fundamental issues are discussed before evaluating the structural analyses results, which are related to the vibration period calculation and the base shear definition for MRSA according to ASCE 7-16. When applying MRSA, the code sets two limits that condition the design base shear calculation. One is that the base shear calculated by the MRSA procedure must be at least equal to the one obtained with ELF method and the second is that the fundamental period used for base shear calculations shall not exceed a prescribed value, even if a higher value is found with modal analysis. These limits are not common among all FBD based codes and are essentially applying empirical restrictions on the designs resulting from a presumably more accurate MRSA. For instance, they are not implemented in Eurocode 8. Table 4.2 shows a

comparison of the vibration periods calculated following the ELF and MRSA procedures. It is observed that the maximum period limit governs the 6-storey and 9-storey designs.

As described in ASCE 7-16 commentary, these limits are implemented to prevent the designer from using over-flexible models that result in periods too long for which demand is too low, and consequently lower strength. The requirement to match the MRSA base shear to 100% ELF base shear, according to the code commentary, intends to improve the collapse performance of MRSA designed buildings. It is nevertheless noted that the application of this rule does not necessarily guarantee that the desired performance is achieved either.

Table 4.2. Comparison of different period definitions results. MRSA vs ASCE 7-16 formulas.

Design	MRSA	Method for Period Calculation		
		1. $T_a = C_t h_n^x$	2. $T_a = 0.1N$	3. $T = C_u T_a$
FBD - 3	0.34	0.254	0.3	0.355
FBD - 6	1.17	0.426	0.6	0.597
FBD - 9	1.41	0.578	0.9	0.809

1. Height dependent formula.

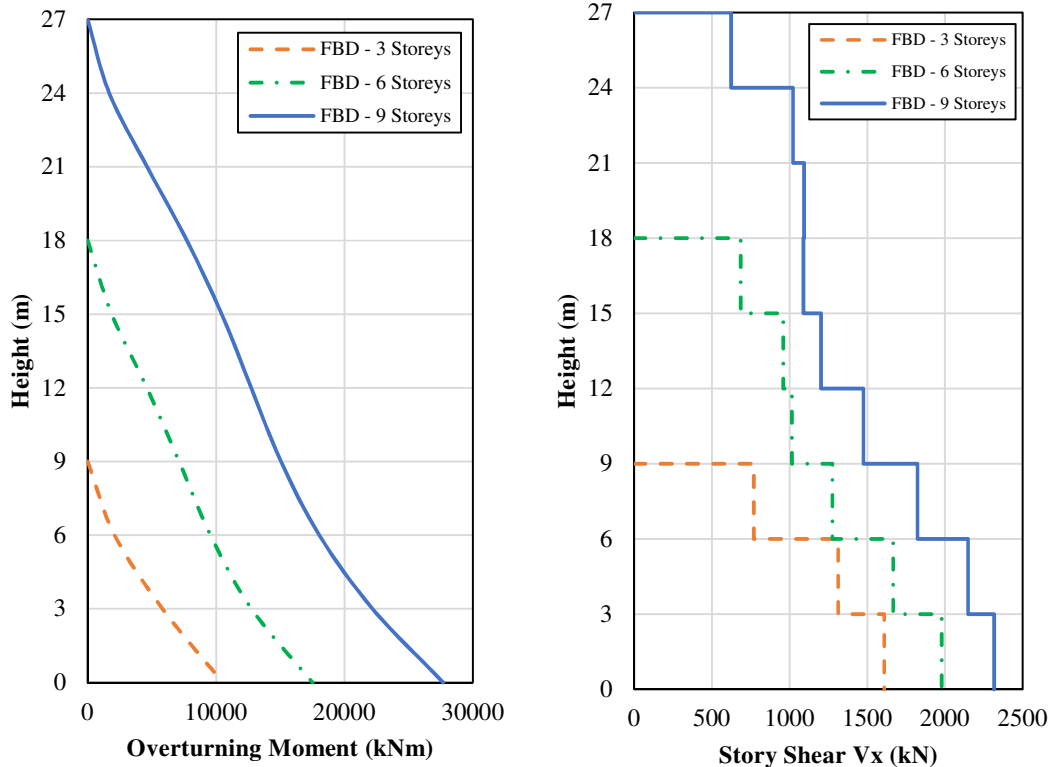
2. Number of storeys (N) dependent formula.

3. Maximum T allowed by the code of design purposes, overrides MRSA if $MRSA > C_u T_a$

A few comments can be made on the points above. The first is that the code is somehow recognising that there are flaws within the FBD procedure that might lead to structures not meeting the desired performance (i.e. too high collapse risk), and that some compensation is necessary. Moreover, the enforcement of the limits of base shear and period seems to be related with the perception that more strength is equal to more safety, as the code requires the designer to use low periods that result in larger acceleration demands and consequently more required strength. This is not necessarily true, as explained in Section 2.3. To account for this code requirement, within a modal analysis framework, the scaling of the base shear was therefore achieved by scaling up the design response spectrum by the appropriate scale factor, prior to performing the structural analysis for the FBD cases. Table 4.3 shows the calculation of the scale factors and compares the base shear obtained by ELF and MRSA

Table 4.3. Scale factors and comparison of base shear (V_b) for MRSA and ELF procedures.

Design	Direction	$V_{b,\text{ELF}}$ (kN)	$V_{b,\text{MRSA}}$ (Elastic) (kN)	R/Ie	$V_{b,\text{MRSA}}$ (Reduced) (kN)	Scale Factor	$V_{b,\text{MRSA}}$ (Design) (kN)
FBD-3	X-Dir	1608.83	7124.82	6.00	1187.47	1.35	1608.83
	Y-Dir	1608.83	7124.82	6.00	1187.47	1.35	1608.83
FBD-6	X-Dir	1978.42	6910.68	6.00	1151.78	1.72	1978.42
	Y-Dir	1978.42	6910.68	6.00	1151.78	1.72	1978.42
FBD-9	X-Dir	2311.79	9526.88	6.00	1587.81	1.46	2311.79
	Y-Dir	2311.79	9526.88	6.00	1587.81	1.46	2311.79

**Figure 4.4. FBD: Moment (left) and Shear (right) design profiles results, MRSA analysis with scaled spectrum.**

MRSA was carried out for the three buildings, considering checks regarding maximum drifts, accidental torsion and P-Delta effects. Figure 4.4 shows the moment and shear profiles for the structures. As expected, demands increase with increasing number of storeys, mainly because of the higher seismic weight. These forces were combined with dead and live loads following

the combination rules of Table 4.1 to obtain the required strength of the structural members (factored loads). Design was completed considering axial-flexure interaction, thus the $0.71D + 1Qe$ load combination case became critical to calculate flexural reinforcement, as lower axial force affects the nominal moment capacity of the wall.

4.2.4 Reinforcement detailing and final design

Reinforcement calculations were carried out for the structural walls only, since they essentially constitute the seismic-force resisting system. Hence, gravity columns design was not performed, since their contribution to lateral force resistance was neglected for the purposes of this study. Special structural walls design is given by Section 18.10 of ACI 318-14 code. It provides procedures for the estimation of axial, flexural and shear strength, as well as requirements on reinforcement arrangement. Most of these formulas are based on extensive experiments and research completed in the past, others are the result of expert judgement. As it is observed in the design profile plots, the moment and shear demands generally decrease at the upper storeys. In many cases, the minimum reinforcement requirements will govern the design.

All walls were designed including boundary elements which extend up to the rooftop. In order to have an optimised design, the reinforcement layout was changed every three floors. The wall behaviour is usually classified according to the shear-span ratio, h_w/l_w where typically if this ratio is less than 2, the wall response is considered to be shear-dominated, and if the ratio is greater than 2, a flexural-dominated response is expected.

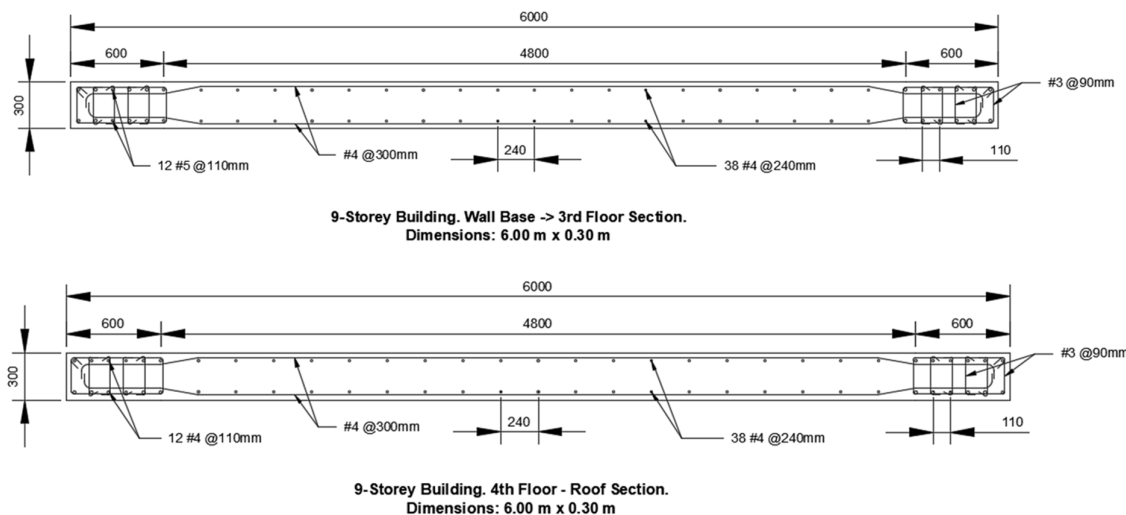
The code makes use of member strength reduction factors (ϕ), which aim to provide a safety margin for the designed structures by reducing the calculated nominal strength of the members, thus requiring more strength to overcome the demands. In this study, reduction factors of 0.85, 0.9 and 0.75 were applied in axial, flexural and shear strength calculations respectively. A factor of 0.75, rather than 0.6, was allowed for shear design because of the capacity design rules implemented.

Table 4.4. Summary of flexural design at wall base for FBD cases.

Design	P _u , Max (kN)	P _u , Min (kN)	M _u (kNm)	M _n (kNm)	c (mm)	φM _n (kNm)	Ω Flexural (Shear Magnification*)	Rebars Boundary	Rebars Web
FBD-3	880	407	5271	7803	463	7022	1.48	12 #5	28 #4
FBD-6	1813	841	8760	11929	688	10736	1.36	12 #6	28 #5
FBD-9	3516	1650	13847	19711	903	17740	1.42	12 #5	38 #4

*Such that capacity design principles are used and a reduction factor of 0.75 instead of 0.6 is allowed for shear.

First, the flexural design of the RC walls was carried out considering axial-flexure interaction. Most of the steel was placed at the boundary elements and the remaining part was equally distributed along the wall web following the minimum and maximum spacing requirements. The flexural design of wall base sections is summarized in Table 4.4. Capacity design was implemented following the recommendations of NEHRP (Moehle et al., 2012). The ratio between nominal and required moment was calculated to get the flexural overstrength, then the shear demand was amplified by this factor to ensure that the flexural yielding mechanism develops first. Next, shear design was carried out. Two layers of bars were used for both horizontal and vertical reinforcement. Finally, axial capacity was checked, and the boundary elements transverse reinforcement was arranged in compliance with spacing rules. Figures 4.5 to 4.7 depict the cross-sections of the designed walls. The detailed extent of the calculation is presented in Appendix A and summary of wall-base section properties is provided in Table 4.5.

**Figure 4.5. (FBD) Force-Based Design, 9-Storeys Building. (Rebar size in Imperial System).**

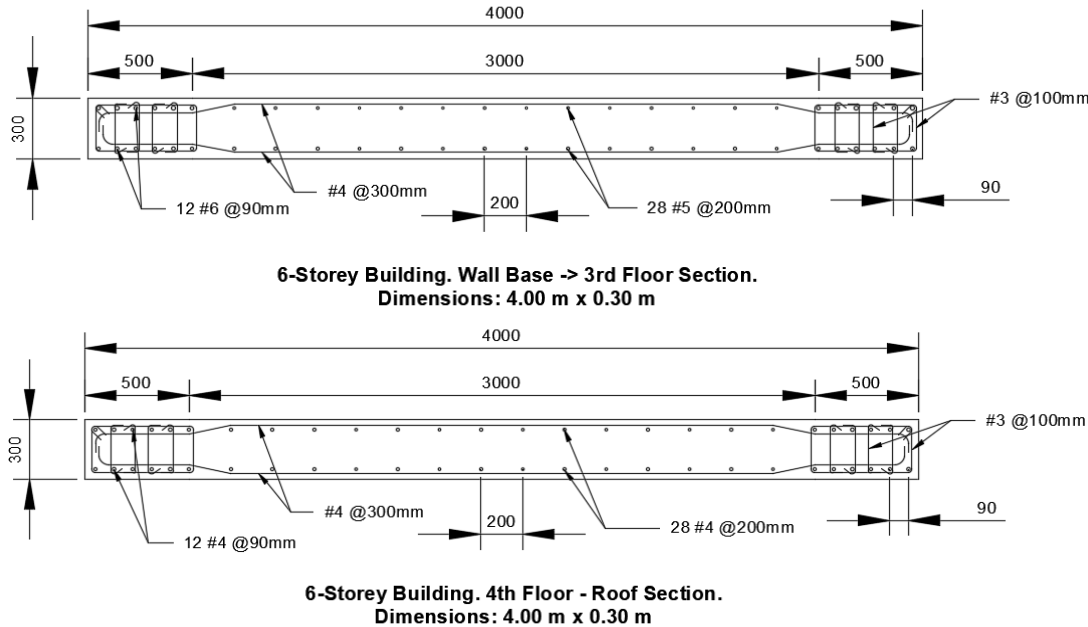


Figure 4.6. (FBD) Force-Based Design, 6-Storeys Building. (Rebar size in Imperial System).

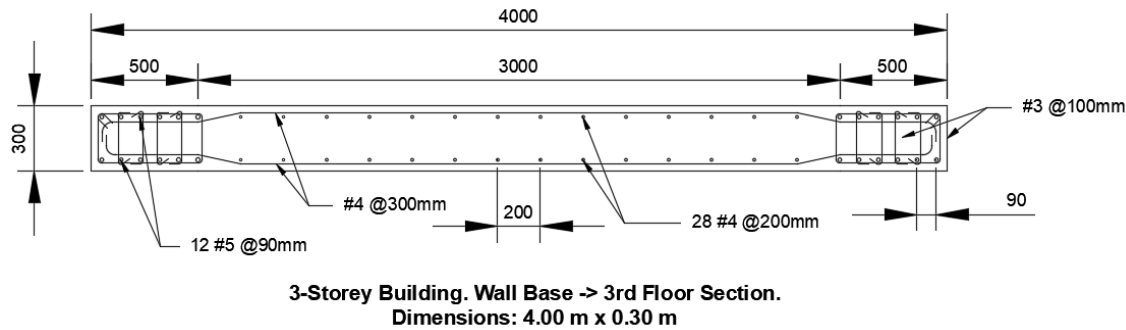


Figure 4.7. (FBD) Force-Based Design, 3-Storeys Building. (Rebar size in Imperial System).

Table 4.5. Summary of FBD design characteristics at wall-base section of all buildings.

Design	Wall Length (mm)	Wall Thickness (mm)	Bound. Elemt. Length (mm)	Total A _s , Horiz. (mm ²)	Total A _s , Vert. (mm ²)	ρ _t , Transv.	ρ _{l,w} - Web Long.	ρ _{l,b} - Bound. Elemt.
FBD - 3	4000	300	500	2580	8412	0.00287	0.00430	0.01600
FBD - 6	4000	300	500	2580	12416	0.00287	0.00667	0.02272
FBD - 9	6000	300	600	2580	9702	0.00287	0.00358	0.01333

4.3 Direct displacement-based design

4.3.1 Displacement spectrum for design

As mentioned earlier, the DBD procedure utilised was the one prescribed by the DBD12 model code (Sullivan et al., 2012) and Priestley et al. (2007). The first step in the design process is to define the seismic demand via a displacement response spectrum. DBD12 requires the design spectrum to have a shape as shown in Figure 4.8, a bilinear spectrum in which the displacement increases linearly with period until reaching a given corner period (T_C) and then remains constant. This linear ascending branch can be obtained from acceleration spectra by making use of the formulation for steady-sinusoidal peak response, Equation 4.2, hence the definition of the corner period is the main parameter to define.

$$\Delta_{(T)} = \frac{T^2}{4\pi^2} S_{A(T)} g \quad (4.2)$$

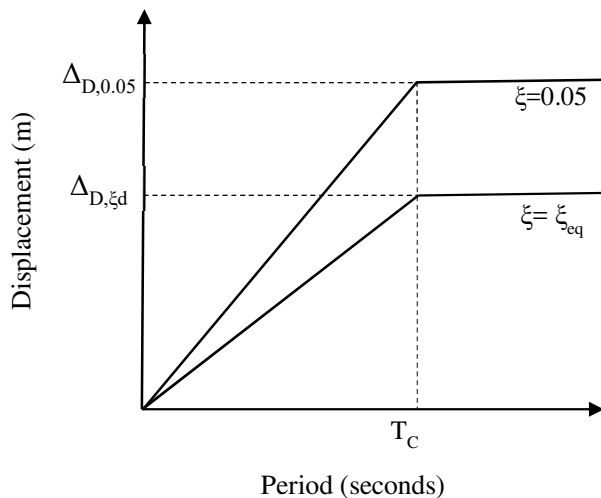


Figure 4.8. Design displacement spectra illustration. 5% damping and reduced by equivalent viscous damping ξ_{eq} .

DBD12 suggests that the corner period should be both magnitude and distance dependent. In recent years, researchers have investigated the issue and have attempted to provide equations for estimation of T_C , e.g. Equation 4.3 (Faccioli et al., 2004) and Equation 4.4 (NEHRP, 2003). These equations are event-dependent as they provide T_C values for a given magnitude and in some cases for a (M,R) pair. One option would be to compute the corner period based on the

magnitude that contributes more to the hazard at the site obtained by hazard disaggregation (Bazzurro & Cornell, 1999), which is discussed in Section 4.3.2.

$$T_C = 1.0 + 2.5(M_W - 5.7) \quad (4.3)$$

$$\log_{10} T_C = -1.25 + 0.3M_W \quad (4.4)$$

The approach taken in this research consisted of identifying the onset of the constant displacement range in the response spectrum generated from the acceleration UHS obtained in PSHA, using Equation 4.2. Then by visual inspection, a T_C value to compute the bilinear “smoothed” spectrum (such as the one described in DDBD12) that better fits the PSHA outcome was identified. This option was applied here such that design spectra would agree with the one used for MRSA in FBD, although T_C has little to no influence in the FBD of the studied buildings. The NSR-10 code includes a formulation for calculating the displacement design spectra. However, its use results in a slight overestimation of maximum displacement demand if compared with the results obtained in PSHA. Application of the adopted approach to estimate the design spectra is shown in Figure 4.9, for which a corner period T_C equal to 2.4 seconds was taken from the bilinear fit to define the spectrum used for design.

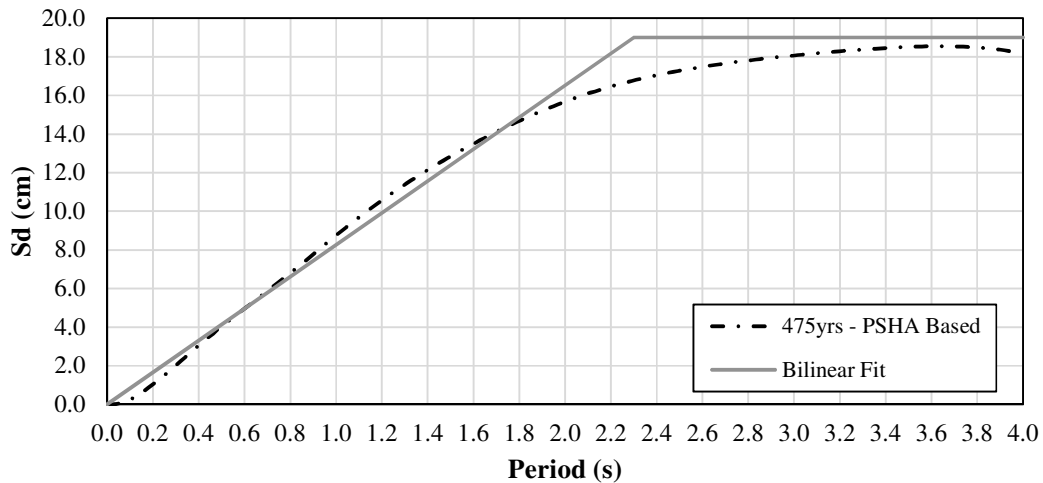


Figure 4.9. Displacement spectra used for design, bilinear fit of PSHA results.

4.3.2 Alternative displacement design spectrum

The issue of adequate computation of the displacement response spectrum at a site, although not related with the DDBD method itself, is still a concern, as a wrong estimation of the corner period and/or peak displacement may lead to unconservative designs. This issue will become more relevant in the subsequent sections.

One could also question the validity of PSHA results for the range of long periods, since PSHA results are highly dependent on the GMPEs chosen, the weights assigned and how each one of them was calibrated. For example, past investigations (Akkar & Bommer, 2006) have shown that the cut-off frequencies used for filtering ground motion records have a major influence on the range of periods a GMPE is reliable for, in spectral displacement estimation. This discussion is beyond the scope of this thesis, but a simplified comparative study was carried out. Displacement demand is computed using GMPEs calibrated for long periods, i.e. (Campbell & Bozorgnia, 2008) “CB08” and (Cauzzi et al, 2015) “CAUZ14”. Results are compared with the original PSHA model and the corner period estimations of Equations 4.3 and 4.4.

Disaggregation was performed for PGA for a 10% probability of exceedance in 50 years and the results of mean M-R disaggregation can be seen in the Figure 4.10. The M-R scenario with highest contribution to the hazard of the site is identified, as shown in Table 4.6. Additional results are presented with disaggregation of $Sa(2.0s)$ (Table 4.7), following the procedure suggested by NEHRP. T_C estimates are shown in Table 4.8.

Table 4.6. M-R results from disaggregation of PGA and 475 years return period.

M-R	Scenario 1
Magnitude (Mw)	7.5
Distance (Km)	110

Table 4.7. M-R results from disaggregation of $Sa(2.0s)$ and 475 Years Return Period.

M-R	Scenario 2	Scenario 3
Magnitude (Mw)	7	7.75
Distance (Km)	40	290

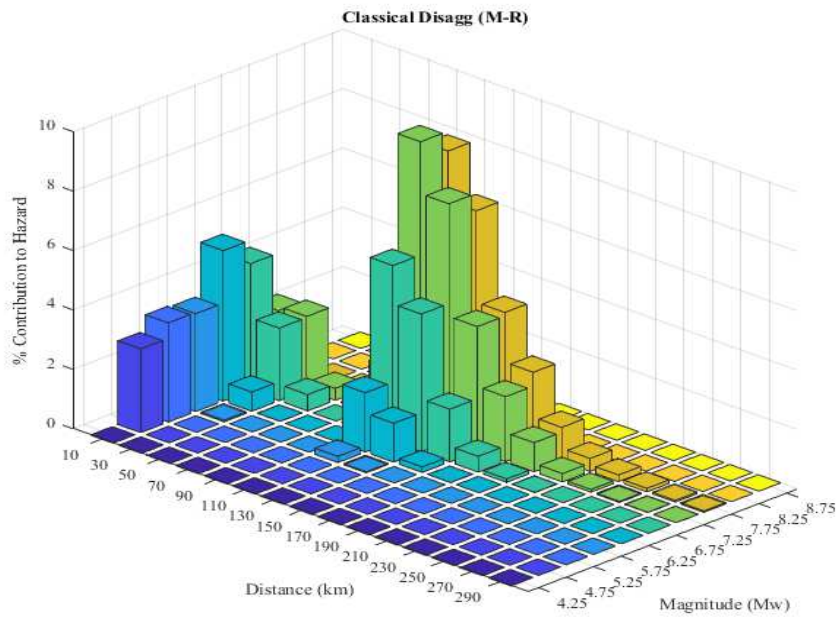


Figure 4.10. Disaggregation for PGA and 475 years return period.

Regarding the T_c estimation, there were significant differences between each one of the methods used. Yet, it appears that results from the original PSHA provide a rather small value for corner period if compared with the alternative hazard models or the equations proposed by NEHRP and Faccioli (2004). For instance, when using CB08, a higher corner period (3.40 sec) and a higher displacement plateau (258 mm) were obtained. These results are closer to the ones obtained with the formula proposed by the NSR-10 code (3.72 sec).

Table 4.8. Comparison T_c (sec) estimates

Method	T_c
Faccioli (2004) – (Scenario 1)	5.50
Faccioli (2004) – (Scenario 2)	4.25
Faccioli (2004) – (Scenario 3)	6.12
NEHRP (2003)	40.0
PSHA (with Akkar14)	2.40
PSHA (with CB08)	3.40
PSHA (with CAUZ14)	3.80
Total Avg. TD (sec)	4.245

The NEHRP (2003) method is the less preferable as it relies only on modal magnitude to compute the displacement demand, neglecting the effects of distance and the fact that more than one magnitude-distance scenario may dominate the hazard in the site (Faccioli & Villani, 2009), as in this case. Taking the displacement spectrum up to such long corner periods might result in an overestimation of the seismic demand, especially when compared to the results obtained by the various combinations of GMPEs tested for the PSHA model. Therefore, computations of Tc made with NEHRP formula were neglected. Table 4.9 shows results for the maximum displacement (δ_{\max}) found by the different methods.

Table 4.9. Comparison δ_{\max} (mm) estimates

Method	δ_{\max}
Faccioli (2004) – (Scenario 1)	253.94
Faccioli (2004) – (Scenario 2)	220.84
Faccioli (2004) – (Scenario 3)	171.30
PSHA (with AKKAR14)	190
PSHA (with CB08)	258
PSHA (with CAUZ14)	244
Avg. δ_{\max} (mm)	236.49

Taking the average of the results suggested that the design displacement spectra should increase linearly up to a maximum displacement of 237 mm at a corner period, Tc, equal to 4.25 seconds. A graphical comparison is made in Figure 4.11. It was observed that CB08, CAUZ14 and the Equations-Based spectra have similar maximum displacement, different than the original (“default”) PSHA results. However, the displacement spectrum calculated with the equations was below all the PSHA-based results in the ascending branch. Therefore, it was less conservative for that range of periods. The CB08 results were the ones that better matched the computed average maximum displacement at long periods, while remaining close to the original PSHA results for the lower range of periods. Among all the considered approaches, this would be the most conservative thus it is proposed as the alternative design spectrum.

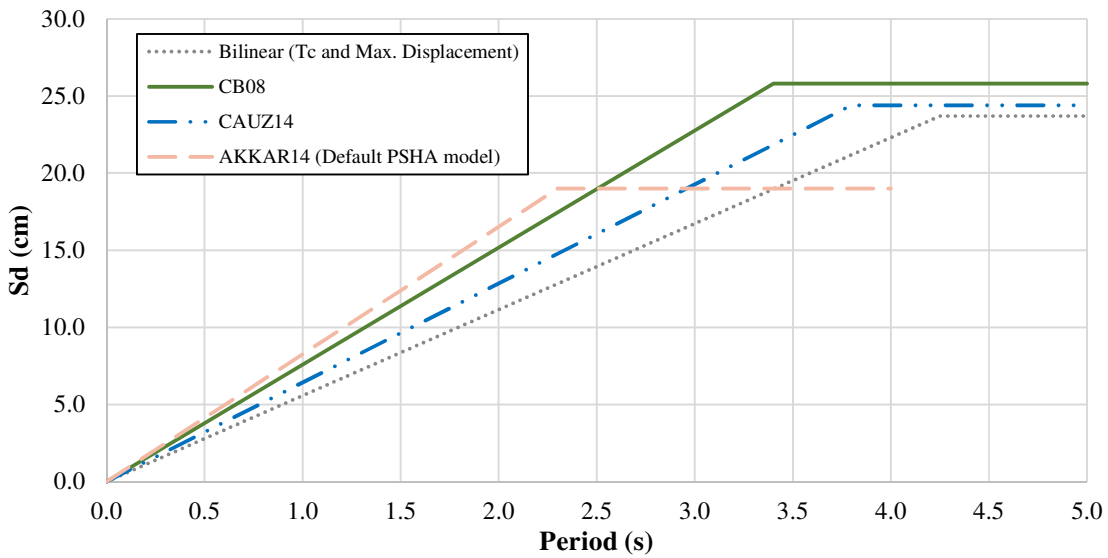


Figure 4.11. Graphical comparison alternative estimates of the design displacement spectra.

4.3.3 Material strengths for design

Design material strengths are given in Chapter 3 of the DBD12 model code. Expected material strengths, rather than characteristic strengths, were used for the design of plastic-hinge regions because the expected strengths are the ones to be developed during ductile response. DBD12 proposes to use $f'_{ce} = 1.3f'_c$ for concrete and $f'_{ye} = 1.1f_y$ for reinforcement steel. In addition, no force-reduction factors were applied in the design of the ductile mechanism, i.e. no reduction factors were used when computing flexural strength at the base section of a RC cantilever wall.

On the other hand, design of regions different than the plastic hinge zone was carried out using characteristic strengths and reduction factors were applied in this case. This was to guarantee the development of the plastic mechanism and also included the design of capacity-protected actions, i.e. shear strength at wall base section. The strength reduction factors from ACI 318-14 were used for sections detailing. Further considerations regarding capacity design and reinforcement detailing are discussed in Section 4.3.7 and Section 4.3.8, respectively.

4.3.4 Desired inelastic mechanism and displacement shapes

As the current study focused on the design of flexure-dominated RC cantilever wall buildings, the intended ductile mechanism to ensure adequate deformation capacity was a plastic hinge at the base. In order to compute the SDOF substitute structure characteristics, it was necessary to determine the expected displacement profile at the desired performance level. Two performance

limit states were defined. The first was a 2% code-prescribed drift limit (2% for consistency, as it is the same limit applied by ASCE 7-16 in the FBD procedure) and the other is a strain limit of 0.06 for the reinforcement steel that dictates the plastic rotation capacity at the wall base.

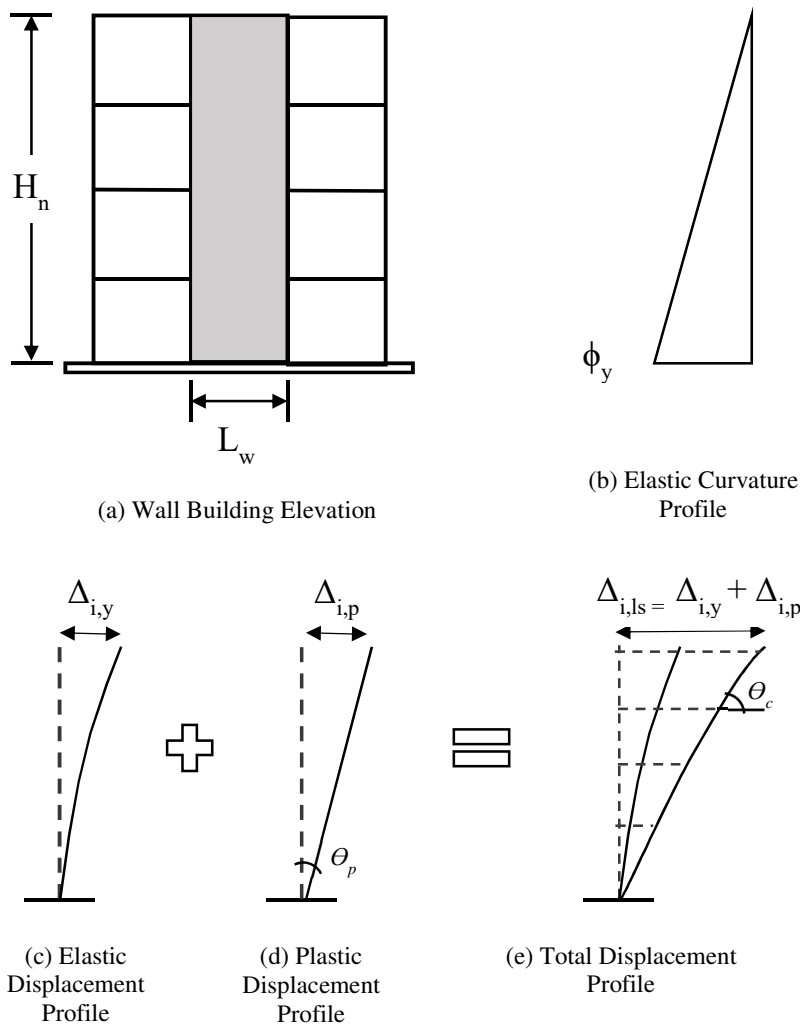


Figure 4.12. Design displaced shape for RC cantilever walls. Adapted from (Sullivan et al., 2012).

The procedure for computation of design displaced shape of RC cantilever walls is illustrated in Figure 4.12. It was observed that the final shape was determined by a combination of an elastic deformation profile and a plastic rotation at the wall base. DDBD is an effective first-mode approach, so the elastic displacement profile was based on a triangular distribution of curvature with height at yield (Priestley et al., 2007). The yield curvature ϕ_y was estimated using

Equation 4.5, based on the yield strain of reinforcement steel ε_y and the effective section depth D .

$$\phi_y = 2.25 \frac{\varepsilon_y}{D} \quad (4.5)$$

The total displacement profile was computed by Equation 4.6, where h_i is the height up to storey i and H_n is the total building height. θ_p is the design plastic rotation, the parameter that accounts for the defined performance limits, i.e. drift limit θ_c and reinforcing steel strain limit ϕ_{ls} . The equations for computing the design plastic rotation are described in Section 6.3.1 of DBD12 Code and Priestley et al. (2007).

$$\Delta_{i,ls} = \Delta_{i,y} + \Delta_{i,p} = \frac{\phi_y}{2} h_i \left(1 - \frac{h_i}{3H_n} \right) + \theta_p h_i \quad (4.6)$$

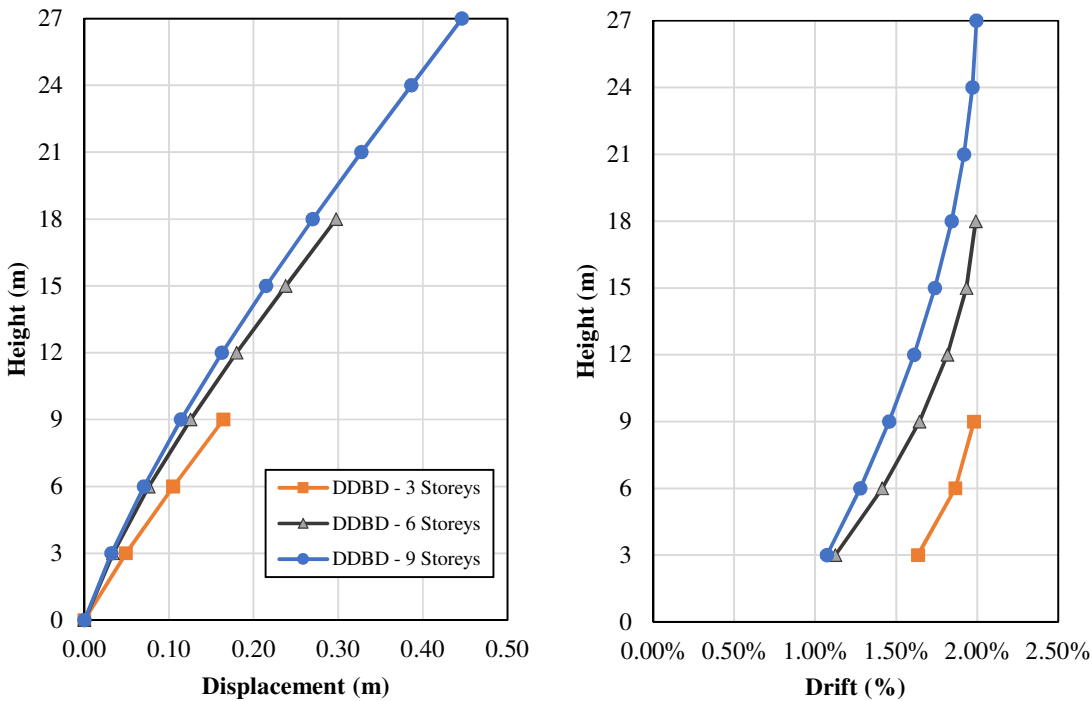


Figure 4.13. Displacement Shapes and Drift Profiles of the three buildings.

Figure 4.13 shows the displaced shapes and drift profiles computed for each of the buildings and it is observed that in all cases the displacement profile at limit state was governed by the 2% storey drift limit. Also notable is that only the estimation of member sizes, the yield strain of reinforcement and the definition of the desired inelastic mechanism were required at this

stage of the process. Torsional effects and higher modes effects were neglected in the calculation of the design displacement profile, given the characteristics of the studied buildings (Sections 5.8 and 5.9 of DBD12).

4.3.5 SDOF substitute structure and structural analysis

The SDOF properties were calculated following DBD12. The design displacement Δ_d was obtained using Equation 4.7 and this is the equivalent SDOF displacement that ensures the drift limits (i.e. 2%) produced by the displaced shapes in the previous section were not exceeded. Also, the SDOF yield displacement Δ_y is calculated by using Equation 4.8. The effective mass m_e and effective height H_e are also computed.

$$\Delta_d = \frac{\sum_{i=1}^n (m_i \Delta_i^2)}{\sum_{i=1}^n (m_i \Delta_i)} \quad (4.7)$$

$$\Delta_y = \frac{\phi_y}{2} H_e^2 \left(1 - \frac{H_e}{3H_n} \right) \quad (4.8)$$

With this information the ductility capacity of the cantilever walls was computed, the equivalent viscous damping (ξ_{eq}) was obtained and the reduced design displacement spectrum was calculated. Table 4.10 summarises the main properties of the SDOF substitute structure for each one of the buildings, the values shown for the DDBD-6 and DDBD-9 designs were modified as explained below and in Section 4.3.6; the adjusted SDOF properties of these cases are shown in Table 4.11.

Table 4.10. Initial properties of the SDOF substitute structure for each designed building.

Design	Design displacement , Δ_d (m)	Effective mass, m_e (kg)	Effective Height, H_e (m)	Yield displacement, Δ_y (m)	Ductility Capacity μ	Equivalent Viscous Damping ξ_{eq}
DDBD – 3	0.123	930798	6.88	0.020	6.04	16.93%
DDBD – 6*	0.205	1738395	13.14	0.075	2.72	13.93%
DDBD – 9*	0.301	2689612	19.34	0.110	2.74	13.98%

*These values need to be modified, see Table 5.11 and Section 5.3.6.

Table 4.11. Properties of the SDOF Substitute Structure after iterative procedure for 6-Storeys and 9-Storeys buildings.

Design	Response displacement Δ_{df} (m)	Displacement adjustment (Δ_{df}/Δ_d)	Expected drift	Yield displacement Δ_y (m)	Ductility Developed μ	Equiv. Viscous Damping $\xi_{eq,f}$
DDBD - 6*	0.145	0.71	1.40%	0.075	1.92	9.77%
DDBD - 9*	0.162	0.54	1.07%	0.110	1.47	7.44%

*These values replace the ones shown in Table 5.7. DDBD-3 remains unchanged.

Calculation of the base shear was carried out using Equation 4.9. To estimate the equivalent stiffness K_e (Equation 4.10) it was necessary to get the effective period T_e , which was read from the reduced design displacement spectra plot. This procedure is illustrated in Figure 2.3 (d), which is plotted again here as Figure 4.14.

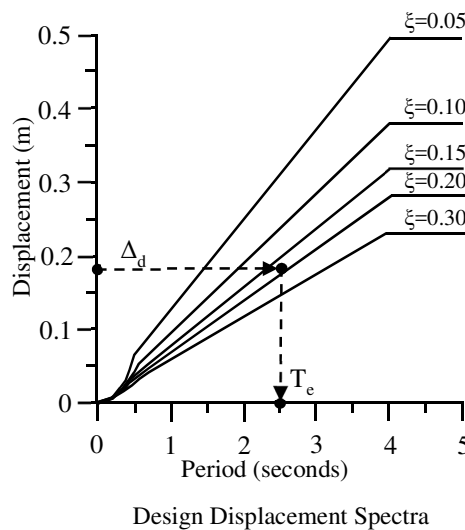


Figure 4.14. Effective period T_e calculation procedure.

There was a possibility that the design displacement of the building exceeded the displacement demand, particularly for very flexible structures. In those cases, it is not possible to obtain an effective period T_e from the reduced design displacement spectra since there is no intersection. In other words, the design seismicity would not produce enough spectral demand to push the equivalent SDOF to that level of displacement and ductility. Instead, a new design displacement ($\Delta_{d,f}$) value must be obtained taking into account the maximum ductility to be developed given

the spectral displacement demand at the site, rather than using the maximum ductility capacity of the building. The 6-storey and 9-storey buildings designed in this study fell in this range. Therefore, for the remainder of this subsection, the results presented for those structures correspond to the ones calculated by the iterative procedure, which is described in Section 4.3.6.

$$V_{base} = K_e \Delta_d + V_{P-\Delta} \quad (4.9)$$

$$K_e = \frac{4\pi^2 m_e}{T_e^2} \quad (4.10)$$

$$V_{P-\Delta} = C \frac{\sum_{i=1}^n P_i \Delta_i}{H_e} \quad (4.11)$$

The required member strengths were found by distributing the design base shear using Equation 4.12. In the V_{base} calculation, P-Delta effects are accounted for using Equation 4.11 and Section 5.6 of the DBD12 Code. All the computations were done using a spreadsheet and did not require any numerical modelling as in the case of FBD. Figure 4.15 shows the shear and overturning moment profiles for all buildings.

$$F_i = \frac{V_{base}(m_i \Delta_i)}{\sum_{i=1}^n (m_i \Delta_i)} \quad (4.12)$$

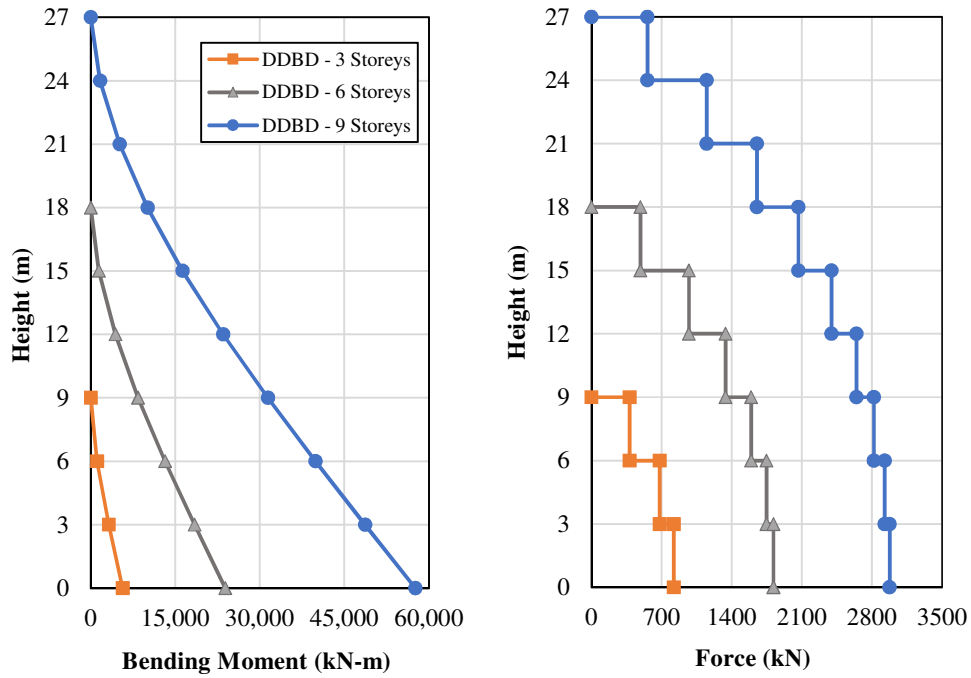


Figure 4.15. DDBD: Moment (left) and Shear (right) design profiles results.

4.3.6 Special Case: Design displacement exceeds the spectral demand

As noted in the previous section, the 6-storey and 9-storey buildings had a design displacement higher than the reduced spectral demand. This meant that these buildings cannot develop the target ductility capacity calculated. Nevertheless, they still entered the inelastic range as the yield displacement was lower than the 5% damped spectra elastic demand (see Figure 4.16).

This case is addressed in Section 3.4.6 of Priestley et al. (2007).

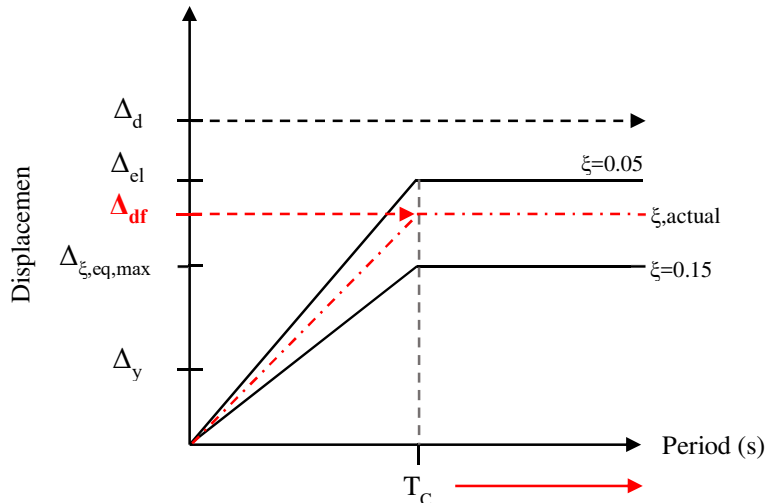


Figure 4.16. Typical case in which displacement capacity (Δ_d) exceeds reduced spectral demand ($\Delta_{\xi,eq}$).

The final response displacement Δ_{df} fell between the corner displacement demand at maximum ductility capacity, $\Delta_{\xi,eq,max}$ in Figure 4.16, and the total displacement capacity of the building Δ_d . Note that in the case of $\Delta_d > \Delta_{el}$ (as illustrated in the same figure) this range was further reduced because the final response displacement must also be below the elastic demand Δ_{el} , since yielding would already have occurred.

A stable solution was found by iteration, starting with a trial final displacement value within the expected displacement range and taking the corner period T_C as reference period. This allowed a new ductility to be computed and consequently a new value for equivalent viscous damping. The reduced displacement design spectra was re-calculated and the process repeated until the trial final displacement value Δ_{df} was equal to the displacement at the corner period T_C of the new design spectra $\Delta_{\xi,eq}$. This iteration process was needed to guarantee that the displacement response computed was compatible with the equivalent viscous damping implied by that displacement demand (Priestley et al., 2007).

Note that no unique solution exists for the effective stiffness K_e , as any period $T \geq T_C$ would be valid for its computation. As the provided strength does not affect the displacement response in this case, the choice of period and effective stiffness would then be limited by P-Delta effect considerations. The procedure described in this section, taking T_C as the reference structural period, was used for the design base shear calculation of the 6- and 9-storey buildings, whose results were included in Section 4.3.5. The adjusted SDOF properties of those buildings were summarised in the Table 4.11.

4.3.7 Capacity design considerations

An approximate method for determining capacity design force levels was applied, as described in Section 9.3 of the DBD12 Code. As mentioned in previous sections, the desired inelastic mechanism for the studied buildings was the development of a plastic hinge at the wall base. Equation 4.13 determines the strength of capacity-protected members S_{CP} , where ϕ^0 is an overstrength factor and ω is a dynamic amplification factor.

$$S_{CP} = \phi^0 \omega S_E \quad (4.13)$$

For plastic hinge regions, the approach to calculate flexural reinforcement is to design for the overturning moment that comes from the analysis without any amplification and compute nominal moment capacity using expected material strengths without any reduction factors. Then, Priestley et al. (2007) suggest performing moment-curvature analysis (including effects of concrete confinement, expected material properties and strain hardening effects), to compute the bending moment developed by the section at the design curvature (calculated during DDBD procedure). The obtained bending moment is likely to be higher than the one accounted for, when choosing flexural reinforcement. The ratio between those two is the overstrength, ϕ^0 . Alternatively, if no detailed analysis is performed a value of overstrength between 1.25 and 1.6 might be assumed, $\phi^0 = 1.25$ was used in this research for capacity-protected actions.

DBD12 provides capacity design envelopes for moments and shears. For moments, the capacity-protected action is the bending moment at the building mid-height, this is the product of the bending moment at the base amplified by the overstrength times a shape factor, that is a function of ductility and the building initial elastic period (calculated using Equation 4.14). The design moments profile has a bilinear shape as the one given by the solid line in Figure 4.17.

$$T_i = \frac{T_E}{\sqrt{\mu}} \quad (4.14)$$

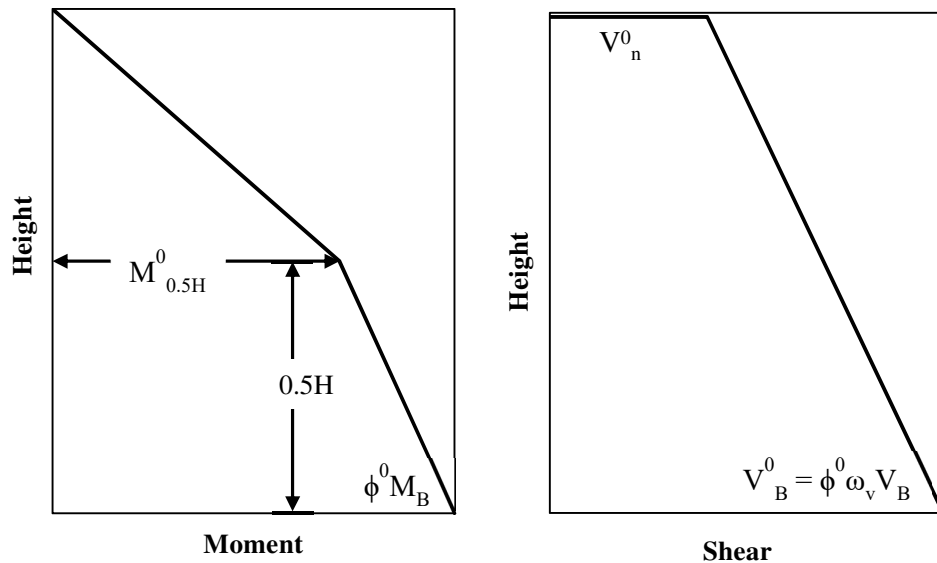


Figure 4.17. Moment and Shear capacity design envelopes described by DBD12.

The overstrength factor was also used to compute the capacity design shear at the base and top of the structure. When dealing with shear, it is also necessary to compute the dynamic amplification factor. Shear reinforcement was calculated for amplified analysis forces, according to the envelope described in DBD12 (Figure 4.17). Shear flexural reinforcement was computed using characteristic strengths and a reduction factor of 0.75, in compliance with the ACI 318-14 procedures. This does not have a big impact on the designs as in most of the studied cases, minimum reinforcement ratio dominates the shear design.

Based on the above, the capacity design approach implemented is summarised as follows:

- Calculate flexural reinforcement for base moment obtained from DDBD, considering the largest and smallest expected values of axial force (load combinations). Expected strengths are used and no reduction factor is applied. The plastic hinge reinforcement extends up the first 3 floors.
- From the 4th floor up to the roof, design was carried out for the moments obtained applying the capacity design envelope that accounts for overstrength proposed in DBD12 Code. Expected strengths were used and no reduction factor was applied.
 - If the resulting design requires more reinforcement than at wall-base, then recalculate capacity design moments profile with overstrength factor = 1 and apply the strength reduction factor (0.9); or maintain same reinforcement as for plastic hinge region, as small inelastic excursions are accepted. (see Priestley et al. (2007), Example 6.2, for instance).
- For shear, design for the forces obtained applying the capacity design envelope that accounts for overstrength and dynamic amplification. Shear capacity must be calculated with characteristic strengths and a reduction factor of 0.75 (equal to FBD) was applied.

4.3.8 Reinforcement detailing and final design

In this study, the steel reinforcement for DDBD was calculated following the same procedure described in Section 4.2.4 for force-based design of the buildings. The only differences in the reinforcement calculation approach were the ones regarding capacity design rules noted previously and the ones concerning expected material strengths and strength reduction factors discussed in Section 4.3.3. Figures 4.18 to 4.20 show the typical cross-sections for each of the buildings designed using DDBD. The detailed extent of the calculation is presented in Appendix B and the wall-base section flexural design and reinforcement values are summarised in Tables

4.12 and 4.13, respectively. A high flexural overstrength was obtained for the DDBD-3 case because the design is governed by minimum reinforcement requirements, producing a nominal capacity much larger than the demand.

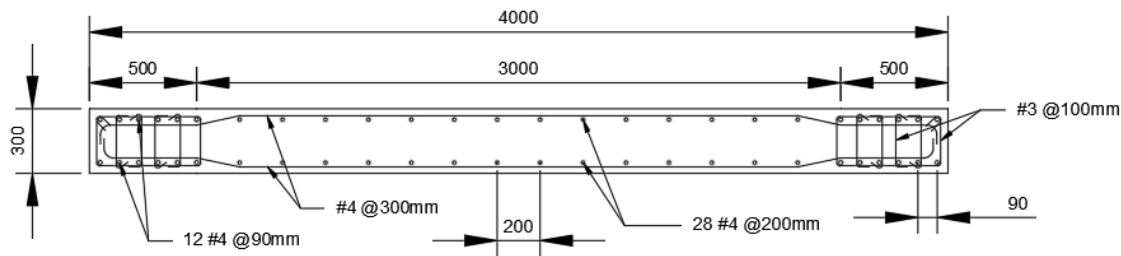
Table 4.12. Summary of flexural design at wall base for DDBD cases.

Design	P _u , Max (kN)	P _u , Min (kN)	M _u (kNm)	M _{n,CS} (kNm)	c (mm)	φM _{n,CS} (kNm)	Ω Flexural (Shear Magnification*)	Rebars Boundary	Rebars Web
DDBD-3	880	407	2827	7159	402	7159	2.53	12 #4	28 #4
DDBD-6	1813	841	11941	13718	636	13718	1.15	4#7 + 8#6	28 #5
DDBD-9	3515.53	1649.71	28793.53	32812.4	1078.5	32812.4	1.14	12#7	38 #6

*Does not apply as shear forces have been modified by capacity design envelopes

Table 4.13. Summary of DDBD geometry and reinforcement at wall-base section of all buildings.

Design	Wall Length (mm)	Wall Thickness (mm)	Bound. Elemt. Length (mm)	Total A _s , Vert. (mm ²)	Total A _s , Horiz. (mm ²)	ρ _t , Transv.	ρ _{l,w} - Web Long.	ρ _{l,b} - Bound. Elemt.
DDBD - 3	4000	300	500	2580	6708	0.00287	0.00430	0.01030
DDBD - 6	4000	300	500	3225	13240	0.00358	0.00667	0.02547
DDBD - 9	6000	300	600	3518	14416	0.00391	0.00556	0.01893



**3-Storey Building. Wall Base → 3rd Floor Section.
Dimensions: 4.00 m x 0.30 m**

Figure 4.18. (DDBD) Displacement-Based Design, 3-Storeys Building. (Rebar size in Imperial System).

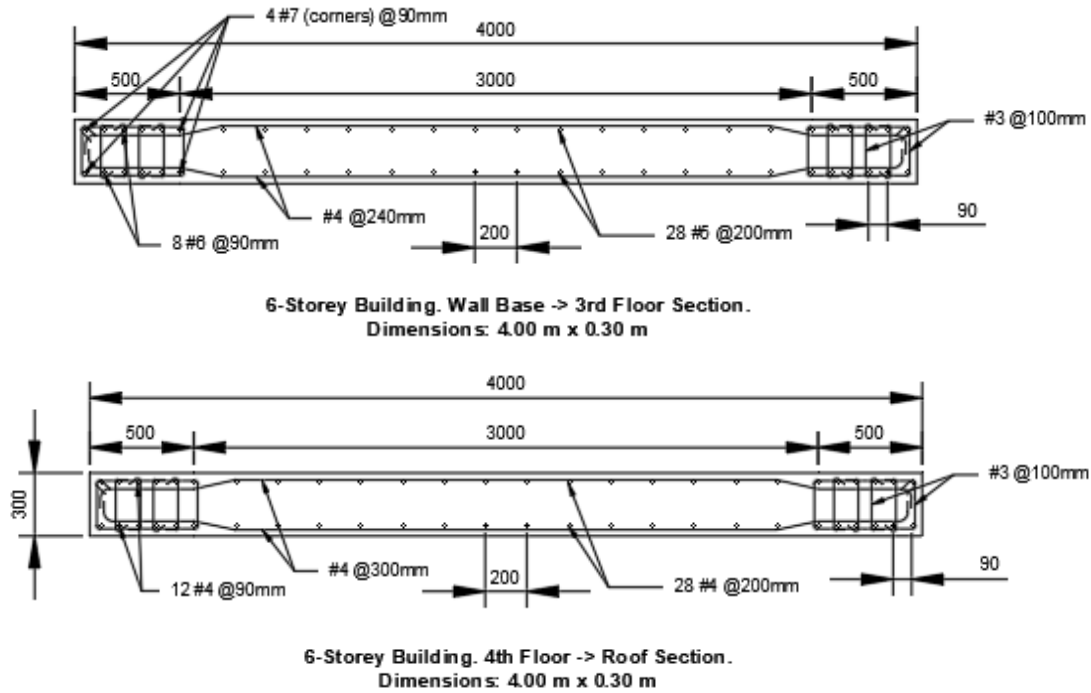


Figure 4.19. (DDBD) Displacement-Based Design, 6-Storeys Building. (Rebar size in Imperial System).

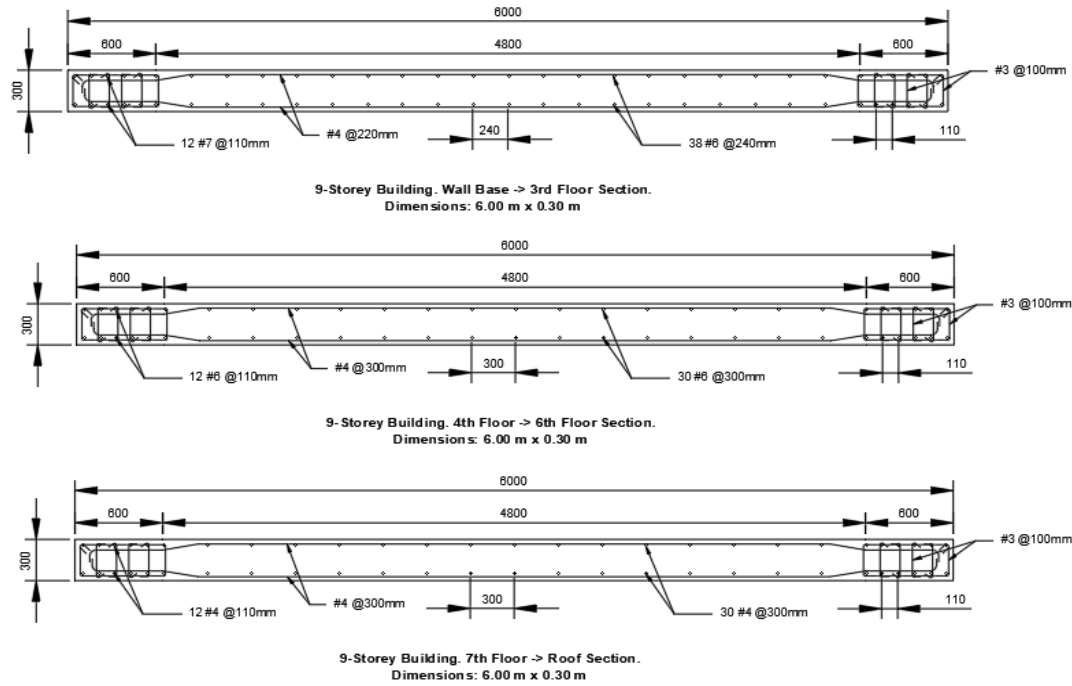


Figure 4.20. (DDBD) Displacement-Based Design, 9-Storeys Building. (Rebar size in Imperial System).

4.4 FBD and DDBD

Table 4.14 summarises the design for shear forces at the building base (i.e. 2 walls) by FBD and DDBD. In all FBD cases and for DDBD-3, the final shear design was given by minimum reinforcement requirements. Capacity design implemented in DDBD approximately doubled the initial values obtained from the structural analysis and this enlarged the differences to FBD in the 6-storey and 9-storey cases. For 3-storey buildings, the initial difference between V_{FBD} and V_{DDBD} was reduced after capacity design rules were applied ($V_{FBD,C}$ and $V_{DDBD,C}$), still, as the minimum reinforcement governed the design in both cases, the final nominal capacities provided are equal. In general, DDBD provided higher values of shear strength than FBD. It is appreciated that the V_{FBD} design values are the result of MRSA analysis scaled to match V_{ELF} .

Table 4.14. Comparison FBD vs DDBD design for shear (in kN) at wall base (2 walls).

# Storeys	FBD - Structural Analysis				DDBD - Structural Analysis		FBD Provided	DDBD Provided	Difference Provided V_n^*
	V_{ELF}	V_{MRSA}	V_{FBD}	$V_{FBD,C}^{**}$	V_{DDBD}	$V_{DDBD,C}^{**}$	$\phi V_{n,FBD}$	$\phi V_{n,DDBD}$	
3	1609	1187	1609	2382	822	2290	3786***	3786***	0
6	1978	1152	1978	2694	1817	4223	3786***	4328	+542
9	2312	1588	2312	3297	2977	6607	5680***	6862	+1182

*Difference with respect to FBD.

**After capacity design, this is the final design value.

***Minimum reinforcement governs design.

Table 4.15 provides the same comparison but for flexural design, capacity design does not change the moment at the base in any method. In FBD, it is observed that scaled M_{MRSA} is lower than M_{ELF} in all cases and the differences increase with increasing number of floors. There are significant differences in the moment capacity provided by FBD and DDBD for the 6 and 9-storey buildings, these differences would have reduced if M_{ELF} , instead of scaled M_{MRSA} , was used in FBD, the reasons behind these differences are explained below. As in shear design, flexural design of DDBD-3 model was governed by minimum requirements. Despite this, Table 4.15 shows that $M_{n,DDBD}$ is “larger” than $\phi M_{n,FBD}$, which occurs because the DDBD flexural design uses expected strengths and no reduction factors.

Table 4.15. Comparison FBD vs DDBD design for moments (in kNm) at wall base (2 walls).

# Storeys	FBD - Structural Analysis			DDBD - Structural Analysis		FBD Provided	DDBD Provided	Difference Provided M_n^*
	M_{ELF}	M_{MRSA} (unscaled)	M_{MRSA} (scaled)	M_{FBD}^{**}	M_{DDBD}	$M_{DDBD,C}^{**}$	$\phi M_{n,FBD}$	
3	10921	7780	10542	10542	5653	5653	14045	14318*** +273
6	25333	10198	17520	17520	23882	23882	21473	27436 +5963
9	44245	19021	27694	27694	57587	57587	35480	65625 +30144

*Difference with respect to FBD.

**After capacity design, this is the final design value.

***Minimum reinforcement governs design.

All buildings comprise two identical walls in each direction. Table 4.16 shows a comparison of the amount of reinforcement placed at the typical wall base section of each building at the end of the design process for both FBD and DDBD methods. The difference of steel area (A_s) and the percentage change of steel ratios (ρ), are computed taking as a reference the values found by the FBD procedure.

As expected, the differences observed in Tables 4.14 and 4.15 are reflected in the reinforcement layouts. For the 3-storey building, the DDBD method requires less longitudinal steel than the FBD method and the difference is accentuated because DDBD-3 design was governed by minimum reinforcement requirements. The opposite is observed for the 6-storey building, where DDBD requires both more flexural and shear reinforcement than FBD, with these differences becoming larger for the 9-storey case. Here, DDBD requires almost 1.5 times the amount of flexural steel as the one of FBD. Thus, for the studied cases, DDBD appears to allocate more reinforcement than FBD as building height/flexibility increases.

One possible reason for this is the fact that the 6-storey and 9-storey buildings designed with DDBD fell in the “special case” range described in Section 4.3.6, as the buildings design displacements exceeded the reduced spectral demand, meaning that the maximum displacement capacity of the buildings could not be exploited by DDBD. This essentially translated into these structures being designed for a stricter drift limit. Moreover, it is recalled that there was no unique effective period definition for the buildings that fall in this range as any period $T > T_c$ would have complied with the DDBD procedure requirements (limit is given by P-Delta effects). In this study, the choice made was to use the corner period T_c for design but if a larger

effective period had been chosen, the stiffness demand would have been reduced and, consequently, a lower base shear would have been obtained. An “optimised” design could be carried out by selecting the largest possible period, which would imply the least strength demand and therefore less reinforcement steel. This issue will be further discussed in Chapter 7. It is noted, however, that this peculiar scenario is more a result of the limitations of current development of DDBD to cope with such scenarios rather than an inherent limitation of the method itself.

Table 4.16. FBD vs DDBD comparison of reinforcement steel placed at typical wall base section for all buildings designed.

Design Method	Total As, Horiz. (mm ²)	Total As, Vertical (mm ²)	ρ _t , Transv.	ρ _{l,w} - Web Long.	ρ _{l,b} - Bound. Ele. Long.
3 - storeys					
DDBD	2580	6708	0.00287	0.00430	0.01030
FBD	2580	8412	0.00287	0.00430	0.01600
<i>Difference*</i>	<i>0</i>	<i>-1704</i>	<i>0.00%</i>	<i>0.00%</i>	<i>-35.63%</i>
6 - storeys					
DDBD	3225	13240	0.00358	0.00667	0.02547
FBD	2580	12416	0.00287	0.00667	0.02272
<i>Difference*</i>	<i>+645</i>	<i>+824</i>	<i>+25.00%</i>	<i>0.00%</i>	<i>+12.09%</i>
9 - storeys					
DDBD	3518	14416	0.00391	0.00556	0.01893
FBD	2580	9702	0.00287	0.00358	0.01333
<i>Difference*</i>	<i>+938</i>	<i>+4714</i>	<i>+36.36%</i>	<i>+55.04%</i>	<i>+42.00%</i>

*Difference with respect to FBD.

A factor that amplified the differences between the calculated flexural reinforcement from one method to the other was the fact that the design bending moment profiles computed for FBD were found using modal analysis. For DDBD, the overturning moment at the base was obtained as an effective fundamental mode procedure where the moments produced by the lateral forces are accumulated from floor-to-floor until the base, like in the ELF procedure. This usually produces larger moments if compared to a modal analysis approach. Figures 4.21 to 4.23 compare the shear and moment profiles for both methods and each building. These were the values obtained from structural analysis therefore do not reflect the capacity design modifications.

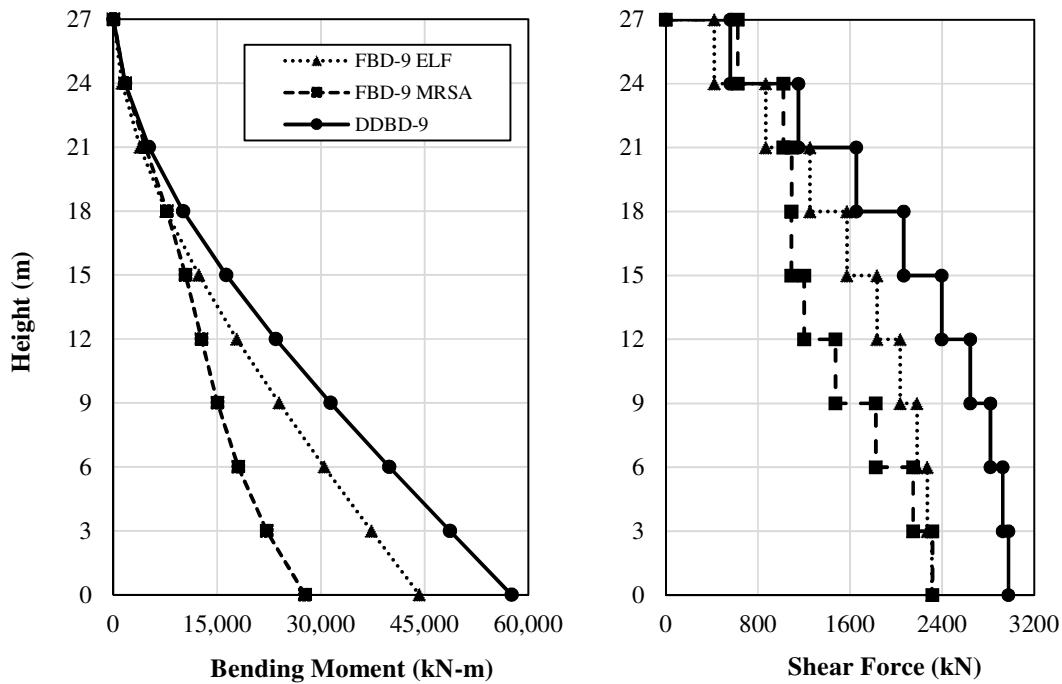


Figure 4.21. 9-Storeys: Moment and Shear profiles obtained from structural analysis. FBD vs DDBD.

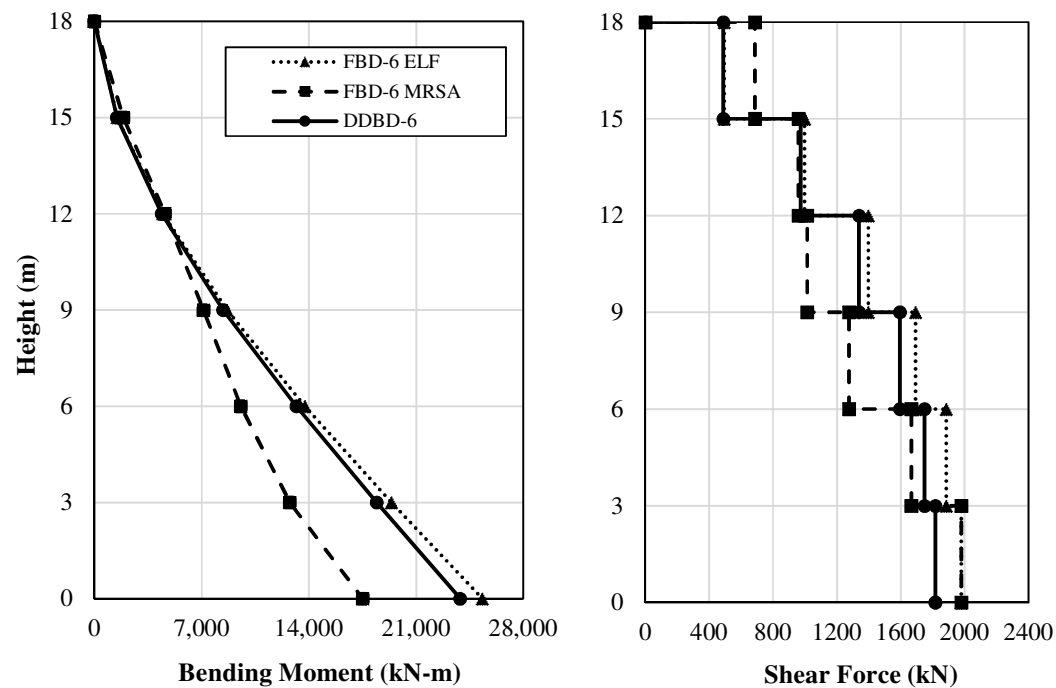


Figure 4.22. 6-Storeys: Moment and Shear profiles obtained from structural analysis. FBD vs DDBD.

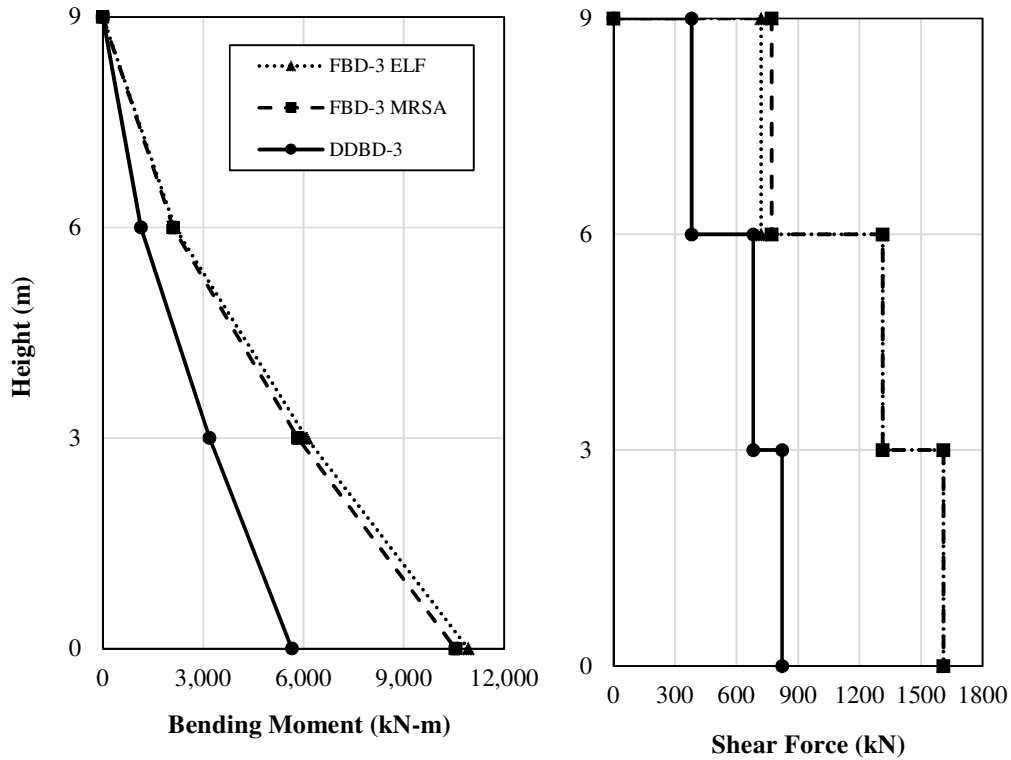


Figure 4.23. 3-Storeys: Moment and Shear profiles obtained from structural analysis. FBD vs DDBD.

Table 4.17 compares the shear and flexural design overstrength values for both methods. As noted previously, for the overturning moment, the final design values are equal to the structural analysis values. Initial values of shear are modified by capacity design hence the shear overstrength relative to final design values is always lower than the one computed from the structural analysis. The high overstrength values for shear design of FBD and for shear and flexural design of DDBD-3 case are observed again, because minimum reinforcement governs those cases. The results of Table 4.17 will be further discussed ahead, when presenting the pushover results in Section 5.6.

Table 4.17. Comparison FBD vs DDBD design overstrength values.

Building Case	Overstrength relative to analysis values				Overstrength relative to final design values			
	Shear		Flexure		Shear		Flexure	
	FBD	DDBD	FBD	DDBD	FBD	DDBD	FBD	DDBD
3-storeys	2.35	4.61	1.33	2.53	1.59	1.65	1.33	2.53
6-storeys	1.91	2.38	1.23	1.15	1.41	1.02	1.23	1.15
9-storeys	2.46	2.30	1.28	1.14	1.72	1.04	1.28	1.14

The fundamental periods are shown in Table 4.18, corresponding to the results calculated using gross initial stiffness, the design method formulation and the bilinear idealization of the pushover curve at yield point computed using the numerical model described in Chapter 5. It is observed that very different assumptions are made in the period computations for each design method, as periods of DDBD are always higher than the FBD models despite the actual differences in stiffness and strength. For instance, for the 3-storey building the cracked-sections period obtained in FBD is almost equal to the gross-stiffness period.

Therefore, pushover results provide a better comparison as T_1 is computed for all models based on a unified criterion, in this case the differences in flexural strength were echoed in the obtained periods. For example, DDBD-9 is stronger than FBD-9, consequently, the DDBD-9 period is shorter than FBD-9. Additionally, the difference between pushover-based and design-method-based periods was computed, it is observed that DDBD-based periods were closer (within less than 0.2s) to the numerical model results than the FBD-based ones. These conclusions are related to the pushover results presented in the following chapter.

Table 4.18. First-mode vibration periods of each building comparison.

Model	Design Method Based T_1 (s)	Gross Stiffness T_1 (s)	Pushover (Yield) Based T_1 (s)
FBD - 3	0.34	0.33	0.72
FBD - 6	1.17	0.92	1.94
FBD - 9	1.41	1.00	2.59
DDBD - 3	1.00	0.36	0.82
DDBD - 6	1.73	0.82	1.90
DDBD - 9	1.98	0.94	2.09

5 NUMERICAL MODELLING

5.1 Introduction

Several approaches are available in the literature to model RC walls behaviour. Some of the most well-known options are fibre models with force-based and displacement-based formulations (Spacone et al., 1996), strut and tie methods, shell panels, multiple vertical line element models (MVLEM) and shear-flexure interaction MVLEM (SFI-MVLEM) (Kolozvari et al., 2018b). A recent state-of-the-art study (Kolozvari et al., 2018a) compared some of these models with experimental tests of cyclic pushovers on walls and noted differences among the different modelling approaches. It concluded that the strut and tie model is the approach that best captures the overall response of RC walls but due to the high number of degrees of freedom involved, its implementation in a building-size model would be rather cumbersome. SFI-MVLEM models represents a good alternative for RC walls with low shear-span ratio (i.e. $h_w/l_w < 2$) in which shear deformations play a major role in the structural response, since they account for shear-flexure interaction. MVLEM is found to be adequate for flexure-dominated walls and its formulation appears to have fewer convergence issues than the fibre-based modelling approach. Fibre models are probably the most widely adopted but its force-based formulation is known to present several convergence issues at high levels of non-linearity which makes its use for collapse assessment difficult. The displacement-based formulation of the fibre model overcomes these convergence issues but requires further discretisation of the elements to obtain a reliable response, which in turn represents a further limitation as models tend to need to become quite large and inefficient.

It is noted that the aforementioned models represent the global load-deformation response of structural walls in an adequate manner, provided they are implemented correctly. However, they tend to overestimate tensile strains and underestimate compressive strains (Kolozvari et al., 2018a). Then, the local responses should be carefully analysed.

5.2 Modelling strategy: RC wall macro-model selection

As the current study required NLTHA analysis of multi-storey buildings with flexure-dominated walls, the MVLEM approach was used to model the RC Walls behaviour. Additionally, initial comparisons of pushover curves were made with fibre approach with force-based formulation. OpenSees (McKenna, 2011; McKenna et al., 2000) software was used for modelling and analysis of the case studies. Initially, each of the six buildings had a fibre model and a MVLEM model for the two design methodologies for a total of 12 computational models. The wall cross-sections are shown in the Sections 4.2.4 and 4.3.8 for FBD and DDBD, respectively.

Some simplifications were introduced in the modelling, as the buildings are symmetric, and the lateral load-resisting system is composed of two RC walls in each direction. No torsional effects were considered, and the gravity columns contribution was neglected. Thus, the structures were expected to have the same strength and stiffness in both directions. The proposed strategy consisted of a 2D planar model of a single wall using either fibre or MVLEM elements. Then, an elastic leaning column with low rotational stiffness was attached to the wall by means of rigid-truss elements. Gravity loads were applied to each node of the leaning column to account for P-Delta effects. Each wall node was loaded with its corresponding axial load calculated via its tributary floor area during the design phase. An illustration of the analytical model is shown in Figure 5.1.

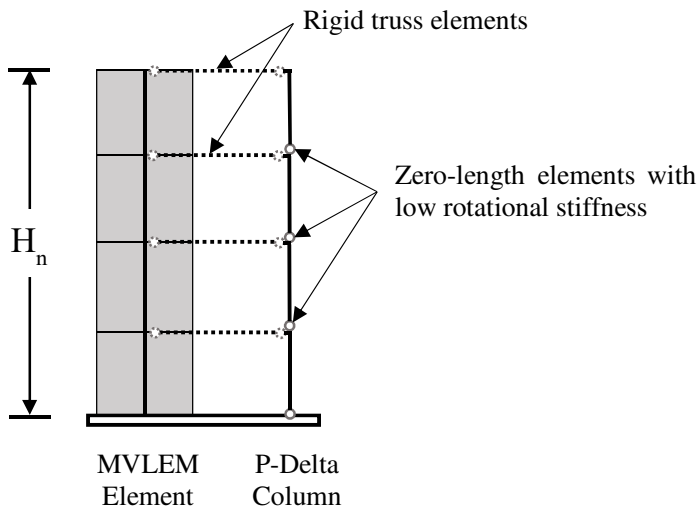


Figure 5.1. Analytical model used for NLTHA in OpenSees. MVLEM model for RC walls.

To define the dynamic properties of the model, half of the floor seismic mass was lumped at the wall nodes of each floor in the translational degree of freedom. With respect to the damping model, it has been recognised that some modelling choices can produce misleading results in NLTHA (Carr, 1997; Hall, 2006), particularly when using Rayleigh damping, which might introduce spurious damping forces in the model. However, it has been shown that this issue has marginal effects on models with fibre formulations (Chopra & McKenna, 2016). An alternative would be to use a modal damping formulation like the ones proposed by Chopra et al. (2016) and Wilson & Penzien (1972). As both numerical models used in this study were fibre-based models (i.e. MVLEM and fibre with force-based formulation), Rayleigh damping as implemented in OpenSees was used, proportional to the mass matrix and the committed stiffness matrix.

5.3 Materials constitutive behaviour

The material constitutive models can have a major influence in the outcome of the analysis. A reasonable choice was made among the existing materials in the OpenSees library and no calibration of parameters against experimental data was performed. The same material models were used for analysis of both FBD and DDBD buildings.

For RC sections, Concrete07 model was used. It is based on the Chang & Mander (1994) stress-strain relationships for confined and unconfined concrete. Unconfined concrete parameters were used for the web section and for the cover concrete while the confined concrete model was applied at the boundary elements region. Input values were computed according to the formulation proposed by the authors and the recommendations found on the OpenSees Wiki⁴, which are presented in Tables 5.1 and 5.2, and the stress-strain curves calculated are shown in Figures 5.2 and 5.3. No contribution of concrete in tension was considered.

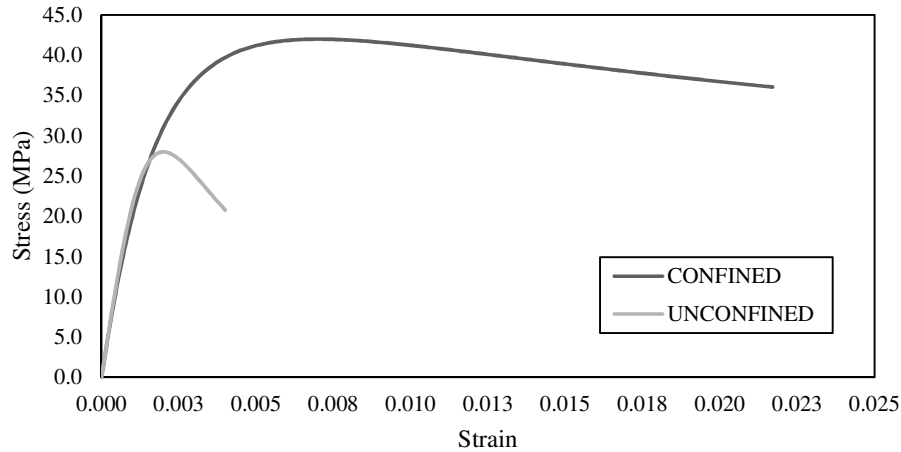
Table 5.1. Parameters to define concrete material model.

Material Type	f'_{c0} (MPa)	ϵ_c	E_c (MPa)	f_t	ϵ_t
Concrete Unconfined	28	0.002	24780	1.00E-05	1.00E-09
Concrete Confined	42	0.007	24780	1.00E-05	1.00E-09

⁴ <http://opensees.berkeley.edu/wiki/>

Table 5.2. Parameters to define steel material model.

Material Type	f_y (MPa)	E_s (MPa)	B_s	R_0	ϵ_u
Reinforcement Steel	420	200000	0.01	18	0.08

**Figure 5.2. Confined and unconfined concrete stress-strain curves. FBD 9-Storeys building.**

For reinforcement steel, Steel02 model was used. It is based on the Giuffre-Menegotto-Pinto (Menegotto & Pinto, 1973) stress-strain relationships for steel, as implemented in OpenSees (Filippou et al., 1983). It does not include rebar buckling failure modes, fatigue or degradation parameters. The coefficients defining the transition from elastic to plastic branches were defined as suggested by the OpenSees Wiki.

This steel uniaxial material was “wrapped” with the MaxMin material in OpenSees such that it sets the stress of the material to zero when a tensile strain of 0.08 is exceeded. This was incorporated to provide a means in which the rebars could fail due to excessive flexural deformation. That is, when the strain exceeded 0.08 a rebar would be deemed to have ruptured and lost its strength, thus indirectly simulating the expected failure mode of the walls. The limit values that define the stress-strain curve were chosen following the recommendations made by Priestley et al. (2007) and Priestley et al. (1996) whereas the coefficients defining the transition from elastic to plastic branches were defined as suggested by the OpenSees Wiki.

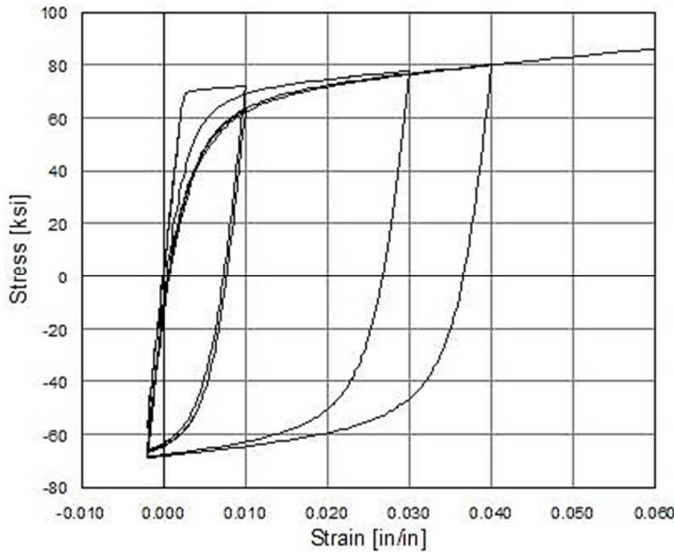


Figure 5.3. Steel02 Material - Giuffré-Menegotto-Pinto Model. (Adapted from OpenSees)

5.4 Fibre model discretisation

Seven different patches with their corresponding meshes constitute the cross-section of the fibre models. Three main patches represent the two boundary elements and the central web, the additional four patches form the cover concrete at the longitudinal and transversal directions (Figure 5.4). No mesh sensitivity analysis was done and the mesh-size used was between 10 and 20mm. The reinforcement bars were modelled as uniaxial fibres distributed accordingly to the design layout. Five integration points were used along each element and a single element per floor was used.

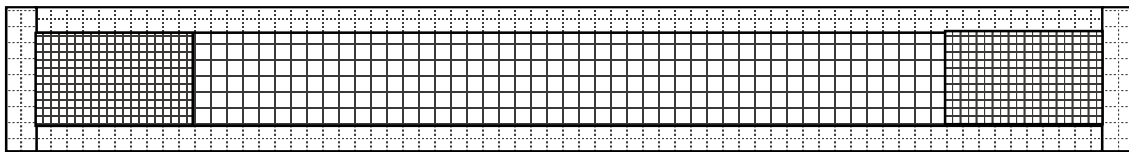


Figure 5.4. Illustration of the wall fibre model discretisation.

5.5 MVLEM discretisation

For the MVLEM, it was necessary to discretise the cross-section of the element into various macro-fibres. Each boundary element was contained in a single macro-fibre while the dimensions of the segments in the web were chosen according to the reinforcement layout. Furthermore, each wall along the building was divided in two elements per storey at the storey mid-height. Figures 5.5 to 5.7 show how the cross-section discretisation was performed.

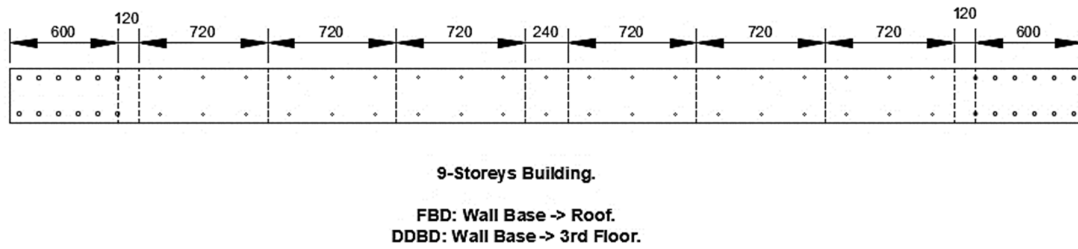


Figure 5.5 - MVLEM Discretisation 6 m Wall, 9-storeys building. Used in FBD (All floors) and DDBD (Ground Floor to 3rd Floor).

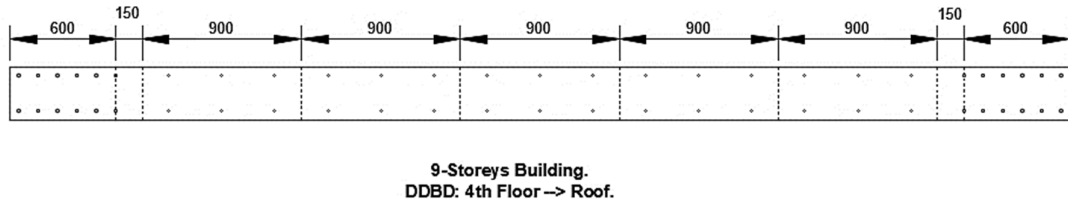


Figure 5.6 - MVLEM Discretisation 6 m Wall, 9-storeys building. Used in DDBD (4th Floor to Roof).

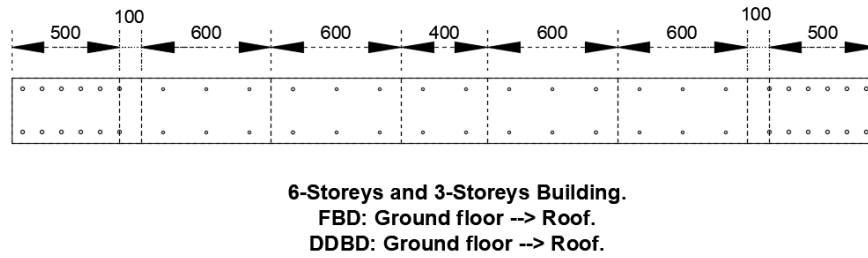


Figure 5.7. MVLEM Discretisation 4 m Wall, 3-Storeys and 6-Storeys building. Used in FBD (All Floors) and DDBD (All Floors).

5.6 Pushover analysis

Nonlinear static analysis (i.e. pushover) was performed on twelve models (six for FBD and six for DDBD) considering both fibre and MVLEM modelling options. Each wall kept the same overall cross-section dimensions over the building's height, but the reinforcement arrangement was changed every 3 floors according to the design layout. The pushover curves provide useful information about the strength and deformation capacity of the building when subjected to an increasing lateral load distributed over the building height. Therefore, it provides a good approximation of the first-mode response of the studied buildings. Figures 5.8 to 5.12 show the

pushover analysis results, with each curve corresponding to a single wall, meaning that the actual building lateral strength would be twice the one illustrated.

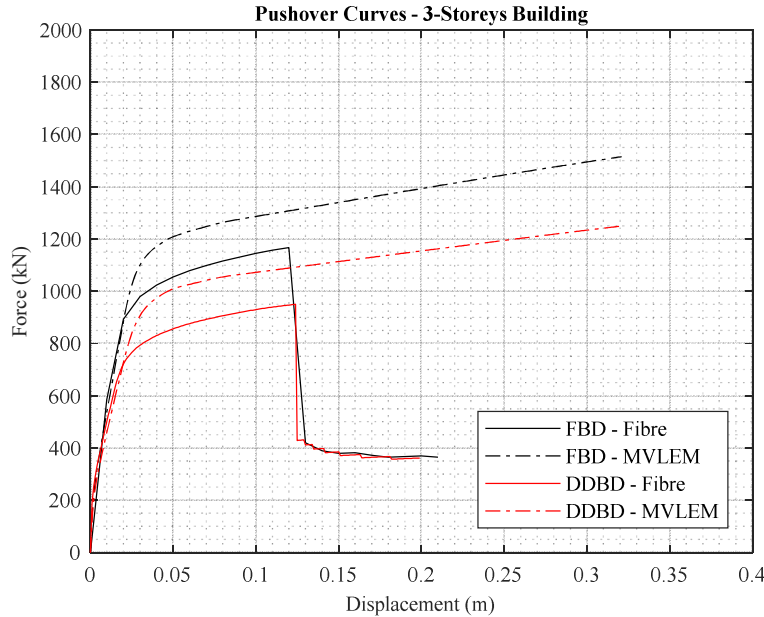


Figure 5.8. Pushover curves comparison between FBD and DDBD for both MVLEM and fibre models. 3-storey Building.

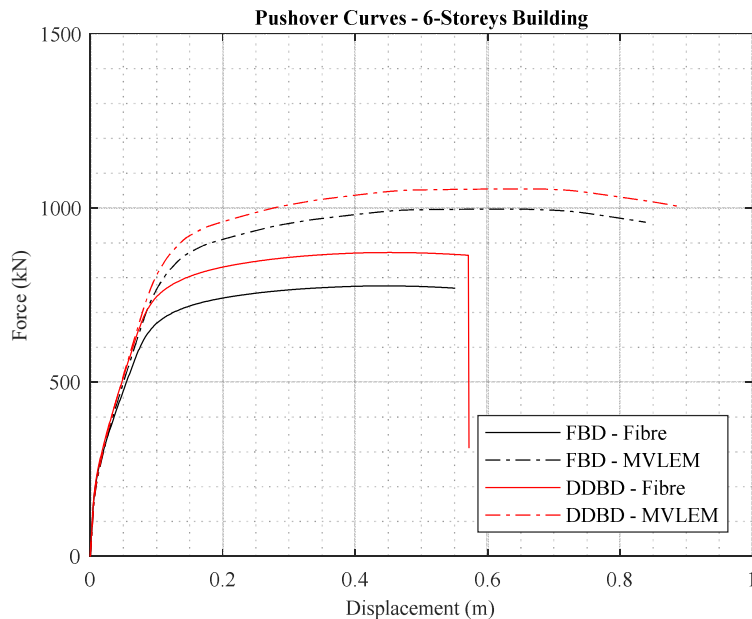


Figure 5.9. Pushover curves comparison between FBD and DDBD for both MVLEM and fibre models. 6-storey Building.

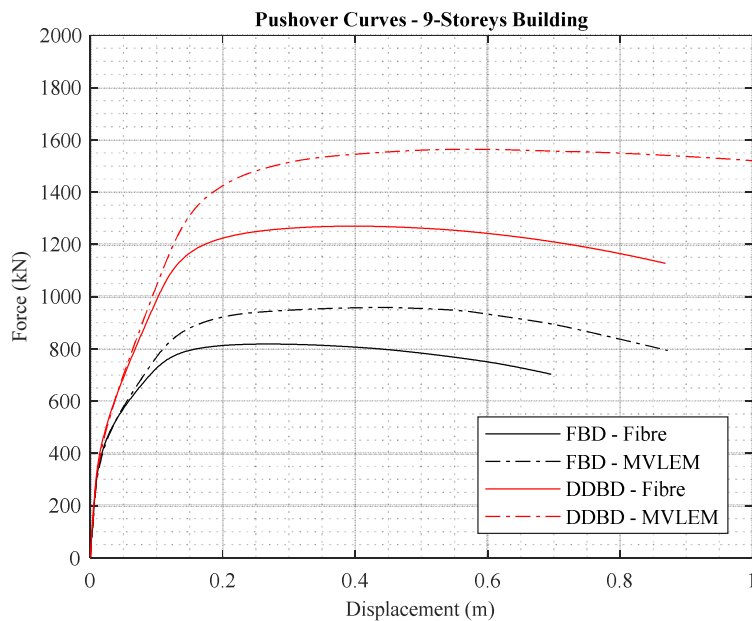


Figure 5.10. Pushover curves comparison between FBD and DDBD for both MVLEM and fibre models. 9-storey building.

From Figures 5.8 to 5.10, it is observed that MVLEM models exhibit more strength and more deformation capacity than fibre models. The difference in strength is very similar throughout all models, but the differences in final displacement are reduced with increasing number of storeys. One of the reasons for this trend might be related to the discretisation of the elements, as very different discretisation schemes were used in each model. Additionally, as it was necessary to work with macro-fibres for the MVLEM model, no distinction could be made between the boundary elements and the cover concrete surrounding them. As a result, a larger cross-sectional area was assigned with confined concrete material properties in MVLEM walls.

It is worth noting the differences between the formulations of each model. For instance, MVLEM uses average stress and strain at each macro-fibre over the height of the element rather than evaluating stress-strain relationship at multiple integration points. Also, for MVLEM, the curvature along the height of the element is assumed as uniform (constant), which might provide less accurate results for local rotations and deformations if compared to fibre beam-column elements (Kolozvari et al., 2018b). This shortcoming was improved by further division of the wall into more elements in the plastic hinge zone.

In some plots, e.g. Figure 5.8, a very steep (almost vertical) linear softening branch can be observed. This is the result of the restriction placed to the maximum tensile strain of the reinforcement steel, as mentioned in Section 5.3. This was not observed in all models, particularly in the MVLEM cases, as the walls failed at the strain limit but the model was not able to represent the descending branch (maybe due to the size of the macrofibres). In these cases, the failure was implied by non-convergence of the model after reaching the strain limit, which stopped the analyses. As such, results were taken up to the point where this maximum strain was reached at first time.

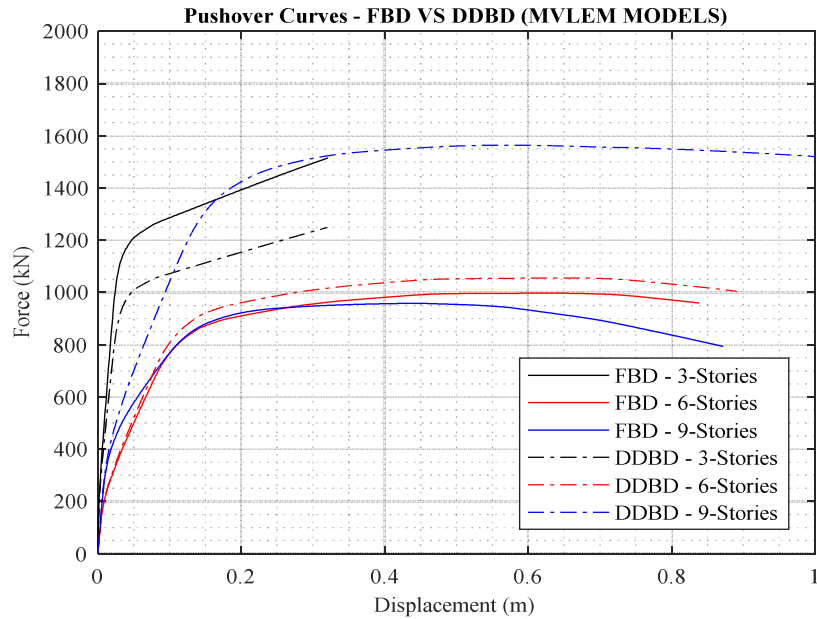


Figure 5.11. Pushover curves comparison FBD vs DDBD with MVLEM wall models.

Figure 5.11 compares all the designs using the MVLEM pushover curves. As expected, the differences between FBD and DDBD observed in the design stage with respect to seismic demands and to provided steel (Section 4.4) are also reflected in the pushover curves. The 3-storey building designed with FBD method shows higher capacity than its DDBD counterpart. The opposite trend is observed for the 9-storey building where DDBD exhibits more than 1.5 times the capacity obtained with FBD. On the other hand, differences between the design methods for the 6-storey buildings are almost negligible, with a difference of around 100kN in strength and about 5cm in displacement capacity being noted. It is also interesting to note how the 6- and 9-storey buildings designed with FBD method exhibit similar strength around the

yield point but diverge with increasing demand due to larger P-Delta effects in the 9-storey model. Finally, a high post-yield stiffness is observed in the 3-storey buildings since P-Delta effects were negligible in this case, whereas pushover curves for the 6- and 9-storey buildings flatten more and exhibit some softening at the post-peak region. Similar conclusions can be drawn with reference to Figure 5.12, which compares each of the designs when using the fibre modelling approach.

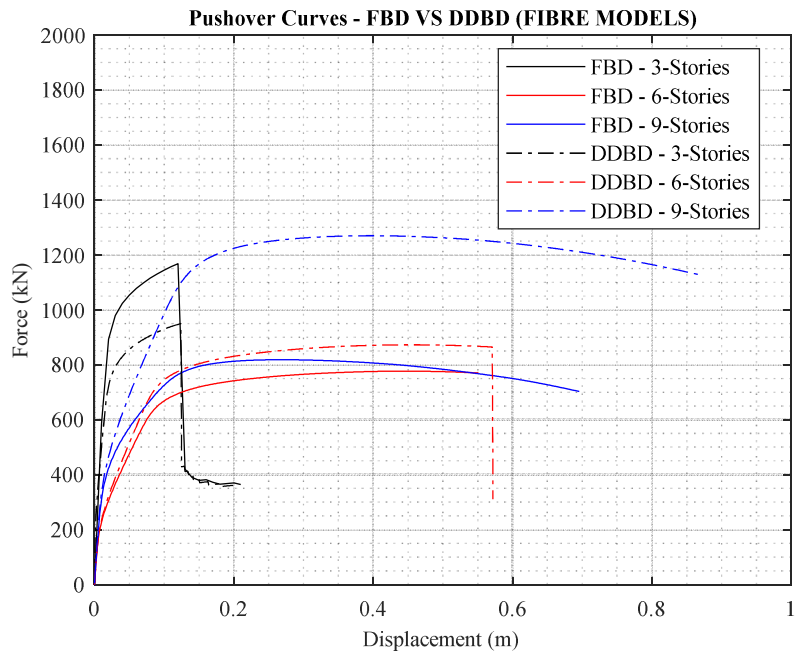


Figure 5.12. Pushover curves comparison FBD vs DDBD with fibre wall models.

The pushover curves, normalised by the buildings weight, are illustrated in Figure 5.13. For both FBD and DDBD, the base shear coefficient tends to decrease with increasing number of storeys. Table 5.3 shows a comparison of the shear overstrength factors and base shear coefficients computed for each designed building.

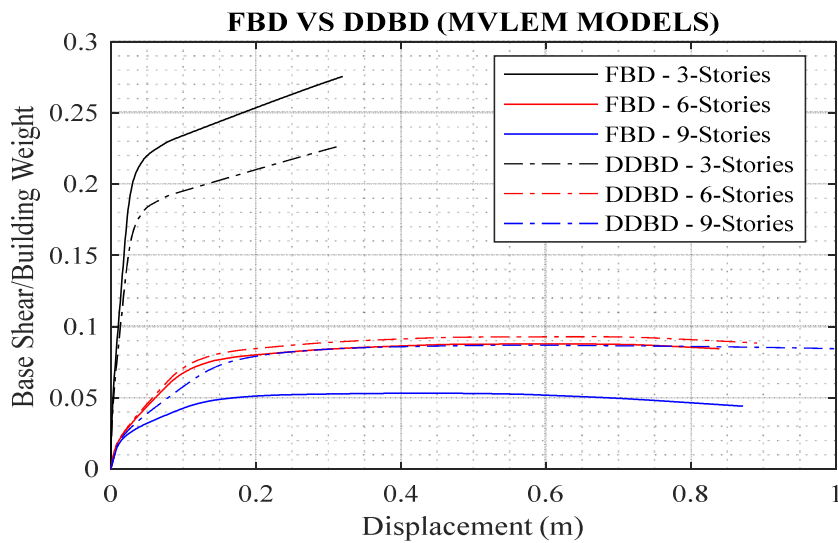


Figure 5.13. Normalised pushover curves for all designs.

Table 5.3. Base shear coefficients and pushover base shear overstrength for all buildings.

Model	Weight (kN)	Base Shear Analysis* V_b (kN)	Base Shear Pushover $V_{b,po}$ (kN)	Pushover Overstrength ($V_{b,po}/V_b$)	Design Overstrength (Table 4.14)	Base Shear coefficient Pushover ($V_{b,po}/W$)	Base Shear coefficient Analysis (V_b/W)
FBD - 3**	10989	1609	2800	1.74	1.59	0.255	0.146
FBD - 6**	22726	1978	2000	1.01	1.41	0.088	0.087
FBD - 9**	35994	2316	1900	0.82	1.72	0.053	0.064
DDBD - 3**	10989	822	2200	2.68	1.70	0.200	0.075
DDBD - 6	22726	1817	2100	1.16	1.02	0.092	0.080
DDBD - 9	35994	2977	3160	1.06	1.04	0.088	0.083

*Taken prior to any capacity design considerations for reinforcement

**Minimum reinforcement governs design

The base shear capacity of the 9-storey building designed with FBD found from pushover analysis, illustrated in Figure 5.14, was lower than the base shear for which it was designed since the overstrength factor is 0.82 (Table 5.3). This might be an initial suggestion of an unconservative design, however a comparison in terms of base moment found in the structural analysis phase versus the base moment obtained by pushover gives a flexural overstrength ratio of 1.67, as shown in Table 5.5.

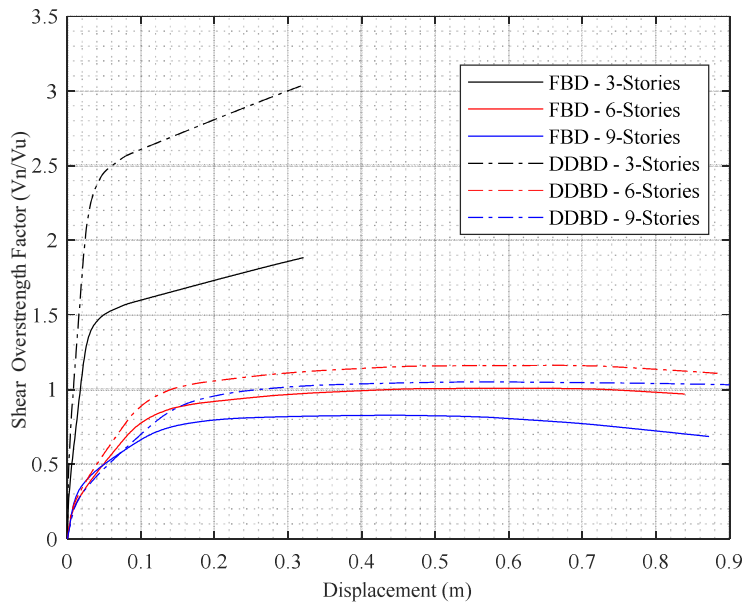


Figure 5.14. Overstrength pushover curves for FBD buildings and DDBD buildings, with MVLEM wall model.

Table 5.4. Comparison analysis and design moments at wall base FBD.

Building Case	FBD - Structural Analysis			FBD Provided	
	M_{ELF}	M_{MRSA} (unscaled)	M_{MRSA} (scaled)	M_{FBD}^{**}	$\phi M_{n,FBD}$
3-storeys	10921	7780	10542	10542	14045
6-storeys	25333	10198	17520	17520	21473
9-storeys	44245	19021	27694	27694	35480

**After capacity design, this is the final design value.

To understand this issue, it is recalled that in FBD, the design base shear was scaled to match the 100% V_{ELF} value. The scaling procedure of ASCE 7-16 consists in multiplying all MRSA forces by the V_{MRSA}/V_{ELF} ratio, which produces a scaled V_{MRSA} equal to the V_{ELF} , however, scaling M_{MRSA} moments by this ratio does not match the MRSA moments with M_{ELF} as it is observed in Table 5.4 and in Figures 4.21 to 4.23. The difference between scaled M_{MRSA} and M_{ELF} increases with increasing number of storeys. This is another reason why the 9-storey building designed by FBD method appears to have less shear strength than required. However,

the comparison in terms of moment overstrength (Table 5.5) shows that the design is indeed adequate.

In Table 5.5, it is also noted that while the pushover results of the FBD-6 and DDBD-6 models are very similar, those buildings were designed for quite different bending moments. The reason behind this similarity comes from the fact that DDBD uses expected material properties for flexural design of plastic hinge regions, meaning that less steel is required per moment demand (if compared to FBD), causing both methods to render similar reinforcement layout.

Table 5.5. Pushover base moment overstrength for all buildings.

Model	Base Moment Analysis* M_b (kNm)	Base Moment Pushover $M_{b,po}$ (kNm)	Pushover Overstrength ($M_{b,po}/M_b$)	Design Overstrength (Table 4.15)
FBD - 3	10542	21200	2.01	1.33
FBD - 6	17520	30362	1.73	1.23
FBD - 9	27694	46260	1.67	1.28
DDBD - 3**	5653	17460	3.09	2.50
DDBD - 6	23882	32181	1.35	1.15
DDBD - 9	57587	72955	1.27	1.14

*Taken prior to any capacity design considerations for reinforcement

**Minimum reinforcement governs design

In Tables 5.4 and 5.5 high values of shear overstrength were observed for FBD cases and high overstrength (both flexural and shear) were found for DDBD-3. This occurred because in those cases minimum reinforcement requirements governed the design. It is also observed that, in general, flexural design overstrength increased in the pushover results for DDBD and FBD (Table 5.5). This trend is not observed for shear overstrength of FBD models, mainly due to the reason explained in the previous paragraph regarding FBD-9 case, but also due to the P-Delta effects observed with FBD-6 and FBD-9 models, which were neglected in the design as allowed by FBD procedure verifications (see Appendix A). Furthermore, it is recalled that pushover results are sensitive to the shape of the applied vector of forces, thus, the results are tailored for the first-mode response of the structures, neglecting the importance of higher modes (Antoniou & Pinho, 2004), particularly in the 6 and 9 storeys buildings. This could have been improved

using an adaptive pushover procedure (Gupta & Kunnath, 2000), however this was not carried out in this study.

5.7 Wall model selected for NLTHA

In the remainder of this dissertation, the numerical model used for RC walls response is the MVLEM model. This is due to its computational efficiency that characterises the structural response up to high levels of nonlinearity, which is ideal for collapse assessment. Furthermore, it has been validated against experimental tests (Kolozvari, et al., 2018c; Orakcal & Wallace, 2006) where it performed similarly or better than fibre-based models, as pointed out in Section 5.1.

6 RISK ASSESSMENT

6.1 Introduction

Collapse risk of the designed structures was assessed following the methodology described in Section 2.5. The collapse assessment methodology involves ground motion record selection, NLTHA and convolution between fragility and hazard to obtain the MAPE for different levels of drift up to structural collapse. In this chapter, some background is provided for each of the procedures performed and the choices made are explained. Finally, results are shown and compared, with the risk consistency of FBD and DDBD methods evaluated.

6.2 Ground motion record selection

Ground motion selection criteria plays an important role in collapse capacity prediction (Goulet et al., 2007). Several approaches can be used to perform this task and there is still no full consensus on which should be the proper way to perform it since advantages and disadvantages exist among each.

Most approaches require hazard disaggregation (Bazzurro & Cornell, 1999) to identify the characteristics of the event that has the highest contribution to the hazard at the site for an IM type and level. This IM relates the PSHA results with the structural analysis hence its choice is closely linked to the particular building being studied. Ground motion records that match the event rupture characteristics (e.g. moment magnitude, distance, epsilon and style of faulting) are selected from databases and used for NLTHA. The selected records can be scaled to match the target IM such that they are consistent with the hazard at the site.

Various studies (Baker & Cornell, 2006; Goulet et al., 2008; Zareian & Krawinkler, 2007) have shown that ignoring spectral shape, characterised by the term epsilon, in the ground motion

record selection process can result in an underestimation of the collapse capacity of the structure and consequently will affect the mean annual rate of collapse. The epsilon value at a period T_i , $\epsilon(T_i)$, is defined as the number of standard deviations by which $\ln Sa(T_i)$ differs from the mean prediction $\mu \ln Sa(M; R; T_i)$, at T_i . The epsilon value can be obtained directly from disaggregation.

Recently, more refined approaches have been developed and several algorithms for ground motion record selection are available in the literature (Georgioudakis et al., 2017; Iervolino et al., 2010; Moschen et al., 2017). Among these are the conditional spectrum (CS) methods (Baker, 2011; Baker & Lee, 2018; Lin et al., 2013) which describe the expected (target) response spectrum associated with a ground motion having an IM specified as $Sa(T^*)$, where T^* is called the conditioning period, to which all results are related. This target spectrum links the ground motion hazard to the structural response and it is computed based on the mean causal earthquake obtained from disaggregation and using the GMPEs of the PSHA model. Therefore, the target spectrum contains the Sa values at all periods T_i associated with a given $Sa(T^*)$ value at the conditioning period. The CS also considers the variability in response spectra at other periods different than T^* (Lin et al., 2013). Correlation between epsilon across all periods is used to estimate the expected value of Sa at T_i given Sa at T^* , from which a conditional mean and a conditional standard deviation are computed. Such approach was adopted in this study and a computationally efficient algorithm (Jayaram et al., 2011) was used to select and scale records from a database until they collectively match the computed target CS.

As such, an IM and intensity level were selected prior to performing disaggregation on the OpenQuake hazard analysis results. In this study, spectral acceleration at the building's first-mode period $Sa(T_1)$ was chosen as the reference IM and a return period of 2475 years was the intensity level instead of the 475 years return period used for design since it is more closely related to the collapse limit state of the buildings. This implies that the disaggregation results must be computed for each one of the 6 buildings designed, as each one of them has a different first mode period, as explained in the following section.

Some authors (e.g. Baker & Cornell, 2006b; Haselton & Baker, 2006) have expressed their concern about the use of $Sa(T_1)$ as IM for risk-based assessments because the structures tend to soften due to damage when subjected to ground shaking resulting in an "elongation" of the first-

mode period. This means that the dynamic properties of T_1 become increasingly less relevant and that a choice of $T > T_1$ may be more suitable. Additionally, multi-storey buildings tend to be influenced by higher modes, especially for mid-rise and high-rise wall buildings, so consideration should also be taken of periods less than T_1 . Thus, it has been proposed (AIS, 2009; Haselton & Baker, 2006) that a range of periods between $0.2T_1$ and $2T_1$ rather than T_1 alone could be used as IM. One alternative IM is AvgSa as proposed in recent studies (Eads et al., 2015; Vamvatsikos & Cornell, 2005), which requires some post-processing of the PSHA results to keep the same IM in the GMPEs and in the NLTHA.

Nevertheless, many previous risk-based studies (Haselton et al., 2008; Ibarra & Krawinkler, 2005) have deemed results adequate when using $Sa(T_1)$ as the IM, making it probably the most common IM used in the field. For example, as noted in the past (Shome & Cornell, 1998) structural analysis results for MDOF structures with T_1 around 1 sec showed no adverse effects when input records were matched over a range of periods instead of T_1 , and authors note that scaling at T_1 is a reasonable choice for medium to long-period structures.

6.2.1 Disaggregation

Disaggregation of the seismic hazard must be performed in order to identify the dominating event for the given IM level. A sensitivity study was performed to identify which branches of the PSHA logic tree contributed more to the hazard of the site. Thus, some branches were eliminated from the original PSHA model helping to improve computational time with little loss in accuracy. This purge of the PSHA logic tree gains more importance when trying to disaggregate the hazard at the site, which would otherwise take too much time in OpenQuake due to the sheer volume of branches to disaggregate. Consequently, the final logic tree used for hazard and disaggregation calculations consists of 3 branches for the two main tectonic regions surrounding the site. Disaggregation was performed in terms of $M-R-\epsilon$ and some of the results are plotted in Figures 6.1 and 6.2, with the rest found in the Appendix C. Each disaggregation analysis was carried out for conditioning period T^* value, corresponding to the first-mode period of each designed building, as shown in Table 6.1

Table 6.1. First-mode vibration periods of each building according to pushover results, used for disaggregation and record selection.

Design Method	Period T_1 (s)		
	3-storey	6-storey	9-storey
FBD	0.72	1.94	2.59
DDBD	1.00	1.73	1.98

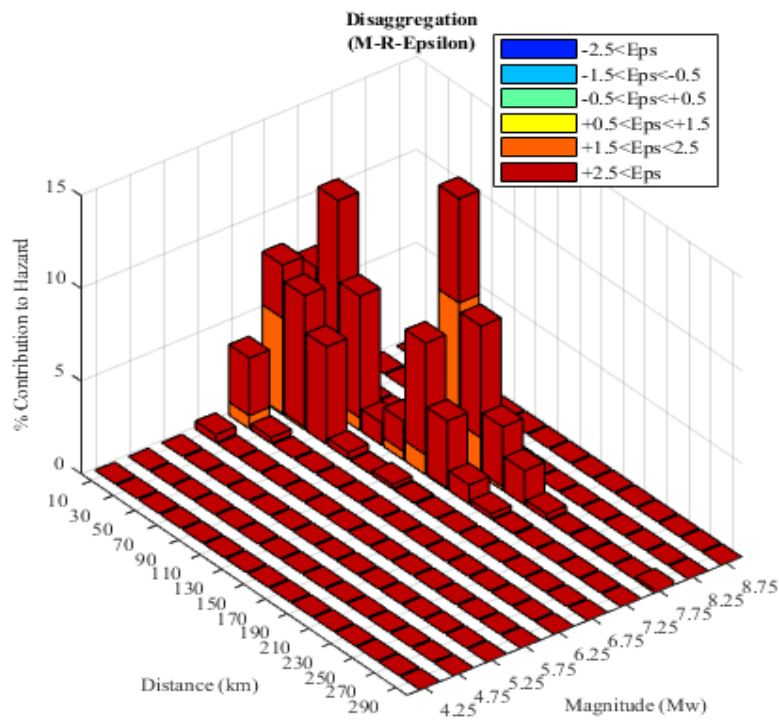


Figure 6.1. Disaggregation DDBD-3, $Sa(T_1=1.00\text{s})$. 2475 years return period.

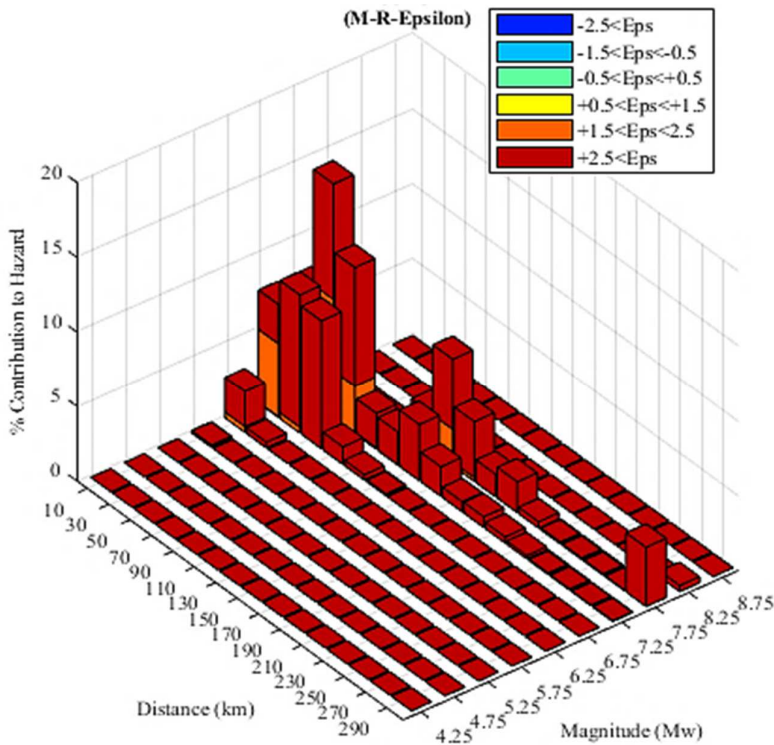


Figure 6.2. Disaggregation FBD-6, $Sa(T_1=1.94s)$. 2475 years return period.

6.2.2 Conditional spectrum computation and ground motion record selection

Using disaggregation results and fundamental period information presented in the previous section, a computationally efficient algorithm (Baker & Lee, 2018; Jayaram et al., 2011) was used to select the ground motion records to be used in the NLTHA of the buildings. As six different buildings were tested, six different sets of records were selected from the PEER NGA-West2 Database (Ancheta et al., 2014). The maximum scaling factor allowed was 4 and a total of 30 records were selected for each set. Figures 6.3 and 6.4, show the conditional spectra computed for the 6-storey building designed with FBD and DDBD, respectively. The other spectrums can be found in Appendix C.

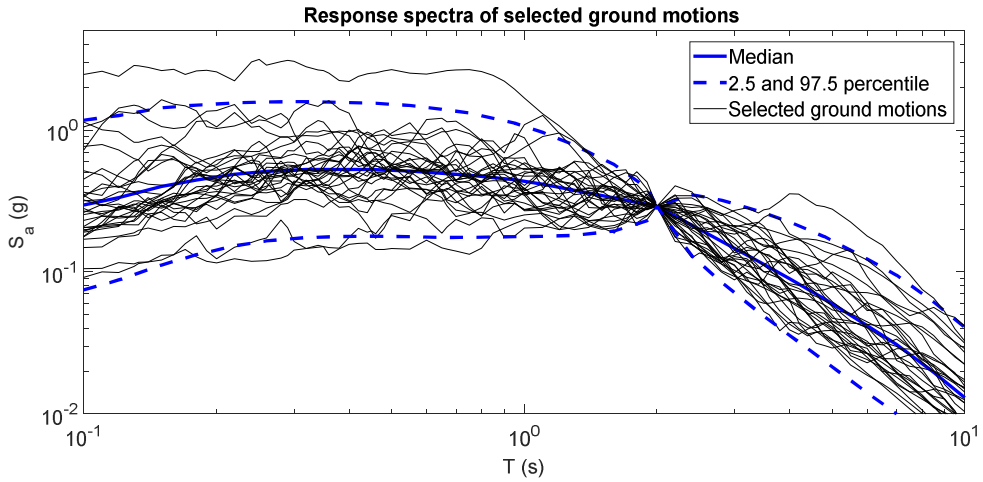


Figure 6.3. FBD-6 Building: Response spectra of selected ground motion records conditioned on $Sa(T_1=1.94\text{s})$.

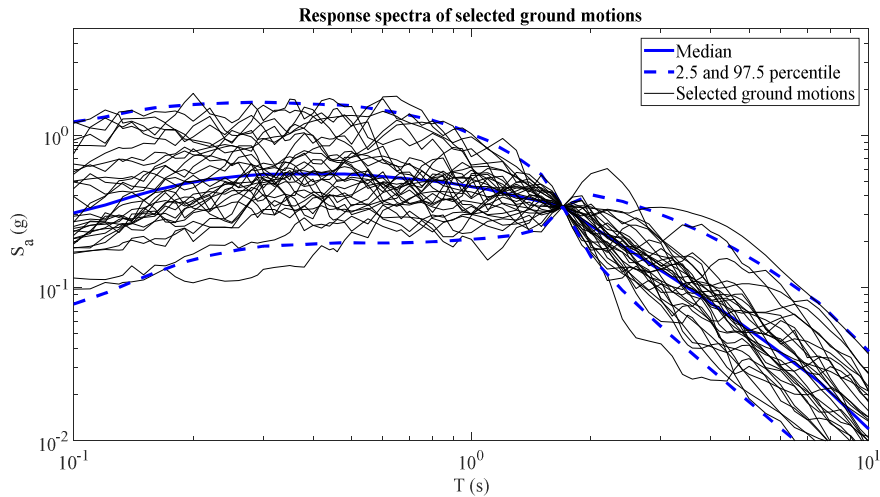


Figure 6.4. DDBD-6 Building: Response spectra of selected ground motion records conditioned on $Sa(T_1=1.7\text{s})$.

6.3 Collapse definition

Collapse is typically defined as the point where lateral instability occurs, i.e. the point at which a large increase in drift/displacements under a small load increment is observed, such that the structure does not retain its load carrying capacity. Hence, the reference EDP used in this study was the maximum peak storey drift ratio (MPSD), which corresponds to the absolute maximum drift observed across all storeys during seismic response. Previous studies in literature (Haselton et al., 2008) found that values between 5% and 6% of roof drift ratio produced collapse of structures, whereas others have conservatively taken 5% peak inter-storey drift as

the reference collapse point (Dabaghi et al., 2019). Still, the maximum drift considered for the NLTHA was 10% as once the structure's numerical model has exceeded such a level of deformation, it has almost certainly collapsed and has no lateral strength capacity remaining.

6.4 Incremental dynamic analysis

As pointed out in Section 2.5.2, the methodology to assess the seismic collapse capacity of the buildings was IDA. IDA evaluates the structural response under a set of ground motions scaled increasingly to multiple intensity levels, with each one of them producing a curve of response versus intensity level. Therefore, this method allows to link IM and EDP, making it possible to estimate the IM level that causes collapse for each ground motion record. As stated previously, the selected IM was $Sa(T_1)$ and the EDP was the maximum peak storey drift ratio (MPSD).

Some concerns arise regarding the “validity” of IDA results due to record scaling (Luco & Bazzurro, 2007). However, as indicated by Vamvatsikos and Cornell (2002), if the IM is chosen in such a way that the EDP is independent of the M and R (for the range of interest) then the scaling of records will produce good results for the distribution of EDP given IM. Therefore, emphasis should be placed on the choice of IM. Additionally, small dispersion on the IM gives small dispersion in EDP, so fewer analyses were needed to obtain a good median estimate. Also, the fact that the scale factor was limited to 4 suggests that the level of bias introduced via scaling on the records during IDA is limited in some respect.

To construct the IDA curves, a decision must be taken in terms of how many runs or IM values (discrete points) should be performed in order to have a good representation of the IDA trace of a single ground motion record while keeping computational efficiency in the overall procedure. In this study, a *Hunt, Trace and Fill* (HTF) algorithm was used to improve the resolution of the IDA curves. As its name suggests, the procedure comprises three different stages. An initial intensity level is set and then the records are rapidly increased while *hunting* for the collapse point. The first collapse point is discarded, and the record is scaled up in smaller increments starting from the previous non-collapse intensity level to more accurately find (*trace*) the collapse point. Then, the remaining runs available are used to *fill* the gaps in the IDA curve. A total of 20 runs per record were set in the HTF algorithm used to analyse the studied buildings. Figures 6.5 to 6.10 show the results of the IDA performed for each of the buildings.

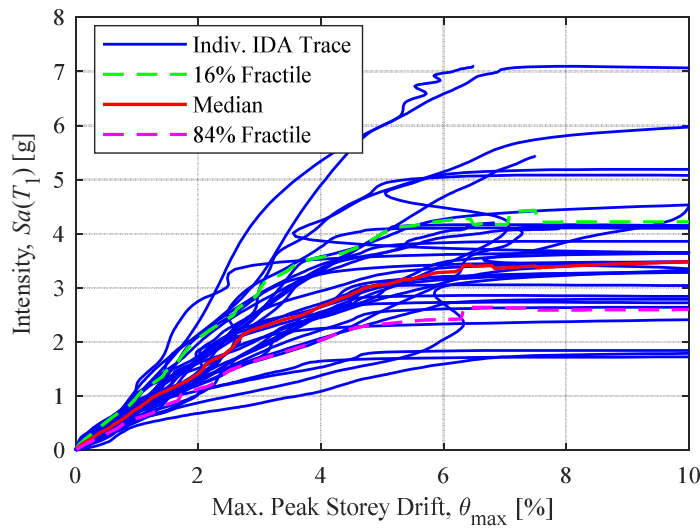


Figure 6.5. FBD 3-Story building IDA curves, $Sa(T_1=0.72s)$.

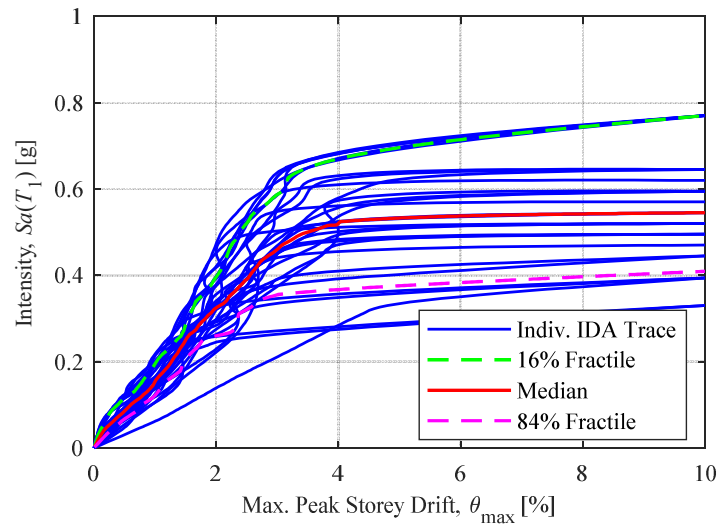


Figure 6.6. FBD 6-Story building IDA curves, $Sa(T_1=1.94s)$.

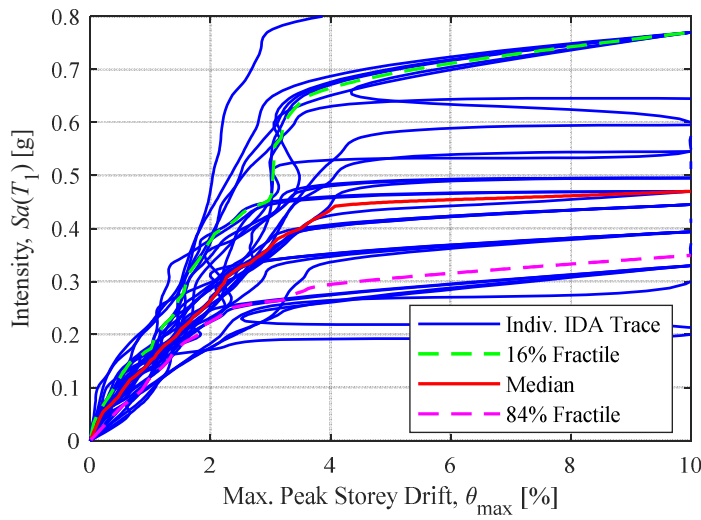


Figure 6.7. FBD 9-Story building IDA curves, $Sa(T_1=2.59s)$.

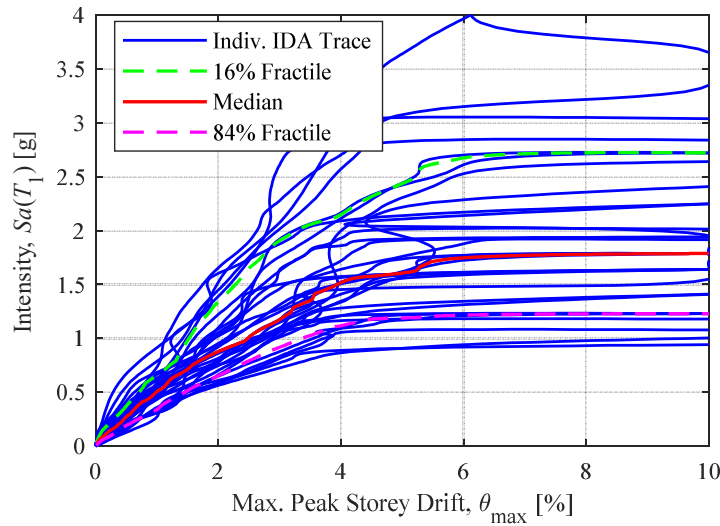
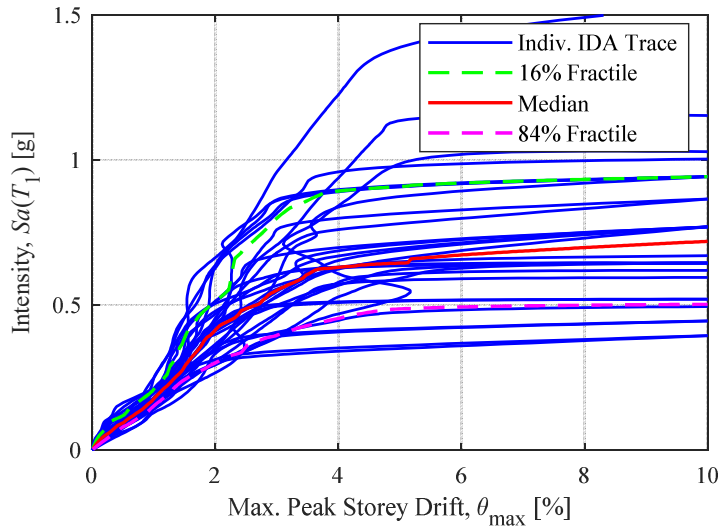
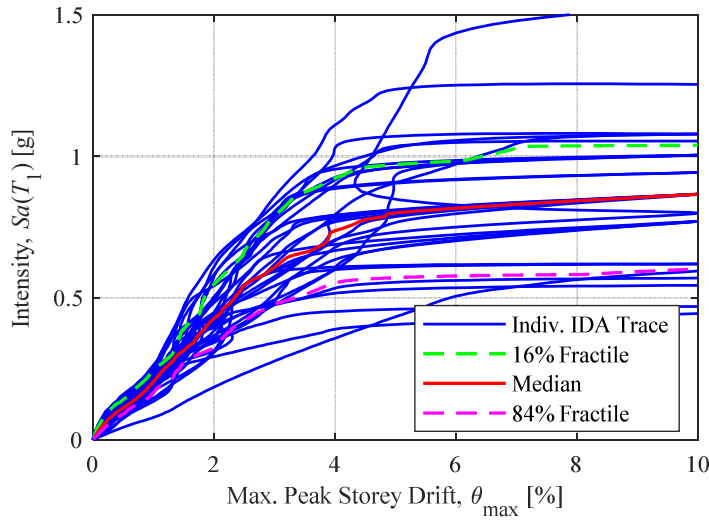


Figure 6.8. DDBD 3-Story building IDA curves, $Sa(T_1=1.00s)$.

Even though the same EDP was used in all the analyses, it is not possible to compare the buildings performance based on the IDA curves, because a different IM was used due to them having different fundamental periods. Instead, comparisons can be made after calculating the collapse risk in terms of the MAFE of a given MPSD value, which is described in Section 6.6.

Figure 6.9. DDBD 6-Story building IDA curves, $Sa(T_1=1.73\text{s})$.Figure 6.10. DDBD 9-Story building IDA curves, $Sa(T_1=1.98\text{s})$.

6.5 Modelling uncertainty

Modelling uncertainty (Bradley, 2013) is related to the epistemic uncertainties involved in the modelling process. For instance, different modelling approaches are available for the structures/materials and different values can be used for the parameters that define them. The IDA curves calculated account only for record-to-record (RTR) variability (aleatory uncertainty). However, inclusion of model uncertainties is of high importance for risk assessment (Gokkaya et al., 2016) as it produces an increase of the probability of collapse, and

consequently, an increase in the mean annual rate of collapse. With respect to drift capacities and demands, it has been shown that the inclusion of the modelling uncertainties leads to slight changes in the median (mean) values of these quantities but has a major impact in the dispersion that may be up to 60%. Similar conclusions were drawn in other studies (Haselton et al., 2008).

In this project, modelling uncertainties are included by a user-input value in the calculation of MAFE. The dispersion value adopted here was taken from a study by Kosić et al. (2016). This study proposed a value of 0.40 for RC walls which should also be increased by 10% if CS is used for ground motion records selection. Therefore, the dispersion value for modelling uncertainty used was 0.45.

6.6 Mean annual frequency of exceedance

The procedure used to calculate the MAFE is the one proposed by Vamvatsikos (2013) which is a modification of the SAC/FEMA expressions (Cornell et al., 2002; SAC/FEMA, 2000b, 2000a) to evaluate seismic performance of structures in a closed-form and probabilistic manner. The MAFE can thus be found by integrating the seismic hazard (fitted by a second-order polynomial) with the structural response given by the median IDA curves (in terms of IM) of each building.

The individual curves of MAFE of maximum peak storey drift (MPSD) and the hazard curves fit plots are shown in Appendix C. Here the curves obtained by each method are compared in Figure 6.11.

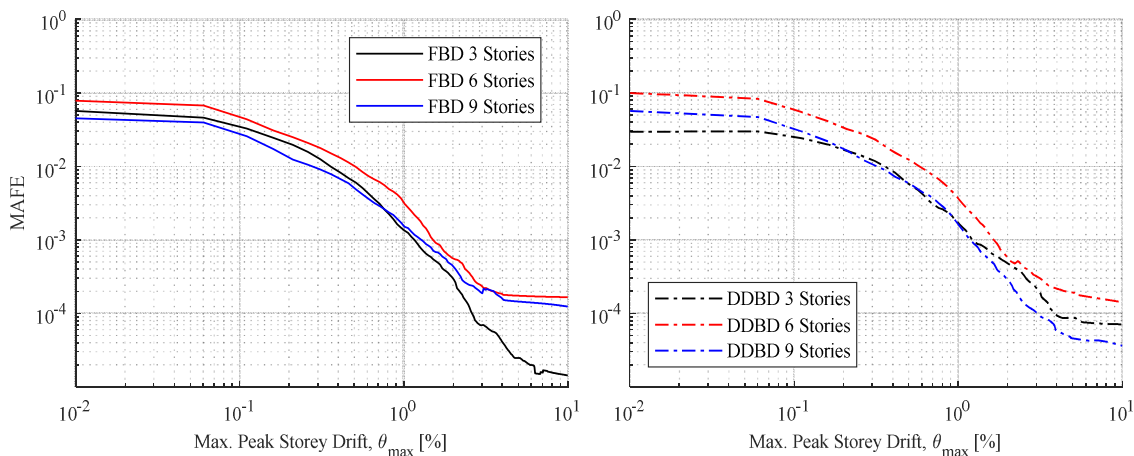


Figure 6.11. Maximum peak storey drift ratio MAFE curves for (left) FBD and (right) DDBD.

In general terms, it can be observed that the curves span a relatively narrow band up to the 4-5% MPSD point. This coincides roughly with the range of drifts for which the median IDA curves flatten-out or begin to start collapsing via the rapid increase in structural demand for each structure. As it is very unlikely that any structure will be standing at larger drifts ratios, the 5% MPSD was conservatively taken as the reference point to analyse the collapse performance. Also, it can be noted how the MAFE tends to saturate beyond this point for each building meaning that they are in fact approaching their collapse capacity. Thus, the MAFE at such point was taken as equal to the mean annual frequency of collapse (MAFC) for the buildings.

For the FBD case, it is observed that the 3-storey building presents the lowest MAFC, followed by the 9-storey building and the 6-storey building, in that order. On the other hand, for DDBD the 9-storey building exhibits the lowest MAFC, followed by the 3-storey and the 6-storey buildings. Hence, it is found that for both FBD and DDBD, the 6-storey building is the one with higher risk of collapse, although the significant overstrength of the 3-storey structures must also be recalled.

Although previous studies (mostly dealing with RC frames) have found that collapse probability (not MAFC) increases with increasing number of stories (Dabaghi et al., 2019; Galanis & Moehle, 2015; Ibarra & Krawinkler, 2005), others have shown that this might not be always the case, especially with RC walls (Gogus & Wallace, 2015). This is mainly because the collapse performance of the buildings is influenced by many parameters, like shear overstrength, moment overstrength, ductility capacity, structural period and P-Delta effects, among others. Furthermore, the comparisons based on the collapse probability might not necessarily hold after integration with the hazard curve, as in MAFC computation.

To provide a better comparison, the collapse margin ratio (CMR) was computed for each of the buildings. The CMR is defined in the FEMA P695 guidelines (FEMA/NEHRP, 2009) as the ratio between the median collapse capacity (\hat{S}_{CT}) and the ground motion intensity at the maximum considered earthquake MCE (S_{MT}), see Equation 6.1. As noted in previous sections, the MCE corresponds to the 2% in 50 years probability of exceedance intensity level and it was taken as the spectral acceleration value at the fundamental period, $Sa(T_1)$, read from the UHS for such hazard level. The median collapse capacity is taken from the median value of the IDA

curve of each building at the collapse MPSD. Table 6.2 shows a summary of the CMR computation for each design and a graphical comparison is shown in Figure 6.12.

$$CMR = \hat{S}_{CT}/S_{MT} \quad (6.1)$$

Table 6.2. Collapse Margin Ratio (CMR) and Mean Annual Frequency of Collapse (MAFC) calculated for all the designs.

Model	\hat{S}_{CT} (g)	S_{MT} (g)	CMR	MAFC
FBD - 3	3.06	0.83	3.68	2.46E-05
FBD - 6	0.53	0.28	1.90	17.38E-05
FBD - 9	0.45	0.19	2.37	14.49E-05
DDBD - 3	1.61	0.61	2.64	8.79E-05
DDBD - 6	0.64	0.32	2.00	18.60E-05
DDBD - 9	0.80	0.27	2.96	4.59E-05

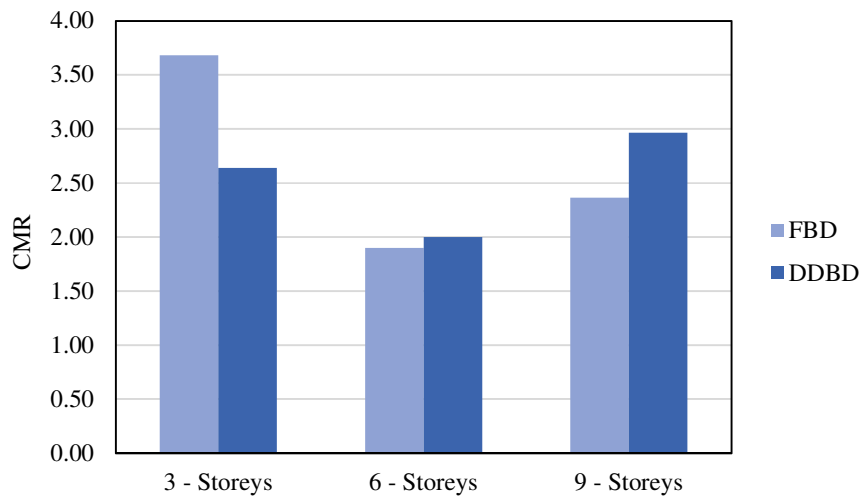


Figure 6.12. CMR comparison for all designs.

The CMR values reflect the behaviour observed in the MAFE curves shown in Figure 6.11 and in the pushover curves shown in Figure 6.13. A normalised pushover plot in terms of MPSD is introduced by Figure 6.13 and the results also resemble what is observed in the MAFE curves. From Figure 6.12, and Tables 6.2 and 6.3 a few comments can be made:

- For FBD case, the FBD-3 design has lower period which implies high demand at MCE, but it has much higher capacity, as observed in the base shear coefficient results (Table

6.3). It also has higher flexural and shear overstrength than the FBD-6 and FBD-9 cases, thus higher CMR. Such high overstrength is found mainly because design was governed by minimum reinforcement requirements. Also, it is reminded that despite being flexure-dominated, the 3-storey models are more sensitive to shear deformations, which were not considered by the numerical model. As such, the FBD-3 MAFC is the lowest among all buildings.

- FBD-6 and FBD-9 have almost the same median collapse intensity but FBD-6 has lower fundamental period so it is subjected to higher demand at MCE, hence its CMR is lower, consequently its MAFC is higher.
- With respect to DDBD, DDBD-9 has larger median capacity than DDBD-6 and longer period, thus it is subjected to less demand at MCE so, as expected, it has higher CMR, and lower MAFC.
- DDBD-9, if compared to DDBD-3, has lower MAFC as its long period means less demand at MCE, while having large capacity (even larger than DDBD-6). This happens despite the high flexural overstrength of DDBD-3 model (given by minimum reinforcement requirements) because DDBD-9 design was biased towards the highest possible strength (special case explained in Section 4.3.6). This is also demonstrated by the base shear coefficient of DDBD-9 which was almost equal to the one of DDBD-6 (Table 6.3), contrary to its tendency to decrease with increasing number of storeys, as observed in FBD cases. If the lowest possible base shear would have been used, then differences like the ones between FBD-3 and FBD-9 should have been found.
- CMR of DDBD buildings varies between 2.0 and 2.96, this is a narrower range than for the FBD cases which vary between 1.90 and 3.68. It is recalled that CMR values found do not account for modelling or any other kind of uncertainty, because CMR computation is based on the median capacity estimate, which remains unchanged as modelling uncertainty only modifies the dispersion (First-order assumption).
- The MAFC seems to vary almost linearly with CMR, with exception of FBD-6 building, as observed in Figure 6.14.

Table 6.3. Summary of parameters involved in collapse performance and collapse risk evaluation for all designs.

Model	\hat{S}_{CT} (g)	S_{MT} (g)	Method-based Period (s)	Pushover -Based Period (s)	μ Pushover	Ω (Flexure)	Ω (Shear)	CMR	MAFC	Base Shear coefficient (V_b/W)
FBD - 3	3.06	0.83	0.34	0.72	7.50	2.01	1.74	3.68	2.46E-05	0.255
FBD - 6	0.53	0.28	1.17	1.94	7.64	1.73	1.01	1.90	17.38E-05	0.088
FBD - 9	0.45	0.19	1.40	2.59	7.25	1.67	0.82	2.37	14.49E-05	0.053
DDBD - 3	1.61	0.61	1.00	0.82	7.50	3.09	2.68	2.64	8.79E-05	0.200
DDBD - 6	0.64	0.32	1.73	1.90	8.09	1.35	1.16	2.00	18.60E-05	0.092
DDBD - 9	0.80	0.27	1.98	2.09	7.69	1.27	1.06	2.96	4.59E-05	0.088

Table 6.3 lists some additional parameters that support the previous comments on the collapse performance and MAFC observed for each building. The collapse performance and MAFC cannot be attributed to a single variable, but rather to the way in which they interact.

An interesting example comes from the comparison of FBD-6 and DDBD-9 cases, as shown in Table 6.4 these models had very similar values of MCE demand, first-mode period, ductility, shear overstrength, and base shear coefficient. However different CMR and MAFC were obtained for each building. In this case, the CMR and MAFC were driven by the median capacity of each building, thus the building with higher median capacity had a higher CMR and lower MAFC. This can also be related to the fact that both models provided essentially equal base shear coefficients regardless the large difference in buildings' weight. Also, it is noted that the differences in median capacity prevailed over the differences in flexural overstrength.

Table 6.4. Comparison of parameters involved in CMR and MAFC for FBD-6 and DDBD-9 models.

Model	\hat{S}_{CT} (g)	S_{MT} (g)	Pushover T1 (s)	μ Pushover	Ω (Flexure)	Ω (Shear)	CMR	MAFC	Base Shear coefficient (V_b/W)	Weight (kN)
FBD - 6	0.53	0.28	1.94	7.64	1.73	1.01	1.90	1.74E-04	0.088	22726.2
DDBD - 9	0.8	0.27	1.98	7.69	1.27	1.06	2.96	4.59E-05	0.088	35993.6

In other cases, the differences in median capacity were somewhat compensated by differences in periods, which affect the MCE demand for each building. This is observed in the similar values of MAFC obtained for FBD-6, DDBD-6 and FBD-9 buildings (Table 6.5).

Table 6.5. Comparison of parameters involved in CMR and MAFC for FBD-6, DDBD-6 and DDBD-9 models.

Model	\hat{S}_{CT} (g)	S_{MT} (g)	Pushover T1 (s)	μ Pushover	Ω (Flexure)	Ω (Shear)	CMR	MAFC	Base Shear coefficient (V _b /W)	Weight (kN)
FBD - 6	0.53	0.28	1.94	7.64	1.73	1.01	1.90	1.74E-04	0.088	22726
DDBD - 6	0.64	0.32	1.73	8.09	1.35	1.16	2.00	1.86E-04	0.092	22726
FBD - 9	0.45	0.19	2.59	7.25	1.67	0.82	2.37	1.45E-04	0.053	35994

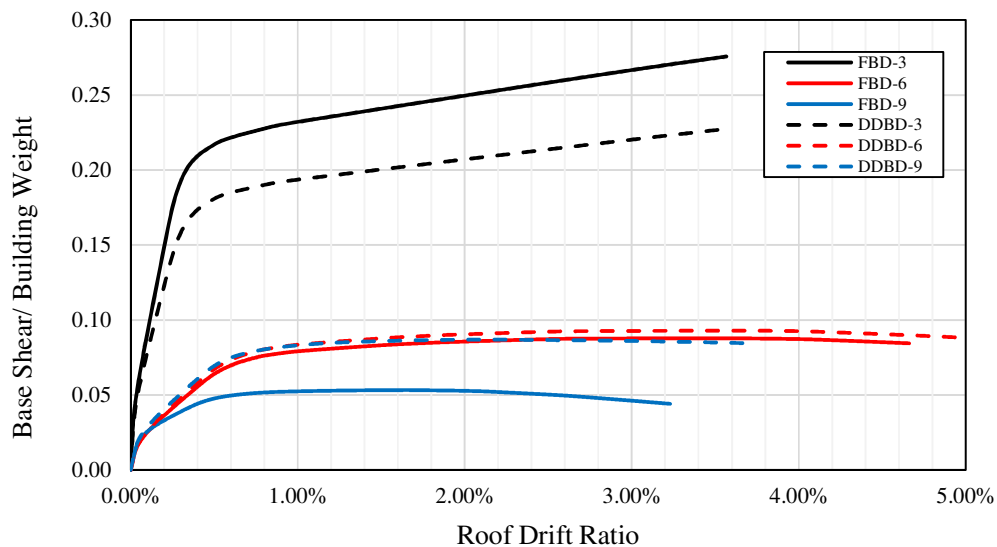


Figure 6.13. Normalized pushover curves in terms of roof drift ratio for all designs.

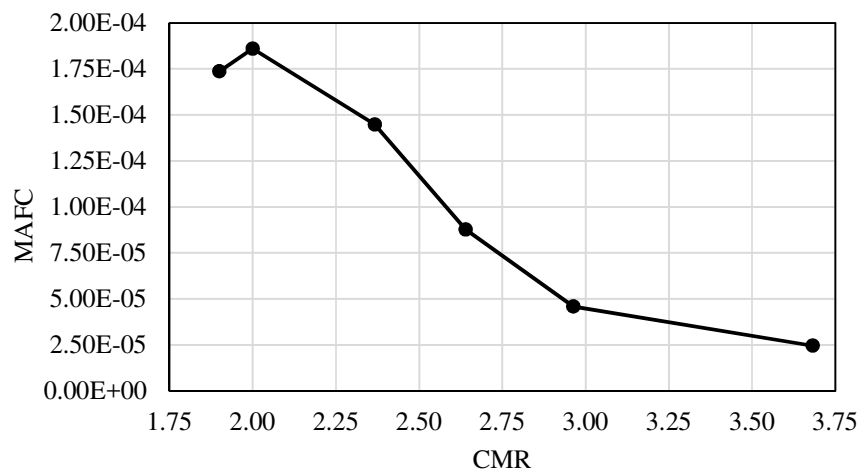


Figure 6.14. Variation of MAFC with CMR for all the studied cases.

6.7 Risk-consistency evaluation

Figure 6.15 shows the MAFE versus drift ratio for all buildings, taking a MPSD of 5% as the reference collapse capacity. This MAFE corresponds to the estimated collapse risk of each design and is marked with the green vertical line in the plot. The exact MAFC values are shown in Table 6.6.

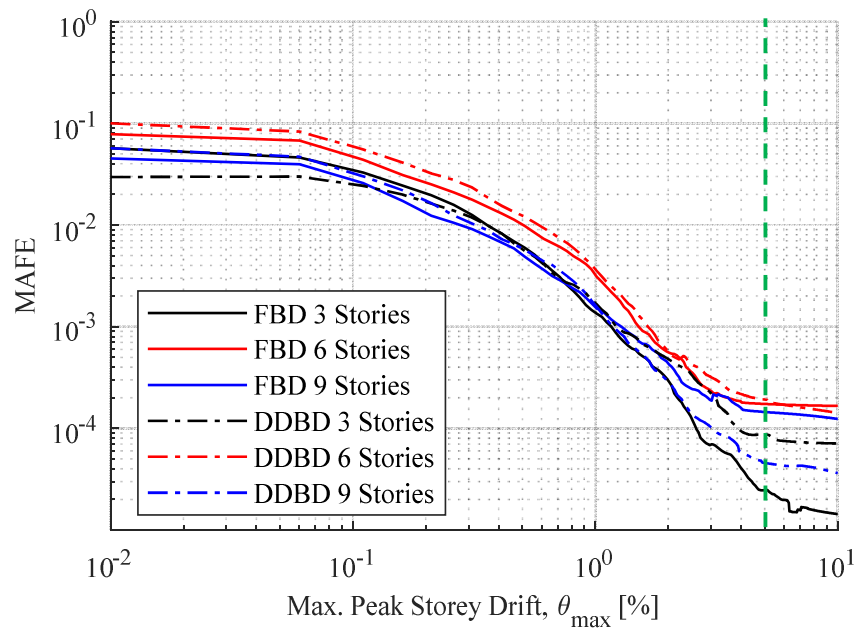


Figure 6.15. All designs comparison, maximum peak storey drift MAFE curves. Green line marks the 5% MPSD.

Table 6.6. Mean Annual Frequency of Collapse (MAFC) comparison FBD vs DDBD.

Design Method	MAFC		
	3-Storeys	6-Storeys	9-Storeys
FBD	2.46E-05	17.38E-05	14.49E-05
DDBD	8.79E-05	18.60E-05	4.59E-05
<i>Ratio FBD/DDBD</i>	0.28	0.93	3.16

Two different concepts of risk consistency are compared: (a) the risk-consistency related to the MAFC of the same building designed by different methods; and (b) the evaluation of the risk consistency, in terms of MAFC, across different buildings designed by the same method.

Referring to (a), from the results obtained, it is observed that the MAFC is essentially equal between FBD and DDBD for the 6-storey building case, this matches with the similarities found

in the final reinforcement layout, pushover curves, base shear coefficients, ductility, fundamental period and overstrength factors. These two structures (FBD-6 and DDBD-6) were also the ones with higher collapse rates among all designs, as previously explained. Therefore, the collapse risk of the 6-storey building was consistent between FBD and DDBD methods, as MAFE curves of both designs followed very similar paths from 2% drift onwards.

On the other hand, for the 3-storey building there is a moderate difference between FBD and DDBD method, expressed by the FBD/DDBD ratio, which is 0.28, implying a lower mean collapse rate for the FBD case. This is because, despite having the same wall geometry, the FBD-3 building featured more reinforcement, thus, more strength than DDBD-3. The difference would be more noticeable if minimum reinforcement requirements would have been ignored in DDBD-3 design, which would have reduced its overstrength factors and consequently its median capacity.

The opposite is observed for the 9-storey building designs. In this case, DDBD is the methodology that produces a significantly lower MAFC, as the collapse rate of the FBD-9 design is 3.16 times larger than its DDBD counterpart. It seems that with increasing number of storeys, the DDBD tended to produce “safer” designs, although it is recalled the design choice biased towards the highest possible strength made for the DDBD-6 and DDBD-9 structures, as they fell in the special design case described in Section 4.3.6. If these buildings would have been designed for the lowest possible base shear, then it is possible that their MAFC would have increased, reducing the differences with FBD, although the effects of period lengthening as consequence of this lower base shear choice would also need to be considered.

Moreover, despite the differences found for the 3-storey and 9-storey cases, the MAFE curves remain relatively close to each other up to the 5% MPSD point hence a moderate degree of consistency is reached between both methods. Some particular issues arose that may explain the differences in the 3- and 9-storey cases but for now, no discernible differences are noted.

Moving on to the second comparison, it is shown that, in general, there is no risk consistency between different buildings designed by the same methodology. This observation applies to both the FBD and DDBD cases as MAFE curves differ from each other for high levels of drift. Hence, this point of view of the “uniform risk” concept is not inherently satisfied by either

design method. An exception to this is found in the comparison of FBD-6 and FBD-9 cases, which had similar MAFC, as explained in the previous section with respect to Table 6.5.

Nevertheless, all designs are within a relatively narrow band up to the 5% MPSD level, which suggests that current FBD design practices and DDBD formulations are on the right track towards this goal. This was observed when computing the difference between the highest and lowest MAFC obtained by each method, which was equal to 1.49E-0.4 and 1.40E-4 for FBD and DDBD cases, respectively.

7 CONCLUSIONS

7.1 Summary and conclusions

Current state of practice in seismic design of building structures focuses on the principles developed in the so-called force-based design (FBD) method, which gives priority to strength in the structural design process. This fundamentally relates to historical development in the field and to how buildings are designed to withstand other actions such as gravity loads. With increased research in the field of earthquake engineering, it has been noted that displacements and ductility capacity are of major importance when designing against seismic actions. Exploiting the ductile behaviour of structures makes it possible to reduce economic costs of construction. Hence, a degree of damage is deemed acceptable under rare ground motions and collapse prevention becomes the primary design objective under very extreme conditions. As damage is more correlated to displacement than forces, the importance of deformations has been addressed by introducing modifications on the FBD procedures. However, member strengths are still the final product of the methodology while displacements are used as a final check. This lack of focus on displacements is further aggravated by a number of flaws in FBD philosophy that have been previously identified (Priestley, 2003).

As a result of the above, alternative design philosophies have been introduced in recent years. Some of them are grouped inside the displacement-based design methods, with Priestley et al. (2007) proposing a direct displacement-based design (DDBD) methodology for the seismic design of buildings. This method addresses many of the fundamental flaws encountered in FBD and turns the whole design procedure around to emphasise displacement capacity and demand from which required member strengths are then derived.

It is then clear that comparisons should be drawn from the structural response of buildings designed by both methods. This dissertation aimed to evaluate the collapse risk consistency between FBD and DDBD methodologies for reinforced concrete (RC) wall buildings. Here, collapse was defined as the point where lateral instability occurs, i.e. the point at which a large increase in drift/displacements under a small load increment is observed, such that the structure does not retain its load carrying capacity. Thus, the engineering demand parameter (EDP) to monitor during structural analysis was the maximum peak storey drift ratio (MPSD). Moreover, collapse risk was evaluated within a probabilistic framework, following the performance-based earthquake engineering (PBEE) framework that allows the expected structural performance under seismic events to be estimated in a probabilistic fashion.

Six buildings were designed, three of them for FBD and three according to DDBD. These correspond to two sets of 3-, 6- and 9-storey buildings. The floor plans and vertical loading conditions were kept equal for both designs, such that the final design differences were given by the seismic demand estimation procedure carried out by each method.

A high seismicity site was selected, namely a seismic category D and soil class C sector in the city of Cali, Colombia. Probabilistic seismic hazard analysis was conducted as it allowed more flexibility on hazard calculations. The design intensity level was taken as the 10% in 50 years probability of exceedance hazard level. The buildings designed by FBD method were calculated following the recommendations of the ASCE 7-16 (ASCE, 2016) building code. For the DDBD cases, the designs were carried out according to the guidelines provided in the DBD12 Model Code (Sullivan et al., 2012) and Priestley et al. (2007). For all designs, the reinforcement steel calculations were detailed according to the ACI 318-14 (ACI, 2014) rules. Capacity design principles were then implemented according to each methodology.

A numerical model of the buildings was built in OpenSees. The macro-model used to simulate the RC cantilever walls response is the multiple vertical line element model (MVLEM), implemented for analysis of flexure-dominated walls. Initially, non-linear static pushover analysis of the buildings was performed to obtain information on the first-mode response of the structures. Ground motion record selection was performed using a computational algorithm (Baker & Lee, 2018) following the conditional spectrum approach. The intensity measure IM

was the spectral acceleration at the fundamental period $Sa(T_1)$ and a total of 30 records were selected for each building.

Incremental Dynamic Analysis (IDA) was applied and a *Hunt, Trace and Fill* algorithm was used to characterise the structural response to increasing intensity. The 5% MPSD was conservatively chosen as the collapse threshold for the designed buildings. Hence, the $Sa(T_1)$ ordinate of the median IDA curve at this reference points describes the median collapse capacity of the structure.

The mean annual frequency of exceedance (MAFE) of the MPSD was computed by integrating the collapse fragility (defined by the median and dispersion of the IDA results characterised in terms of intensity) of each building with the corresponding hazard curve. This process was carried out using a closed-form equation proposed by Vamvatsikos (2013). Also, modelling uncertainty was incorporated in the MAFE computation by means of an user-specified input value based on existing studies (Kosić et al., 2016). The collapse margin ratio (CMR) as defined in the FEMA P695 guidelines was used to support the analysis of the MAFE results and the mean annual frequency of collapse (MAFC) was, again, taken with respect to the 5% MPSD reference threshold. The evaluation of the risk consistency across methods and within methods was performed and the results observed in this study lead to the following conclusions outlined next.

7.1.1 Design methods

Fundamental differences between both design methods were observed. FBD characterises seismic demand based on the acceleration response spectra and a period estimation. However, it has been shown that the latter is dependent on strength, meaning that iteration is often needed (although not commonly applied) to correctly estimate the seismic demands. This assumption, in addition to the common perception that higher strength equals more safety, is implied in various steps of the design procedure, e.g. the ASCE 7-16 base-shear scaling requirement when using MRSA and the limitations on the maximum allowable structural period for seismic considerations.

On the other hand, DDBD characterises seismic demand in terms of a displacement response spectrum, but the process is reversed. In FBD, the period is the input and the acceleration is the output while in DDBD, the designer uses a target displacement demand to compute the

structural period and required stiffness, as the relationship between strength and stiffness is acknowledged, then the required strengths are also determined based on this target displacement. Contrary to FBD, DDBD foresees different ductility capacity and force-reduction factors for different building configurations. Finally, DDBD uses modified capacity design rules and assumes expected material strengths for reinforcement calculation of the plastic hinge region. Hence, it should produce less expensive designs if compared to structures designed for the same level of demand applying the FBD method, which was observed in the case of the 6-storey building pair examined here.

Some issues were found in the determination of the displacement design spectrum for DDBD method. Firstly, the design spectrum is based on an estimation of the corner period, which might lay in the long-period range (e.g. $T>4s$) where there is a great variability on the estimation of spectral ordinates, particularly because the DDBD procedure suggests that the estimation of the corner period and peak displacement should be expressed as functions of magnitude and distance. Moreover, most GMPEs in PSHA models are calibrated with spectral accelerations and based in analogic records, which reduces the choices available with which to perform a correct hazard estimation in terms of displacements at long periods.

Significant differences were observed in the reinforcement layout of the buildings design by both methods. Except for the 3-storey case, in general, DDBD estimated larger demands (and thus, more required steel) with increasing number of floors than the FBD method using MRSA. This is reflected in the pushover curves of the 3- and 9-storey buildings in particular. In the 3-storey case, DDBD estimated a lower seismic demand, almost half, than the one estimated by FBD and reinforcement was governed by minimum reinforcement ratio rules. Conversely for the 9-storey case, DDBD estimated a much larger flexural demand than FBD, consequently more steel was required. These differences were reduced when the FBD was carried out using the ELF method. Despite being designed for different bending moment demands, the differences of FBD-6 and DDBD-6 designs were negligible. This was due to the fact that DDBD method uses expected material strengths for the design while FBD uses characteristic material strengths and applies strength reduction factors.

It is worth pointing out that the DDBD of the 6- and 9-storey buildings were “special cases” as the building displacement capacities exceed the displacement demand at the site for the design

intensity level. As explained in Section 4.3.6, iteration was needed to find the actual displacement response developed because of the demand at the site and the equivalent viscous damping implied by it. In this range, there was no unique solution to calculate the structural stiffness of the building. For these cases, the solution with the maximum possible strength was conservatively chosen and it was noted that more economic designs could have been found.

7.1.2 Collapse assessment and risk-consistency

The assumption of collapse at a 5% MPSD agrees with the observed drift ratio at which the median IDA curve of each building flattened out. The differences in CMR found between buildings were explained by the interaction of several factors as number of storeys, fundamental periods, median capacity, ductility and overstrength. These differences were generally extrapolated to the MAFC calculation.

For instance, buildings with high median capacity and long period (e.g. DDBD-9) exhibited a lower MAFC than buildings with high median capacity and shorter period (e.g. DDBD-3). This interaction of factors was also shown when comparing FBD-6 and DDBD-6 cases, since both had very similar values of ductility and overstrength (flexure and shear). However, DDBD-6 had higher median capacity than FBD-6 and larger base shear coefficient, but almost equal pushover-based period; as a result DDBD-6 had larger CMR and lower MAFC. It is also noticed that the DDBD-6 design provided a slightly larger reinforcement area than FBD-6.

Therefore, in some cases, the CMR and MAFC were controlled by the median capacity of each building, thus the building with higher median capacity had lower MAFC. In other cases, the differences in median capacity were somewhat compensated by differences in periods, which influence the MCE demand for each building (Section 6.6).

Contrary to what has been found in previous studies of collapse risk for RC frames, in this study no clear trend was observed in terms of how the MAFC and CMR vary with number of storeys for RC wall buildings. This again points out that a single factor is not always enough to predict the collapse performance of the structures.

Two different concepts of risk-consistency were evaluated: one corresponding to risk-consistency between design methods for the same building, which is the main aim of this

research, and risk consistency across buildings designed by the same methodology, i.e. “design method consistency”.

It was observed that the collapse risk can be considered consistent between FBD and DDBD methods for one of the design cases (6-storey building). MAFE curves of both designs followed essentially the same path to collapse. On the other hand, some differences were obtained for the 3-storey and 9-storey cases. The MAFE curves remained relatively close each other up to 4% to 5% MPSD where the differences then started to become noticeable.

When evaluating the risk consistency within design method, it was shown that there is no risk consistency between different buildings designed by the same methodology. This observation applied to both FBD and DDBD cases, although the FBD-6 and FBD-9 designs reached similar values of MAFC. What was more interesting, was that if the difference between the highest and lowest MAFC obtained by each method is computed, the values obtained were very similar (1.49E-0.4 for FBD and 1.40E-4 for DDBD). Thus, it could be said that the degree of within-method “inconsistency” is essentially the same.

7.2 Future research

In this work, the whole process from hazard estimation and buildings design up to collapse risk assessment was carried out for three different number of storeys RC wall buildings designed following FBD and DDBD, with the final aim being to evaluate the collapse risk consistency between both methods. Further research is needed to assess the impact of different design choices in the collapse performance of the structures. A comparison in terms of mean annual loss estimations can also be carried out, and consistency can be compared for damage levels other than collapse.

This study was limited to analysis of RC cantilever wall buildings. Further research could be extended to different building typologies and configurations. Also, different hazard levels could be used to provide a more extensive comparison of both methods.

For FBD cases, different design choices can be made to test the influence of some prescriptions that might not be applied in building codes different than ASCE 7-16. For example, redesigning the FBD buildings ignoring the limits on the structural period and the minimum base shear

requirements, as these are not enforced by other FBD building codes (e.g. EC8). Designs can also be carried out with a different method of structural analysis like the ELF method, which is a fundamental-mode approach, with similar level of complexity to the one used in DDBD. The impact of these choices on the MAFC computation should be addressed.

More research is needed on the characterisation of the displacement demand given by the displacement response spectrum in DDBD method, such that future editions of the DDBD model code include equations for its estimation. For instance, hazard maps of corner period and peak displacement values can be produced similar to what has been done in previous versions of ASCE, or a derivation might be established from the spectral acceleration maps that are used in several parts of the world. On the other hand, new force-reduction factors based on particular building characteristics, rather than structural typologies, could be tested within the FBD methodology, to improve the estimation of the structural response in the non-linear range and possibly reduce the scatter in collapse risk of buildings designed by the same methodology.

8 REFERENCES

- AIS-300, Yamín, L. E., Jaramillo, J. D., Aycardi, L. E., Carreño, M. L., Cano, L., ... Velásquez, C. A. (2010). Estudio General de Amenaza Sísmica de Colombia 2009, 1–206.
- Akkar, S., & Bommer, J. J. (2006). Influence of long-period filter cut-off on elastic spectral displacements. *Earthquake Engineering and Structural Dynamics*, 35(9), 1145–1165. <https://doi.org/10.1002/eqe.577>
- Ancheta, T. D., Darragh, R. B., Stewart, J. P., Seyhan, E., Silva, W. J., Chiou, B. S. J., ... Donahue, J. L. (2014). NGA-West2 Database. *Earthquake Spectra*, 30(3), 989–1005. <https://doi.org/10.1193/070913EQS197M>
- Antoniou, S., & Pinho, R. (2004). Advantages and limitations of adaptive and non-adaptive force-based pushover procedures. *Journal of Earthquake Engineering*, 8(4), 497–522. <https://doi.org/10.1080/13632460409350498>
- Araya-Letelier, G., Parra, P. F., Lopez-Garcia, D., Garcia-Valdes, A., Candia, G., & Lagos, R. (2019). Collapse risk assessment of a Chilean dual wall-frame reinforced concrete office building. *Engineering Structures*, 183(December 2017), 770–779. <https://doi.org/10.1016/j.engstruct.2019.01.006>
- Asociación Colombiana de Ingeniería Sísmica (AIS). Reglamento Colombiano de Construcción Sismo Resistente NSR-10 (2009). Bogota: Comisión Asesora Permanente para el Regimen de Construcciones Sismo Resistentes.
- Baker, J. W. (2011). Conditional Mean Spectrum: Tool for Ground-Motion Selection. *Journal of Structural Engineering*, 137(3), 322–331. [https://doi.org/10.1061/\(ASCE\)ST.1943-541X.0000215](https://doi.org/10.1061/(ASCE)ST.1943-541X.0000215)
- Baker, J. W., & Cornell, C. A. (2006a). Spectral shape, epsilon and record selection. *Earthquake Engineering and Structural Dynamics*, 35(9), 1077–1095. <https://doi.org/10.1002/eqe.571>
- Baker, J. W., & Cornell, C. A. (2006b). Which spectral acceleration are you using? *Earthquake Spectra*, 22(2), 293–312. <https://doi.org/10.1193/1.2191540>
- Baker, J. W., & Lee, C. (2018). An Improved Algorithm for Selecting Ground Motions to Match a

- Conditional Spectrum. *Journal of Earthquake Engineering*, 22(4), 708–723. <https://doi.org/10.1080/13632469.2016.1264334>
- Bazzurro, P., & Cornell, C. A. (1999). Disaggregation of seismic hazard. *Bulletin of the Seismological Society of America*, 89(2), 501–520. <https://doi.org/10.1785/0120060093>
- Bradley, B. A. (2013). A critical examination of seismic response uncertainty analysis in earthquake engineering. *Earthquake Engineering & Structural Dynamics*, 42(11), 1717–1729. <https://doi.org/10.1002/eqe.2331>
- Campbell, K. W., & Bozorgnia, Y. (2008). NGA Ground Motion Model for the Geometric Mean Horizontal Component of PGA, PGV, PGD and 5% Damped Linear Elastic Response Spectra for Periods Ranging from 0.01 to 10 s. *Earthquake Spectra*, 24(1), 139–171. <https://doi.org/10.1193/1.2857546>
- Carr, A. (1997). Damping Models for Inelastic Analyses. In *Asia-Pacific Vibration Conference '97* (pp. 42–48). Kyongju, Korea.
- Cauzzi, C., Faccioli, E., Vanini, M., & Bianchini, A. (2015). Updated predictive equations for broadband (0.01–10 s) horizontal response spectra and peak ground motions, based on a global dataset of digital acceleration records. *Bulletin of Earthquake Engineering*, 13(6), 1587–1612. <https://doi.org/10.1007/s10518-014-9685-y>
- Chang, G. A., & Mander, J. B. (1994). *Seismic Energy Based Fatigue Damage Analysis of Bridge Columns: Part 1 - Evaluation of Seismic Capacity*. (Vol. NCEER-94-0). State University of New York, Buffalo, N.Y. <https://doi.org/Technical Report NCEER-94-0006>
- Chopra, A. K., & McKenna, F. (2016). Modeling viscous damping in nonlinear response history analysis of buildings for earthquake excitation. *Earthquake Engineering & Structural Dynamics*, 45(2), 193–211. <https://doi.org/10.1002/eqe.2622>
- Cornell, C. A. (1968). ENGINEERING SEISMIC RISK ANALYSIS, 58(5), 1583–1606.
- Cornell, C. A., Jalayer, F., Hamburger, R. O., & Foutch, D. A. (2002). Probabilistic Basis for 2000 SAC Federal Emergency Management Agency Steel Moment Frame Guidelines. *Journal of Structural Engineering*, 128(4), 526–533. [https://doi.org/10.1061/\(ASCE\)0733-9445\(2002\)128:4\(526\)](https://doi.org/10.1061/(ASCE)0733-9445(2002)128:4(526))
- Cornell, C., & Krawinkler, H. (2000). Progress and challenges in seismic performance assessment. Retrieved from <http://peer.berkeley.edu/news/2000spring/index.html>
- Dabaghi, M., Saad, G., & Allhassania, N. (2019). Seismic Collapse Fragility Analysis of Reinforced Concrete Shear Wall Buildings. *Earthquake Spectra*, 35(1), 383–404. <https://doi.org/10.1193/121717EQS259M>
- Eads, L., Miranda, E., & Lignos, D. G. (2015). Average spectral acceleration as an intensity measure for collapse risk assessment. *Earthquake Engineering & Structural Dynamics*, 44(12), 2057–2073. <https://doi.org/10.1002/eqe.2575>
- Esteva, L. (1968). *Bases para la formulacion de decisiones de diseño sismico*. Universidad Autonoma

- Nacional de Mexico.
- Faccioli, E., Paolucci, R., & Rey, J. (2004). Displacement Spectra for Long Periods. *Earthquake Spectra*, 20(2), 347–376. <https://doi.org/10.1193/1.1707022>
- Faccioli, E., & Villani, M. (2009). Seismic hazard mapping for Italy in terms of broadband displacement response spectra. *Earthquake Spectra*, 25(3), 515–539. <https://doi.org/10.1193/1.3159004>
- FEMA/NEHRP. (2009). *Quantification of Building Seismic Performance Factors. FEMA P695*.
- Filippou, F. C., Popov, E. P., & Bertero, V. V. (1983). *Effects of Bond Deterioration on Hysteretic Behavior of Reinforced Concrete Joints*. Berkeley, CA.
- Fox, M. J., Sullivan, T. J., & Beyer, K. (2014). Comparison of force-based and displacement-based design approaches for RC coupled walls in New Zealand. *Bulletin of the New Zealand Society for Earthquake Engineering*, 47(3), 190–205. <https://doi.org/10.1089/acm.2011.0493>
- Galanis, P. H., & Moehle, J. P. (2015). Development of Collapse Indicators for Risk Assessment of Older-Type Reinforced Concrete Buildings. *Earthquake Spectra*, 31(4), 1991–2006. <https://doi.org/10.1193/080613EQS225M>
- Garcia, J., Weatherill, G., Pagani, M., Rodriguez, L., & Poggi, V. (2017). Building an Open Seismic Hazard Model for South America : the Sara-Psha Model. *16th World Conference on Earthquake - WCEE*, 1–13. <https://doi.org/10.1021/jm0707424>
- Georgiouidakis, M., Fragiadakis, M., & Papadrakakis, M. (2017). Multi-criteria selection and scaling of ground motion records using Evolutionary Algorithms. *Procedia Engineering*, 199, 3528–3533. <https://doi.org/10.1016/j.proeng.2017.09.504>
- Gogus, A., & Wallace, J. W. (2015). Seismic Safety Evaluation of Reinforced Concrete Walls through FEMA P695 Methodology. *Journal of Structural Engineering*, 141(10), 04015002. [https://doi.org/10.1061/\(ASCE\)ST.1943-541X.0001221](https://doi.org/10.1061/(ASCE)ST.1943-541X.0001221)
- Gokkaya, B. U., Baker, J. W., & Deierlein, G. G. (2016). Quantifying the impacts of modeling uncertainties on the seismic drift demands and collapse risk of buildings with implications on seismic design checks. *Earthquake Engineering & Structural Dynamics*, 45(10), 1661–1683. <https://doi.org/10.1002/eqe.2740>
- Goulet, C. A., Haselton, C. B., Mitrani-Reiser, J., Beck, J. L., Deierlein, G. G., Porter, K. A., & Stewart, J. P. (2007). Evaluation of the seismic performance of a code-conforming reinforced-concrete frame building—from seismic hazard to collapse safety and economic losses. *Earthquake Engineering & Structural Dynamics*, 36(13), 1973–1997. <https://doi.org/10.1002/eqe.694>
- Goulet, C. A., Watson-Lamprey, J., Baker, J., Haselton, C., & Luco, N. (2008). Assessment of Ground Motion Selection and Modification (GMSM) Methods for Non-Linear Dynamic Analyses of Structures. In *Geotechnical Earthquake Engineering and Soil Dynamics IV* (pp. 1–10). Reston, VA: American Society of Civil Engineers. [https://doi.org/10.1061/40975\(318\)3](https://doi.org/10.1061/40975(318)3)
- Gulkan, P., & Sozen, M. (1974). Inelastic Responses of Reinforced Concrete Structure to Earthquake

- Motions. *ACI Journal*, 71(12), 604–610. <https://doi.org/10.14359/7110>
- Gupta, B., & Kunnath, S. K. (2000). Adaptive Spectra-Based Pushover Procedure for Seismic Evaluation of Structures. *Earthquake Spectra*, 16(2), 367–392. <https://doi.org/10.1193/1.1586117>
- Haselton, C. B., Goulet, C. A., Mitrani-reiser, J., Beck, J. L., Deierlein, G. G., Porter, K. A., & Stewart, J. P. (2008). *An Assessment to Benchmark the Seismic Performance of a Code-Conforming Reinforced Concrete Moment-Frame Building*.
- Haselton, C., & Baker, J. W. (2006). Ground motion intensity measures for collapse capacity prediction: choice of optimal period and effect of spectral shape. *8th National Conference on Earthquake Engineering*, 10p.
- Ibarra, L. F., & Krawinkler, H. (2005). *Global Collapse of Frame Structures under Seismic Excitations*. <https://doi.org/10.1002/eqe>
- Iervolino, I., Galasso, C., & Cosenza, E. (2010). REXEL: computer aided record selection for code-based seismic structural analysis. *Bulletin of Earthquake Engineering*, 8(2), 339–362. <https://doi.org/10.1007/s10518-009-9146-1>
- Jayaram, N., Lin, T., & Baker, J. W. (2011). A Computationally efficient ground-motion selection algorithm for matching a target response spectrum mean and variance. *Earthquake Spectra*, 27(3), 797–815. <https://doi.org/10.1193/1.3608002>
- Jhon F. Hall. (2006). Problems encountered from the use (or misuse) of Rayleigh damping. *Earthquake Engineering and Structural Dynamics*, 35(5), 525–545. <https://doi.org/10.1002/eqe.541>
- Kanamori, H., & McNally, K. C. (1982). Variable rupture mode of the subduction zone along the Ecuador-Colombia coast. *Bulletin of the Seismological Society of America*, 72(4), 1241–1253. Retrieved from <https://authors.library.caltech.edu/48542/1/1241.full.pdf>
- Kolozvari, K., Arteta, C., Fischinger, M., Gavridou, S., Hube, M., Isaković, T., ... Wallace, J. W. (2018). Comparative Study on State-of-the-art Macroscopic Models for Planar Reinforced Concrete Walls. *ACI Structural Journal*, (November). <https://doi.org/10.14359/51710835>
- Kolozvari, K., Orakcal, K., & Wallace, J. W. (2018). New opensees models for simulating nonlinear flexural and coupled shear-flexural behavior of RC walls and columns. *Computers & Structures*, 196(December), 246–262. <https://doi.org/10.1016/j.compstruc.2017.10.010>
- Kolozvari, K., Terzic, V., Miller, R., & Saldana, D. (2018). Assessment of dynamic behavior and seismic performance of a high-rise rc coupled wall building. *Engineering Structures*, 176(April), 606–620. <https://doi.org/10.1016/j.engstruct.2018.08.100>
- Kosič, M., Dolšek, M., & Fajfar, P. (2016). Dispersions for the pushover-based risk assessment of reinforced concrete frames and cantilever walls. *Earthquake Engineering & Structural Dynamics*, 45(13), 2163–2183. <https://doi.org/10.1002/eqe.2753>
- Lin, T., Haselton, C. B., & Baker, J. W. (2013). Conditional spectrum-based ground motion selection. Part I: Hazard consistency for risk-based assessments. *Earthquake Engineering & Structural*

- Dynamics*, 42(12), 1847–1865. <https://doi.org/10.1002/eqe.2301>
- Luco, N., & Bazzurro, P. (2007). Does amplitude scaling of ground motion records result in biased nonlinear structural drift responses? *Earthquake Engineering & Structural Dynamics*, 36(13), 1813–1835. <https://doi.org/10.1002/eqe.695>
- McGuire, R. K. (1995). Probabilistic seismic hazard analysis and design earthquakes: closing the loop. *Bulletin of the Seismological Society of America*, 85(5), 1275–1284. <https://doi.org/10.1111/j.1365-2709.1995.tb05630.x>
- McKenna, F. (2011). OpenSees: A framework for earthquake engineering simulation. *Computing in Science and Engineering*, 13(4), 58–66. <https://doi.org/10.1109/MCSE.2011.66>
- McKenna, F., Fenves, G., & Scott, M. (2000). Open system for earthquake engineering simulation (OpenSees). Berkeley, CA.: University of California.
- Menegotto, M., & Pinto, P. E. (1973). Method of Analysis for Cyclically Loaded R. C. Plane Frames Including Changes in Geometry and Non-Elastic Behavior of Elements under Combined Normal Force and Bending. *Proceedings of IABSE Symposium*, 15–22. <https://doi.org/http://doi.org/10.5169/seals-13741>
- Moehle, J., & Deierlein, G. G. (2004). A framework methodology for performance-based earthquake engineering. *Proceedings of the 13 Th World Conference on Earthquake Engineering*, (679), 3812–3814. <https://doi.org/10.1061/9780784412121.173>
- Moehle, J. P., Ghodsi, T., Hooper, J. D., Fields, D. C., & Gedhada, R. (2012). *Seismic Design of Cast-in-Place Concrete Special Structural Walls and Coupling Beams A Guide for Practicing Engineers. NEHRP Seismic Design Technical Brief No. 6*. Gaithersburg, MD.
- Moschen, L., Medina, R. A., & Adam, C. (2017). A Ground Motion Record Selection Approach Based on Multiobjective Optimization. *Journal of Earthquake Engineering*, 2469(August), 1–19. <https://doi.org/10.1080/13632469.2017.1342302>
- NEHRP. (2003). *NEHRP Recommended Provisions for Seismic Regulations for New Buildings and Other Structures. FEMA 450-2 / 2003 Edition. Part 2: Commentary*.
- Noh, N. M., & Tesfamariam, S. (2018). Seismic Collapse Risk Assessment of Code-Conforming RC Moment Resisting Frame Buildings Designed With 2014 Canadian Standard Association Standard A23.3. *Frontiers in Built Environment*, 4(January 2019). <https://doi.org/10.3389/fbuil.2018.00053>
- Orakcal, K., & Wallace, J. W. (2006). Flexural modeling of reinforced concrete walls - Experimental verification. *ACI Structural Journal*, 103(2), 196–206.
- Park, R., & Paulay, T. (1975). *Reinforced Concrete Structures*. (Wiley, Ed.). Wiley. <https://doi.org/10.1002/9780470172834>
- Porter, K. A. (2009). An Overview of PEER's Performance-Based Earthquake Engineering Methodology. In *Ninth International Conference on Applications of Statistics and Probability in Civil Engineering (ICASP9)*. San Francisco. <https://doi.org/10.1.1.538.4550>

- Priestley, M.J.N. Calvi, G.M. Kowalsky, M. J. (2007). Direct Displacement-Based Seismic Design of Structures. In *2007 NZSEE Conference ABSTRACT*: (pp. 1–8). [https://doi.org/10.1016/S0141-0296\(01\)00048-7](https://doi.org/10.1016/S0141-0296(01)00048-7)
- Priestley, M. J. N. (2003). Myths and Fallacies in Earthquake Engineering , Revisited. *The Ninth Mallet - Milne Lecture*. Pavia, Italy: European School for Advanced Studies In Reduction of Seismic Risk (ROSE School).
- Priestley, M. J. N., & Amaris, A. D. (2002). *Dynamic Amplification of Seismic Moments and Shear Forces in Cantilever Walls*. (ROSE Resea). Pavia, Italy: IUSS Press.
- Priestley, M. J. N., Calvi, G. M., & Kowalsky, M. J. (2007). *Displacement-Based Seismic Design of Structures*. Pavia, Italy: IUSS Press.
- Priestley, M. J. N., Seible, F., & Calvi, G. M. (1996). *Seismic Design and Retrofit of Bridges*. (J. W. & Sons, Ed.). Hoboken, NJ, USA: John Wiley & Sons, Inc. <https://doi.org/10.1002/9780470172858>
- SAC/FEMA. (2000a). *Recommended Seismic Design Criteria for New Steel Moment-Frame Buildings, Report No. FEMA-350*. Washington, DC.
- SAC/FEMA. (2000b). *Recommended Seismic Evaluation and Upgrade Criteria for Existing Welded Steel Moment-Frame Buildings, Report No. FEMA-351*. Washington, DC. <https://doi.org/10.1017/CBO9781107415324.004>
- SEAOC. (1996). *Recommended Lateral Force Requirements and Commentary including Errata*.
- Shibata, A., & Sozen, M. A. (1976). The Substitute-Structure Method for Earthquake-Resistant Design of Reinforced Concrete Frames. *Journal of the Structural Division*, 02(1), 1–18.
- Shome, N., & Cornell, A. C. (1998). Normalization and Scaling Accelerograms for Nonlinear Structural Analysis. In *Proceedings of the 6th U.S. National Conference on Earthquake Engineering, Paper 243*. Seattle, Washington.
- Silva, V., Crowley, H., Pagani, M., Monelli, D., & Pinho, R. (2014). Development of the OpenQuake engine, the Global Earthquake Model's open-source software for seismic risk assessment. *Natural Hazards*, 72(3), 1409–1427. <https://doi.org/10.1007/s11069-013-0618-x>
- Spacone, E., Filippou, F. C., & Taucer, F. F. (1996). FIBRE BEAM–COLUMN MODEL FOR NON-LINEAR ANALYSIS OF R/C FRAMES: PART II. APPLICATIONS. *Earthquake Engineering & Structural Dynamics*, 25(7), 727–742. [https://doi.org/10.1002/\(SICI\)1096-9845\(199607\)25:7<727::AID-EQE577>3.3.CO;2-F](https://doi.org/10.1002/(SICI)1096-9845(199607)25:7<727::AID-EQE577>3.3.CO;2-F)
- Sullivan, T. J., Priestley, M. J. N., & Calvi, G. M. (2012). *A Model Code for the Displacement-Based Seismic Design of Structures*. DBD12. (2012th ed.). Pavia, Italy: IUSS Press.
- UNESCO. (1972). *Report of consultative meeting of experts on the statistical study of natural hazards and their consequences. Document SC/WS/500* ,.
- Vamvatsikos, D. (2013). Derivation of new SAC/FEMA performance evaluation solutions with second-order hazard approximation. *Earthquake Engineering & Structural Dynamics*, 42(8), 1171–1188.

- <https://doi.org/10.1002/eqe.2265>
- Vamvatsikos, D., & Cornell, C. A. (2002). Incremental dynamic analysis. *Earthquake Engineering & Structural Dynamics*, 31(3), 491–514. <https://doi.org/10.1002/eqe.141>
- Vamvatsikos, D., & Cornell, C. A. (2005). Developing efficient scalar and vector intensity measures for IDA capacity estimation by incorporating elastic spectral shape information. *Earthquake Engineering & Structural Dynamics*, 34(13), 1573–1600. <https://doi.org/10.1002/eqe.496>
- Wilson, E. L., & Penzien, J. (1972). Evaluation of orthogonal damping matrices. *International Journal for Numerical Methods in Engineering*, 4(1), 5–10. <https://doi.org/10.1002/nme.1620040103>
- Zareian, F., & Krawinkler, H. (2007). Assessment of probability of collapse and design for collapse safety. *Earthquake Engineering & Structural Dynamics*, 36(13), 1901–1914. <https://doi.org/10.1002/eqe.702>

APPENDIX A. FORCE-BASED DESIGN

Force-based design of the studied buildings was carried out following the recommendations of the ASCE 7-16 and ACI 318-14 standards. Here, main checks and calculations are presented for the three structures designed.

A.1 General Requirements

The seismic response parameters are chosen based on the UHS obtained from PSHA and the Site Class C conditions defined in Chapter 3. The computed spectral acceleration values are presented in Table A.1, where subscript “s” denotes short-periods, “1” denotes one-second period, F_a and F_v are short-period and velocity-based site coefficients, respectively; subscript “M” stands for modified parameter and subscript “D” correspond to design parameters. Importance factor I_e equal to 1 and Risk Category II are assumed for all buildings, and designs are carried out for Seismic Design Category D. The analysis procedure used for seismic design is the Modal Response Spectrum Analysis (MRSA).

Table A1. Seismic response parameters for seismic design requirements.

MCE		Site Coefficients	
S_s	S_1	F_a	F_v
1.42	0.315	1.000	1.485
Adjusted MCE		Design Parameters	
S_{MS}	S_{M1}	S_{DS}	S_{D1}
1.42	0.467	0.947	0.312

Table A2 shows the design coefficients used for all designs, as per Table 12.2-1 of ASCE 7-16. The structural configuration of the buildings is given in Figure 4.1 of this document.

Table A2. Response modification “R”, overstrength “ Ω_0 ” and deflection amplification coefficients.

Location	Response Direction	Building Frame Type	R	Ω_0	Cd
Cali, Colombia	N-S	Special RC Structural Walls	6	2.5	5
	E-W	Special RC Structural Walls	6	2.5	5

Wind loads are not considered, then the design of the buildings is governed by the two following load combinations (Equations A1 and A2). The seismic actions E are considered by Equation A3, where the redundancy factor ρ is assumed equal to 1.0 for all buildings, to be consistent through both design methods. Table A3 shows the final load combinations used for design.

$$1.2D + 0.5L \pm 1.0E \quad (\text{A1})$$

$$0.9D \pm 1.0E \quad (\text{A2})$$

$$E = \rho Q E \pm 0.2 S_{DS} D \quad (\text{A3})$$

Table A3. Load combinations used for FBD-3, FBD-6 and FBD-9 designs.

Load Combinations
1.39D + 0.5L + 1Qe
1.39D + 0.5L - 1Qe
0.71D + 1Qe
0.71D - 1Qe

The values of the applied dead and live loads and material strengths are described in Section 4.1. The details of the computational model used for structural analyses of FBD buildings are provided in Section 4.2.3 of this thesis.

A.2 Period Estimation and Base-Shear Calculation

In Section 4.2.3 the requirements regarding base shear calculation when using MRSA were discussed, particularly the ones requiring that the MRSA-computed base shear must be cross-checked against the ELF-computed base shear, such that the minimum base shear used for design is equivalent to 100% of the ELF calculation. The formulation for structural period and the base shear determination according to Equivalent Lateral Force (ELF) method are given in

Section 12.8 of the ASCE 7-16 Standard. The period limit established by the standard governs the design of the three buildings, as shown in Table 4.2, presented here again as Table A4 for convenience.

Table A4. Comparison of different period definitions results. MRSA vs ASCE 7-16 formulas.

Design	Method for Period Calculation			
	MRSA	1. $T_a = C_t h_n^x$	2. $T_a = 0.1N$	3. $T = CuTa$
FBD - 3	0.34	0.254	0.3	0.355
FBD - 6	1.17	0.426	0.6	0.597
FBD - 9	1.41	0.578	0.9	0.809

1. Height dependent formula.

2. Number of storeys dependent formula.

3. Maximum T allowed by the code of design purposes, overrides MRSA if MRSA>CuTa

Table A5 shows the results obtained for the ELF base shear computation of each building. It is noticed that the base shear increases with increasing number of stories while the base shear coefficient decreases.

Table A5. ELF base shear and base shear coefficients computed for FBD buildings.

Model	Weight (kN)	Base Shear Analysis* V _b (kN)	Base Shear Coefficient Analysis (V _b /W)
FBD - 3	10988.694	1608.83	0.1464
FBD - 6	22726.188	1978.4	0.0871
FBD - 9	35993.61	2316.15	0.0643

*Taken prior to any capacity design considerations for reinforcement

A.3 ELF Vertical Distribution of Seismic Forces and Accidental Torsion Checks

For simplicity, accidental torsion is checked following ELF procedures, the base shear is vertically distributed along the structure according to Section 12.8 of ASCE 7-16. This distribution is presented in Tables A6, A7 and A8 for the FBD-3, FBD-6 and FBD-9 designs respectively. The accidental torsion and torsion irregularity checks of the FBD-9 design is shown in Tables A9 and A10, given the symmetry of the buildings and the results obtained for this model, the accidental torsion results for FBD-3 and FBD-6 are omitted here, as all design passed the checks.

Table A6. (ELF) FBD-3 building, vertical distribution of seismic forces

Level	Hi (m)	Weight (kN)	Wh^k	Whk/SUM (Cvx)	Force Fx (kN)	Story Shear Vx (kN)	OVT Moment Mx (kN-m)
3 (Roof)	9	3163.70	28473.28	0.45	719.29	719.29	0.00
3	6	3912.50	23474.99	0.37	593.03	1312.32	2157.88
2	3	3912.50	11737.49	0.18	296.51	1608.83	6094.84
Total		10988.69	63685.76	1.00	1608.83	--	10921.34

Table A7. (ELF) FBD-6 building, vertical distribution of seismic forces

Level	Hi (m)	Weight (kN)	Wh^k	Whk/SUM (Cvx)	Force Fx (kN)	Story Shear Vx (kN)	OVT Moment Mx (kN-m)
6 (Roof)	18	3163.70	65519.76	0.25	493.67	493.67	0.00
6	15	3912.50	66928.08	0.25	504.28	997.95	1481.01
5	12	3912.50	52965.90	0.20	399.08	1397.04	4474.88
4	9	3912.50	39173.80	0.15	295.16	1692.20	8665.99
3	6	3912.50	25607.11	0.10	192.94	1885.14	13742.59
2	3	3912.50	12380.12	0.05	93.28	1978.42	19398.01
Total	0	22726.19	262574.78	1.00	1978.42	--	25333.27

Table A8. (ELF) FBD-9 building, vertical distribution of seismic forces

Level	Hi (m)	Weight (kN)	Wh^k	Whk/SUM (Cvx)	Force Fx (kN)	Story Shear Vx (kN)	OVT Moment Mx (kN-m)
9 (Roof)	27	3333.69	149829.58	0.18	419.54	419.54	0.00
9	24	4082.49	160153.37	0.19	448.45	868.00	1258.63
8	21	4082.49	137270.67	0.17	384.38	1252.38	3862.63
7	18	4082.49	114889.43	0.14	321.71	1574.08	7619.76
6	15	4082.49	93079.99	0.11	260.64	1834.72	12342.01
5	12	4082.49	71938.72	0.09	201.44	2036.16	17846.17
4	9	4082.49	51606.77	0.06	144.51	2180.67	23954.65
3	6	4082.49	32313.89	0.04	90.48	2271.15	30496.65
2	3	4082.49	14514.96	0.02	40.64	2311.79	37310.10
Total	0	35993.61	825597.38	1.00	2311.79	--	44245.49

Table A9. (ELF) FBD-9 Computation of forces for accidental torsion checks.

Level	Force Fx (kN)	N-S Dimension (m)	N-S Torsion (kNm)	E-W Dimension (m)	E-W Torsion (kNm)
9 (Roof)	419.54	24.00	503.45	24.00	503.45
9	448.45	24.00	538.14	24.00	538.14
8	384.38	24.00	461.25	24.00	461.25
7	321.71	24.00	386.05	24.00	386.05
6	260.64	24.00	312.77	24.00	312.77
5	201.44	24.00	241.73	24.00	241.73
4	144.51	24.00	173.41	24.00	173.41
3	90.48	24.00	108.58	24.00	108.58
2	40.64	24.00	48.77	24.00	48.77

Table A10. (ELF) FBD-9 Torsion irregularity check.

Story	Story Displ. North End (cm)	Story Displ. South End (cm)	Story Drift North End (cm)	Story Drift South End (cm)	Avg Drift (cm)	Max Drift / Avg	CHECK
9	6.68	7.38	0.99	1.10	1.05	1.053	REGULAR
8	5.69	6.28	1.00	1.10	1.05	1.048	REGULAR
7	4.69	5.18	0.97	1.07	1.02	1.049	REGULAR
6	3.72	4.11	0.94	1.03	0.99	1.046	REGULAR
5	2.78	3.08	0.85	0.95	0.90	1.056	REGULAR
4	1.93	2.13	0.75	0.83	0.79	1.051	REGULAR
3	1.18	1.30	0.60	0.66	0.63	1.048	REGULAR
2	0.58	0.64	0.41	0.45	0.43	1.047	REGULAR
1	0.17	0.19	0.17	0.19	0.18	1.056	REGULAR

A.4 Modal Analysis Results

Tables A11 to A13 show the dynamic properties of each structure obtained by modal analysis of the numerical models, using structural analysis software. The total number of modes used in each building was selected to have at least 95% of mass participation, in general 12 modes were used.

Table A11. FBD-3 Modal response characteristics.

Mode	Period (sec)	Rel.mas.UX (%)*	Rel.mas.UY (%)*	Cur.mas.UX (%)**	Cur.mas.UY (%)**	Description
1	0.34	59.38	15.00	59.38	15.000	1st Mode - X
2	0.34	74.38	74.38	15.00	59.380	1st Mode - Y
3	0.20	74.38	74.38	0.00	0.000	1st Mode - Torsion
4	0.08	80.61	90.04	6.23	15.660	2nd Mode -Y
5	0.08	96.27	96.27	15.66	6.230	2nd Mode -X
6	0.05	96.27	96.27	0.00	0.000	2nd Mode - Torsion
7	0.04	96.63	98.94	0.36	2.670	3rd Mode - Y
8	0.04	99.30	99.30	2.67	0.360	3rd Mode - X
9	0.03	99.30	99.30	0.00	0.000	4th Mode - Torsion

*Accumulated modal mass. **Current mode mass.

Table A12. FBD-6 Modal response characteristics.

Mode	Period (sec)	Rel.mas.UX (%)	Rel.mas.UY (%)	Cur.mas.UX (%)	Cur.mas.UY (%)	Description
1	1.17	0.00	67.26	0.000	67.260	1st Mode - Y
2	1.17	67.26	67.26	67.260	0.000	1st Mode - X
3	0.70	67.26	67.26	0.000	0.000	1st Mode - Torsion
4	0.21	89.08	67.26	21.820	0.000	2nd Mode -X
5	0.21	89.08	89.08	0.000	21.820	2nd Mode -Y
6	0.13	89.08	89.08	0.000	0.000	2nd Mode - Torsion
7	0.09	95.87	89.08	6.790	0.000	3rd Mode - X
8	0.09	95.87	95.87	0.000	6.790	3rd Mode - Y
9	0.06	97.38	97.00	1.510	1.130	4th Mode - X
10	0.06	98.51	98.51	1.130	1.510	4th Mode - Y
11	0.05	98.51	98.51	0.000	0.000	3rd Mode Torsion
12	0.04	99.43	98.53	0.920	0.020	5th Mode - X

*Accumulated modal mass. **Current mode mass.

Table A13. FBD-9 Modal response characteristics.

Mode	Period (sec)	Rel.mas.UX (%)	Rel.mas.UY (%)	Cur.mas.UX (%)	Cur.mas.UY (%)	Description
1	1.41	65.36	0.00	65.360	0.00	1st Mode - X
2	1.41	65.36	65.36	0.000	65.36	1st Mode - Y
3	0.86	65.36	65.36	0.000	0.00	1st Mode - Torsion
4	0.26	86.70	65.42	21.340	0.06	2nd Mode -X
5	0.26	86.76	86.76	0.060	21.34	2nd Mode -Y
6	0.16	86.76	86.76	0.000	0.00	2nd Mode - Torsion
7	0.11	87.07	93.43	0.320	6.67	3rd Mode - Y
8	0.11	93.74	93.74	6.670	0.32	3rd Mode - X
9	0.07	93.74	93.74	0.000	0.00	3rd Mode - Torsion

10	0.07	94.64	95.92	0.900	2.18	4th Mode - Y
11	0.07	96.82	96.82	2.180	0.90	4th Mode - X
12	0.05	97.38	97.72	0.560	0.90	5th Mode - Y

*Accumulated modal mass. **Current mode mass.

A.5 MRSA Base Shear Scaling Factors

To comply with the 100% ELF base shear requirement, a scaling factor was computed and applied to the design acceleration response spectrum. Therefore, the obtained scaled spectrum is used for MRSA analyses and members design. Table A14 shows the scale factor computation and the final base shear used for design.

Table A14. Scale factors for 100% ELF requirement and final base shear (Vb) for MRSA procedure.

Design	Direction	Vb,ELF (kN)	Vb,MRSA (Elastic) (kN)	R/Ie	Vb,MRSA (Reduced) (kN)	Scale Factor	Vb,MRSA (Design) (kN)
FBD-3	X-Dir	1608.83	7124.82	6.00	1187.47	1.35	1608.83
	Y-Dir	1608.83	7124.82	6.00	1187.47	1.35	1608.83
FBD-6	X-Dir	1978.42	6910.68	6.00	1151.78	1.72	1978.42
	Y-Dir	1978.42	6910.68	6.00	1151.78	1.72	1978.42
FBD-9	X-Dir	2311.79	9526.88	6.00	1587.81	1.46	2311.79
	Y-Dir	2311.79	9526.88	6.00	1587.81	1.46	2311.79

A.6 Drift and P-Delta Checks

Drift and P-Delta checks are carried out following Sections 12.8 and 12.9 of ASCE 7-16 Standard. Results are shown in Tables A15 to A20. According to the Standard, if the stability coefficient is lower than 0.10, P-Delta effects can be neglected in the analysis. The verification is based on the MRSA analysis without limits in the structural period, as this implies a more flexible structure, also, 40% of story live load is used in the verification. As it is observed in the Tables, none of the buildings exceed the stability coefficient limit, so P-Delta effects are neglected in design.

Table A15. FBD-3 Drift check.

Story	Inter-story Height (m)	Story Displacement δ (cm)	Reduced δ (cm)	Story Drift (cm)	Story Drift*Cd (cm)	Drift Ratio (%)	CHECK	Drift limit (%)
3	3.00	4.56	0.76	0.32	1.62	0.539%	OK!!	
2	3.00	2.62	0.44	0.29	1.43	0.475%	OK!!	2%
1	3.00	0.91	0.15	0.15	0.76	0.253%	OK!!	

Table A16. FBD-6 Drift check.

Story	Inter-story Height (m)	Story Displacement δ (cm)	Reduced δ (cm)	Story Drift (cm)	Story Drift*Cd (cm)	Drift Ratio (%)	CHECK	Drift limit (%)
6	3.00	24.83	4.14	0.94	4.68	1.558%	OK!!	
5	3.00	19.22	3.20	0.91	4.54	1.514%	OK!!	
4	3.00	13.77	2.30	0.84	4.18	1.392%	OK!!	
3	3.00	8.76	1.46	0.71	3.55	1.183%	OK!!	2%
2	3.00	4.50	0.75	0.52	2.58	0.858%	OK!!	
1	3.00	1.41	0.24	0.24	1.18	0.392%	OK!!	

Table A17. FBD-9 Drift check.

Story	Inter-story Height (m)	Story Displacement δ (cm)	Reduced δ (cm)	Story Drift (cm)	Story Drift*Cd (cm)	Drift Ratio (%)	CHECK	Drift limit (%)
9	3.00	25.06	4.18	0.63	3.15	1.050%	OK!!	
8	3.00	21.28	3.55	0.63	3.13	1.042%	OK!!	
7	3.00	17.53	2.92	0.61	3.03	1.008%	OK!!	
6	3.00	13.90	2.32	0.57	2.87	0.956%	OK!!	
5	3.00	10.46	1.74	0.53	2.63	0.875%	OK!!	2%
4	3.00	7.31	1.22	0.46	2.30	0.767%	OK!!	
3	3.00	4.55	0.76	0.37	1.87	0.622%	OK!!	
2	3.00	2.31	0.39	0.27	1.33	0.442%	OK!!	
1	3.00	0.72	0.12	0.12	0.60	0.200%	OK!!	

Table A18. FBD-3 Stability coefficient check for P-Delta verifications.

Story	Story Drift (mm)	Story Shear (kN)	Story Dead Load (kN)	Story Live Load (kN)	Total Story Load (kN)	Accumulated Story Load (kN)	Stability Coefficient (Θ)	CHECK
3	16.17	770.94	3163.70	576.00	3739.70	3739.70	0.0052	OK!!
2	14.25	1312.67	3912.50	576.00	4488.50	8228.20	0.0060	OK!!
1	7.58	1608.83	3912.50	576.00	4488.50	12716.69	0.0040	OK!!

Table A19. FBD-6 Stability coefficient check for P-Delta verifications.

Story	Story Drift (mm)	Story Shear (kN)	Story Dead Load (kN)	Story Live Load (kN)	Total Story Load (kN)	Accumulated Story Load (kN)	Stability Coefficient (Θ)	CHECK
6	46.75	685.87	3163.70	576.00	3739.70	3739.70	0.0170	OK!!
5	45.42	959.67	3912.50	576.00	4488.50	8228.20	0.0260	OK!!
4	41.75	1013.80	3912.50	576.00	4488.50	12716.69	0.0349	OK!!
3	35.50	1275.93	3912.50	576.00	4488.50	17205.19	0.0319	OK!!
2	25.75	1666.20	3912.50	576.00	4488.50	21693.69	0.0224	OK!!
1	11.75	1978.40	3912.50	576.00	4488.50	26182.19	0.0104	OK!!

Table A20. FBD-9 Stability coefficient check for P-Delta verifications.

Story	Story Drift (mm)	Story Shear (kN)	Story Dead Load (kN)	Story Live Load (kN)	Total Story Load (kN)	Accumulated Story Load (kN)	Stability Coefficient (Θ)	CHECK
9	31.50	622.70	3333.69	576.00	3909.69	3909.69	0.0132	OK!!
8	31.25	1021.31	4082.49	576.00	4658.49	8568.18	0.0175	OK!!
7	30.25	1092.42	4082.49	576.00	4658.49	13226.67	0.0244	OK!!
6	28.67	1090.03	4082.49	576.00	4658.49	17885.16	0.0314	OK!!
5	26.25	1201.12	4082.49	576.00	4658.49	22543.65	0.0328	OK!!
4	23.00	1474.28	4082.49	576.00	4658.49	27202.14	0.0283	OK!!
3	18.67	1822.71	4082.49	576.00	4658.49	31860.63	0.0218	OK!!
2	13.25	2147.67	4082.49	576.00	4658.49	36519.12	0.0150	OK!!
1	6.00	2316.15	4082.49	576.00	4658.49	41177.61	0.0071	OK!!

A.7 Structural Design of the Walls

The structural analysis is performed considering the computed load combination factors. Strength demands on structural members (here only RC walls are designed) are obtained, CQC modal combination is used to compute the overall response. Tables A21 to A23 show the factored loads per wall for design, the total loads per orthogonal direction of the building can be computed taking 2 times the values shown.

Table A21. FBD-3 Final loads for wall design (load values for a single wall).

Story / Support Level	Axial (kN)		Shear(kN)		Moment (kNm)	
	1.39D + 0.5L +1Qe	0.71D + 1Qe	1.39D + 0.5L +1Qe	0.71D + 1Qe	1.39D + 0.5L +1Qe	0.71D + 1Qe
3 / R	258.52	117.87	385.47	385.47	1052.37	1052.37
2 / 3	569.46	262.53	656.34	656.34	2916.60	2916.60
1 / 2	880.24	407.09	804.42	804.42	5270.95	5270.95

Table A22. FBD-6 Final loads for wall design (load values for a single wall).

Story / Support Level	Axial (kN)		Shear(kN)		Moment (kNm)	
	1.39D + 0.5L +1Qe	0.71D + 1Qe	1.39D + 0.5L +1Qe	0.71D + 1Qe	1.39D + 0.5L +1Qe	0.71D + 1Qe
6 / R	258.52	117.87	342.94	342.94	939.36	939.36
5 / 6	569.51	262.53	479.84	479.84	2306.82	2306.82
4 / 5	880.40	407.16	506.90	506.90	3562.70	3562.70
3 / 4	1191.32	551.79	637.97	637.97	4783.56	4783.56
2 / 3	1502.23	696.42	833.10	833.10	6382.52	6382.52
1 / 2	1813.08	841.04	989.20	989.20	8760.22	8760.22

Table A23. FBD-9 Final loads for wall design (load values for a single wall).

Story / Support Level	Axial (kN)		Shear(kN)		Moment (kNm)	
	1.39D + 0.5L +1Qe	0.71D + 1Qe	1.39D + 0.5L +1Qe	0.71D + 1Qe	1.39D + 0.5L +1Qe	0.71D + 1Qe
9 / R	333.40	154.08	311.35	311.35	841.17	841.17
8 / 9	731.26	341.07	510.65	510.65	2313.62	2313.62
7 / 8	1129.05	528.03	546.21	546.21	3865.47	3865.47
6 / 7	1526.84	715.00	545.02	545.02	5218.78	5218.78
5 / 6	1924.64	901.97	600.56	600.56	6368.38	6368.38
4 / 5	2322.43	1088.93	737.14	737.14	7528.55	7528.55
3 / 4	2720.22	1275.90	911.35	911.35	9024.19	9024.19
2 / 3	3118.00	1462.86	1073.83	1073.83	11096.96	11096.96
1 / 2	3515.53	1649.71	1158.07	1158.07	13847.17	13847.17

The reinforcement detailing is carried out following Chapter 18 of ACI 318-14, design is completed taking into account axial-flexure interaction, thus the $0.71D + 1Qe$ load combination case becomes critical to calculate flexural reinforcement, as lower axial force affects the nominal moment capacity of the wall. Horizontal reinforcement for shear loads is completed

with the equations provided in the code, results are shown in Tables A24 to A26. The minimum horizontal reinforcement ratio (ρ_t) is 0.0025, vertical reinforcement in the web must be equal or larger than the horizontal one (Tables A27 to A29). A reduction factor $\phi=0.75$ is used for shear calculations and $\phi=0.9$ for flexural design (Tables A27 to A32). The rebars layout is changed every three floors to have a more “optimized” design, horizontal reinforcement is calculated only for the base and assumed to be equal for the rest of the building, because these bars are not needed in the OpenSees numerical model, furthermore, the shear design is governed by minimum reinforcement requirements so the same shear solution is used for the whole building. Boundary elements reinforcement results are shown in Tables A33 to A35, verification of how many storeys need boundary elements was performed but only one example is shown here (Table A36), as boundary elements were extended until roof top in all buildings. Transversal reinforcement is calculated for the boundary elements as presented in Tables A37 to A39. All results correspond to design of a single wall.

Table A24. FBD-3 Web horizontal reinforcement verification.

Story	Spacing (mm)	Total #Bars	#Rebar Type	As,Horiz (mm ²)	Horizontal Ratio (pt)	CHECK As	CHECK Spacing	ϕV_n provided (kN)
Base	300	18	4	2322	0.00287	OK!!	OK!!	1893.20

Table A25. FBD-6 Web horizontal reinforcement verification.

Story	Spacing (mm)	Total #Bars	#Rebar Type	As,Horiz (mm ²)	Horizontal Ratio (pt)	CHECK As	CHECK Spacing	ϕV_n provided (kN)
Base	300	18	4	2322	0.00287	OK!!	OK!!	1893.20
4th	300	18	4	2322	0.00287	OK!!	OK!!	1893.20

Table A26. FBD-9 Web horizontal reinforcement verification.

Story	Spacing (mm)	Total #Bars	#Rebar Type	As,Horiz (mm ²)	Horizontal Ratio (pt)	CHECK As	CHECK Spacing	ϕV_n provided (kN)
Base	300	18	4	2322	0.00287	OK!!	OK!!	2839.80
4th	300	18	4	2322	0.00287	OK!!	OK!!	2839.80
6th	300	18	4	2322	0.00287	OK!!	OK!!	2839.80

Table A27. FBD-3 Web vertical reinforcement verification.

Story	Spacing (mm)	Total #Bars	#Rebar Type	As,Vertical (mm ²)	Vertical Ratio (ρl)	CHECK	CHECK Spacing
Base	200	28	4	3612	0.00430	OK!!	OK!!

Table A28. FBD-6 Web vertical reinforcement verification.

Story	Spacing (mm)	Total #Bars	#Rebar Type	As,Vertical (mm ²)	Vertical Ratio (ρl)	CHECK	CHECK Spacing
Base	200	28	5	5600	0.00667	OK!!	OK!!
4th	200	28	4	3612	0.00430	OK!!	OK!!

Table A29. FBD-9 Web vertical reinforcement verification.

Story	Spacing (mm)	Total #Bars	#Rebar Type	As,Vertical (mm ²)	Vertical Ratio (ρl)	CHECK	CHECK Spacing
Base	240	38	4	4902	0.00358	OK!!	OK!!
4th	240	38	4	4902	0.00358	OK!!	OK!!
6th	240	38	4	4902	0.00358	OK!!	OK!!

Table A30. FBD-3 Summary design for flexure.

Story	Pu, Max (kN)	Pu, Min (kN)	Mu (kNm)	Mn,CS (kNm)	c (mm)	φMn,CS (kNm)	Shear Magnification*	Rebars Boundary	Rebars Web
3	258.52	117.87	1052.37	6795.30	390.00	6115.79	--		
2	569.46	262.53	2916.60	7304.30	426.10	6573.88	2.50		
Base	880.24	407.09	5270.95	7802.60	462.50	7022.38	1.48	12 #5	28 #4

*Such that capacity design principles are used and a reduction factor of 0.75 instead of 0.6 is allowed for shear.

Table A31. FBD-6 Summary design for flexure.

Story	Pu, Max (kN)	Pu, Min (kN)	Mu (kNm)	Mn,CS (kNm)	c (mm)	$\phi M_{n,CS}$ (kNm)	Shear Magnification*	Rebars Boundary	Rebars Web
6	258.52	117.87	939.36	5538.80	361.40	4984.88	--		
5	569.51	262.53	2306.82	6056.80	401.50	5451.08	2.63		
4	880.40	407.16	3562.70	6560.70	441.00	5904.62	1.84	12 # 4	28 #4
3	1191.32	551.79	4783.56	11046.5	615.00	9941.82	2.31		
2	1502.23	696.42	6382.52	11496.1	652.20	10346.50	1.80		
Base	1813.08	841.04	8760.22	11929.3	688.30	10736.30	1.36	12#6	28#5

*Such that capacity design principles are used and a reduction factor of 0.75 instead of 0.6 is allowed for shear.

Table A32. FBD-9 Summary design for flexure.

Story	Pu, Max (kN)	Pu, Min (kN)	Mu (kNm)	Mn,CS (kNm)	c (mm)	$\phi M_{n,CS}$ (kNm)	Shear Magnification*	Rebars Boundary	Rebars Web
9	333.40	154.08	841.17	10142.0	455.10	9127.80	--		
8	731.26	341.07	2313.62	11167.2	508.40	10050.5	4.83		
7	1129.05	528.03	3865.47	12170.5	561.60	10953.4	3.15	12#4	38 #4
6	1526.84	715.00	5218.78	13159.0	616.80	11843.1	2.52		
5	1924.64	901.97	6368.38	14125.0	671.50	12712.5	2.22		
4	2322.43	1088.93	7528.55	15073.1	726.70	13565.8	2.00	12#4	38 #4
3	2720.22	1275.90	9024.19	17912.9	794.50	16121.6	1.98		
2	3118.00	1462.86	11096.96	18819.6	848.20	16937.7	1.70		
Base	3515.53	1649.71	13847.17	19711.3	903.00	17740.2	1.42	12 #5	38 #4

*Such that capacity design principles are used and a reduction factor of 0.75 instead of 0.6 is allowed for shear.

Table A33. FBD-3 Boundary element vertical reinforcement verification.

Story	Spacing (mm)	Total #Bars	#Rebar	As,Vertical (mm ²)	Vertical Ratio (pl,b)	CHECK	CHECK Spacing
Base	90	12	12 #5	2400	0.016	OK!!	OK!!

Table A34. FBD-6 Boundary element vertical reinforcement verification.

Story	Spacing (mm)	Total #Bars	#Rebar	Asb,Vertical (mm ²)	Vertical Ratio (pl,b)	CHECK	CHECK Spacing
Base	90	12	12#6	3408	0.0227	OK!!	OK!!
4th	90	12	12 # 4	1548	0.0103	OK!!	OK!!

Table A35. FBD-9 Boundary element vertical reinforcement verification.

Story	Spacing (mm)	Total #Bars	#Rebar	Asb,Vertical (mm ²)	Vertical Ratio (pl,b)	CHECK	CHECK Spacing
Base	110	12	12 #5	2400	0.0133	OK!!	OK!!
4th	110	12	12#4	1548	0.0086	OK!!	OK!!
7th	110	12	12#4	1548	0.0086	OK!!	OK!!

Table A36. FBD-6 Boundary element requirement check.

Story	N.A. - c (mm) (For Mn,CS and Pu)	δu (mm) - Design Displacement	lw (mm)	hw(mm)	δu/hw >=0.005	Check Factor	Boundary Element Required?
6	361.4	206.92	4000	18000	0.0115	386.63	NO!
5	401.5	206.92	4000	18000	0.0115	386.63	YES!
4	441.0	206.92	4000	18000	0.0115	386.63	YES!
3	615.0	206.92	4000	18000	0.0115	386.63	YES!
2	652.2	206.92	4000	18000	0.0115	386.63	YES!
Base	688.3	206.92	4000	18000	0.0115	386.63	YES!

Table A37. FBD-3 Boundary element transversal reinforcement spacing verification.

Requirement	Value	Check
0.3Agf'c (kN)	1260	
Pu vs 0.3Agf'c	0.699	Tie every (hx) distance (f'c<70)
Dist. Tied bars hx,max 1	200	
Dist. Tied bars hx,max 2	200	
hx,max Limit (mm)	200	
so (mm)	150	
Spacing Limit (mm)	100	Use this one!!

Table A38. FBD-6 Boundary element transversal reinforcement spacing verification.

Requirement	Value	Check
0.3Agf'c (kN)	1260	
Pu vs 0.3Agf'c	1.439	Must tie all bars, check max spacing
Dist. Tied bars hx,max 1	200	
Dist. Tied bars hx,max 2	200	
hx,max Limit (mm)	200	
so (mm)	150	
Spacing Limit (mm)	95.28	Use this one!!

Table A39. FBD-9 Boundary element transversal reinforcement spacing verification.

Requirement	Value	Check
0.3Agfc (kN)	1512	
Pu vs 0.3Agfc	2.325	Must tie all bars, check max spacing
Dist. Tied bars hx,max 1	200	
Dist. Tied bars hx,max 2	200	
hx,max Limit (mm)	200	
so (mm)	150	
Spacing Limit (mm)	95.28	Use this one!!

The final product of the design process are the cross-sections of the walls, which were presented in Figures 4.5 to 4.7 of Chapter 4.

APPENDIX B. DIRECT DISPLACEMENT-BASED DESIGN

B.1 General requirements

The general assumptions prior to start the design with DDBD procedure and the procedure itself, have been thoughtfully explained in Section 4.3 of this thesis. In the following, the calculations performed at each step are summarized for all the designs. Design is performed based on the Displacement-Based Design book by Priestley et al. (2007) and the Displacement-Based Design Model Code (DDBD12) by Sullivan et al. (2012). References are included in Chapter 9.

B.2 Wall allowable plastic rotations and design displacement profiles

The desired inelastic deformation mechanism of the buildings is the plastic hinge at the wall base. The deformation at maximum response is calculated based on the rotations at this section of the wall, therefore, the rotation limits of the wall must be established. Two kind of limits are considered: a non-structural limit given by the 2% drift damage control requirement of the code, and a structural limit related to the maximum plastic rotation allowed by the wall geometry and reinforcement limit strains. The lowest of these two limits and the elastic rotations (given by the yield curvature) are used to compute the expected displaced shape of the building at maximum response. The plastic rotation limits calculation is shown in Tables B1 to B3.

Table B1. DDBD-3 Wall allowable plastic rotations.

Parameter	Value
Yield curvature ϕ_y,w	0.0012
Limit State Curv. ϕ_{ls}	0.0180
Drift Limit, θ_c	2%
Plastic Rotation (non-struct) θ_p,ns	0.0148
Plastic Rotation (Structural) θ_p,max	0.0158
Design Plastic Rotation θ_p	0.0148

Table B2. DDBD-6 Wall allowable plastic rotations.

Parameter	Value
Yield curvature $\varphi_{y,w}$	0.0012
Limit State Curv. φ_{ls}	0.0180
Drift Limit, θ_c	2%
Plastic Rotation (non-struct) $\theta_{p,ns}$	0.0096
Plastic Rotation (Structural) $\theta_{p,max}$	0.0215
Design Plastic Rotation θ_p	0.0096

Table B3. DDBD-9 Wall allowable plastic rotations.

Parameter	Value
Yield curvature $\varphi_{y,w}$	0.0008
Limit State Curv. φ_{ls}	0.0120
Drift Limit, θ_c	2%
Plastic Rotation (non-struct) $\theta_{p,ns}$	0.0096
Plastic Rotation (Structural) $\theta_{p,max}$	0.0272
Design Plastic Rotation θ_p	0.0096

The design displacement and drift profiles are plotted in Figure 4.13 of Chapter 4, here the computations are shown in Tables B4 to B6.

Table B4. DDBD-3 Design displacement profile calculation.

Storey	Height (m)	mi (kg)	Δy_i	Δp_i	Δi	Drifts θ_i
3	9	322497.25	0.0312	0.1332	0.1644	1.98%
2	6	398827.52	0.0162	0.0888	0.1050	1.87%
1	3	398827.52	0.0046	0.0444	0.0490	1.63%

Table B5. DDBD-6 Design displacement profile calculation.

Storey	Height (m)	mi (kg)	Δy_i	Δp_i	Δi	Drifts θ_i
6	18	322497.25	0.1247	0.1729	0.2976	1.99%
5	15	398827.52	0.0938	0.1441	0.2379	1.93%
4	12	398827.52	0.0647	0.1153	0.1799	1.82%
3	9	398827.52	0.0390	0.0864	0.1254	1.64%
2	6	398827.52	0.0185	0.0576	0.0761	1.41%
1	3	398827.52	0.0049	0.0288	0.0337	1.12%

Table B6. DDBD-9 Design displacement profile calculation.

Storey	Height (m)	mi (kg)	Δy_i	Δp_i	Δi	Drifts θ_i
9	27	339825.69	0.1871	0.2593	0.4464	2.00%
8	24	416155.96	0.1561	0.2305	0.3866	1.97%
7	21	416155.96	0.1258	0.2017	0.3275	1.92%
6	18	416155.96	0.0970	0.1729	0.2699	1.84%
5	15	416155.96	0.0706	0.1441	0.2147	1.74%
4	12	416155.96	0.0472	0.1153	0.1625	1.61%
3	9	416155.96	0.0277	0.0864	0.1142	1.46%
2	6	416155.96	0.0128	0.0576	0.0705	1.28%
1	3	416155.96	0.0033	0.0288	0.0322	1.07%

B.3 Equivalent SDOF properties

Next step in DDBD design process is to compute the SDOF Substitute Structure properties for each building based on the expected displaced shapes. This allows to compute the design displacement, effective mass and effective height of the system. Results are shown in Tables B7 to B9.

Table B7. DDBD-3 Equivalent SDOF properties.

Storey	$mi * \Delta i$	$mi * \Delta i^2$	$mi * \Delta i * hi$	Design displacement [Δd] (m)	Effective mass [me] (kg)	Effective Height [He] (m)
3	53020.97	8717.04	477188.70			
2	41870.91	4395.82	251225.44			
1	19553.52	958.66	58660.55	0.123	930798.21	6.88
SUM	114445.39	14071.52	787074.69			

Table B8. DDBD-6 Equivalent SDOF properties.

Storey	$mi \Delta i$	$mi \Delta i^2$	$mi \Delta i hi$	Design displacement [Δd] (m)	Effective mass [me] (kg)	Effective Height [He] (m)
6	95984.86	28567.97	1727727.41			
5	94888.55	22575.76	1423328.19			
4	71765.02	12913.40	861180.29			
3	50023.44	6274.25	450210.97	0.205	1738394.64	13.14
2	30354.76	2310.30	182128.58			
1	13449.96	453.58	40349.88			
SUM	356466.59	73095.27	4684925.31			

Table B9. DDBD-9 Equivalent SDOF properties.

Storey	mi Δi	mi Δi^2	mi $\Delta i h_i$	Design displacement [Δd] (m)	Effective mass [me] (kg)	Effective Height [He] (m)
9	151713.48	67731.72	4096263.94			
8	160874.80	62189.91	3860995.15			
7	136279.29	44627.61	2861865.02			
6	112324.66	30317.55	2021843.81			
5	89331.35	19175.72	1339970.18	0.301	2689612.33	19.34
4	67619.80	10987.32	811437.54			
3	47510.45	5424.03	427594.01			
2	29323.74	2066.25	175942.42			
1	13380.11	430.19	40140.32			
SUM	808357.65	242950.29	15636052.40			

B.4 Equivalent viscous damping and spectrum scaling factor

Then, a yield displacement is computed for the equivalent SDOF system, with this and the design displacement it is possible to obtain the ductility capacity and the equivalent viscous damping associated with it. The values found for each design are presented in Table B10.

Table B10. Equivalent viscous damping and spectrum scaling factor computation.

Design	Yield displacement [Δy] (m)	Ductility Capacity μ	Equiv. Viscous Damp. ξ_{eq}	Spectrum scaling factor (η) R, ξ_{eq}
DDBD-3	0.020	6.040	16.79%	0.610
DDBD-6	0.075	2.717	13.93%	0.663
DDBD-9	0.110	2.741	13.98%	0.662

B.5 Effective period, stiffness and design base shear

As explained in Section 4.3.6 of Chapter 4, iteration was needed to compute the base shear of the DDBD-6 and DDBD-9 designs, as the displacement capacity of these buildings exceeds the reduced spectral displacement demand at the site. The DDBD-3 building is just at the limit of the reduced displacement spectra, so no iteration is needed. When structures fall in this range, i.e. the constant displacement range of the displacement response spectrum, the period and consequently the base shear can be chosen by the designer because any period equal or larger

than the corner period is allowed. Thus, the longer the effective period, the lowest the base shear, which is only limited by P-Delta effects verifications. For the DDBD-3, DDBD-6 and DDBD-9 designs, the effective period is taken equal to the corner period, thus, the buildings are designed for the strongest possible variant. Final values of design ductility, design equivalent viscous damping, design displacement and effective period are shown in Table B11. The effective stiffness, P-Delta effects and design base shear calculations are shown in Table B12.

Table B11. Final design properties and effective period calculation for all buildings.

Design	Effective Period T_e (s)	Design Ductility μ	Design Eq. Viscous Damp. ξ_{eq}	Final Design Displacement Δ_d (m)	Displ. Adjustment ($\Delta_{df}/\Delta_d, initial$)
DDBD-3	2.4	5.733	16.07%	0.117	0.949
DDBD-6*	2.4	1.917	9.77%	0.145	0.705
DDBD-9*	2.4	1.473	7.44%	0.162	0.537

*Original displacement capacity exceeded the demand, iteration performed to calculate actual displacement and damping values.

Table B12. Base shear and overturning moment calculation for all designs.

Design	Design Effective Stiffness K_e (kN/m)	Base Shear [V _b] (kN) (No P-Δ)	P-Delta Coefficient (C) (if <0.1 neglect)	P-Δ component [V _{P-Δ}] (kN)	Base Shear + P-Δ [V _b] (kN)	Overturning Moment Base [M _{oT}] (kN-m)
DDBD-3	6379.59	744.53	0.208	77.48	822.01	5653.19
DDBD-6	11914.77	1723.29	0.109	93.84	1817.12	23881.87
DDBD-9	18434.31	2977.15	0.074	--	2977.15	57587.07

B.6 Vertical distribution of seismic forces and stability coefficient check

The lateral forces are vertically distributed along the structure, proportional to the product of mass and displacements (i.e. an inelastic displacement profile), contrary to FBD which uses a height-proportional displacement profile (Priestley et al., 2007). The values are shown in Tables B13 to B15, these values are per orthogonal direction of the building, so they need to be divided by 2 to get the forces on a single wall.

Table B13. DDBD-3 Vertical distribution of shear and moments (values for 2 walls).

Storey	mi Δi	Fi (kN)	Height	Vi (kN)	Mi (kN-m)
3	53020.97	380.82	9	380.82	0.00
2	41870.91	300.74	6	681.56	1142.47
1	19553.52	140.44	3	822.01	3187.17
0	0.00	0.00	0		5653.19
SUM	114445.39	822.01			

Table B14. DDBD-6 Vertical distribution of shear and moments (values for 2 walls).

Storey	mi Δi	Fi (kN)	Height	Vi (kN)	Mi (kN-m)
6	95984.86	489.29	18	489.29	0.00
5	94888.55	483.70	15	973.00	1467.88
4	71765.02	365.83	12	1338.83	4386.86
3	50023.44	255.00	9	1593.82	8403.34
2	30354.76	154.74	6	1748.56	13184.81
1	13449.96	68.56	3	1817.12	18430.50
0	0.00	0.00	0		23881.87
SUM	356466.59	1817.12			

Table B 15. DDBD-9 Vertical distribution of shear and moments (values for two walls).

Storey	mi Δi	Fi (kN)	Height	Vi (kN)	Mi (kN-m)
9	151713.48	558.76	27	558.76	0.00
8	160874.80	592.50	24	1151.25	1676.27
7	136279.29	501.91	21	1653.16	5130.02
6	112324.66	413.69	18	2066.85	10089.52
5	89331.35	329.00	15	2395.86	16290.08
4	67619.80	249.04	12	2644.90	23477.65
3	47510.45	174.98	9	2819.88	31412.34
2	29323.74	108.00	6	2927.88	39871.97
1	13380.11	49.28	3	2977.15	48655.60
0	0.00	0.00	0		57587.07
SUM	808357.65	2977.15			

The Tables B16 to B18 show the verifications of the stability coefficient, this is the parameter that governs the base shear when displacement capacity exceeds the displacement demand at the site and cannot be larger than 0.3. As it is observed in Tables B17 and B18 there is a large margin to work with in DDBD-6 and DDBD-9 designs, this means that base shear for those buildings can be significantly reduced by picking a longer effective period for design.

Table B16. DDBD-3 Stability coefficient verification.

Story	Story Drift (m)	Story Shear (kN)	Story Dead Load (kN)	Story Live Load (kN)	Total Story Load (kN)	Accumulated Story Load (kN)	Stability Coefficient (Θ)	CHECK
3	0.059	380.82	3163.70	576.00	3739.70	3739.70	0.195	OK!!
2	0.056	681.56	3912.50	576.00	4488.50	8228.20	0.225	OK!!
1	0.049	822.01	3912.50	576.00	4488.50	12716.69	0.253	OK!!

Table B17. DDBD-6 Stability coefficient verification

Story	Story Drift (m)	Story Shear (kN)	Story Dead Load (kN)	Story Live Load (kN)	Total Story Load (kN)	Accumulated Story Load (kN)	Stability Coefficient (Θ)	CHECK
6	0.060	489.29	3163.70	576.00	3739.70	3739.70	0.152	OK!!
5	0.058	973.00	3912.50	576.00	4488.50	8228.20	0.163	OK!!
4	0.055	1338.83	3912.50	576.00	4488.50	12716.69	0.173	OK!!
3	0.049	1593.82	3912.50	576.00	4488.50	17205.19	0.177	OK!!
2	0.042	1748.56	3912.50	576.00	4488.50	21693.69	0.175	OK!!
1	0.034	1817.12	3912.50	576.00	4488.50	26182.19	0.162	OK!!

Table B18. DDBD-9 Stability coefficient verification.

Story	Story Drift (m)	Story Shear (kN)	Story Dead Load (kN)	Story Live Load (kN)	Total Story Load (kN)	Accumulated Story Load (kN)	Stability Coefficient (Θ)	CHECK
9	0.032	558.76	3333.69	576.00	3909.69	3909.69	0.075	OK!!
8	0.032	1151.25	4082.49	576.00	4658.49	8568.18	0.079	OK!!
7	0.031	1653.16	4082.49	576.00	4658.49	13226.67	0.082	OK!!
6	0.030	2066.85	4082.49	576.00	4658.49	17885.16	0.086	OK!!
5	0.028	2395.86	4082.49	576.00	4658.49	22543.65	0.088	OK!!
4	0.026	2644.90	4082.49	576.00	4658.49	27202.14	0.089	OK!!
3	0.023	2819.88	4082.49	576.00	4658.49	31860.63	0.088	OK!!
2	0.021	2927.88	4082.49	576.00	4658.49	36519.12	0.086	OK!!
1	0.017	2977.15	4082.49	576.00	4658.49	41177.61	0.080	OK!!

B.7 Capacity design envelopes

Capacity design rules in DDBD procedure have been explained in Section 4.3.7 of Chapter 4 of this thesis, Figure 4.17 shows schematically the capacity design envelopes proposed in the methodology. These rules have been applied prior to RC wall reinforcement design and results of final design forces are shown in Tables B19 to B21.

Table B19. DDBD-3 Capacity design shear and moments (single wall) used for design.

Story / Support Level	Axial (kN)		Capacity Design Shear(kN)	Capacity Design Moment (kN-m)
	$1.39D + 0.5L + 1Qe$	$0.71D + 1Qe$		
3 / R	258.52	117.87	839.19	2365.87
2 / 3	569.46	262.53	992.14	2596.23
1 / 2	880.24	407.09	1145.09	2826.60

Table B20. DDBD-6 Capacity design shear and moments (single wall) used for design.

Story / Support Level	Axial (kN)		Capacity Design Shear(kN)	Capacity Design Moment (kNm)
	$1.39D + 0.5L + 1Qe$	$0.71D + 1Qe$		
6 / R	258.52	117.87	1020.47	2335.12
5 / 6	569.51	262.53	1238.70	4670.23
4 / 5	880.40	407.16	1456.92	7005.35
3 / 4	1191.32	551.79	1675.15	9340.46
2 / 3	1502.23	696.42	1893.38	10640.70
1 / 2	1813.08	841.04	2111.61	11940.93

Table B21. DDBD-9 Capacity design shear and moments (single wall) used for design.

Story / Support Level	Axial (kN)		Capacity Design Shear(kN)	Capacity Design Moment (kNm)
	$1.39D + 0.5L + 1Qe$	$0.71D + 1Qe$		
9 / R	333.40	154.08	1267.74	3837.15
8 / 9	731.26	341.07	1522.20	7674.29
7 / 8	1129.05	528.03	1776.66	11511.44
6 / 7	1526.84	715.00	2031.12	15348.58
5 / 6	1924.64	901.97	2285.58	19477.25
4 / 5	2322.43	1088.93	2540.04	23605.92
3 / 4	2720.22	1275.90	2794.51	27734.58
2 / 3	3118.00	1462.86	3048.97	28264.06
1 / 2	3515.53	1649.71	3303.43	28793.53

B.8 Structural design of the walls

The structural analysis is performed considering the computed capacity design envelopes of the previous section. As in the Force-Based Design case of the Appendix A, the reinforcement detailing is carried out following Chapter 18 of ACI 318-14. The only difference with the procedures described in ACI 318-14 is that in DDBD flexural design of the walls expected material strengths are used instead of characteristic strengths, and no strength-reduction factors are applied. This is also explained in Section 4.3.3 of Chapter 4 of this thesis. For shear design, and further calculations, all the requirements of the standard are applied. All results correspond to design of a single wall.

Horizontal reinforcement for shear loads is completed with the equations provided in the code, results are shown in Tables B22 to B24. Flexural design results are shown in Tables B25 to B30. The rebars layout is changed every three floors to have a more “optimized” design, horizontal reinforcement is calculated only for the base and assumed to be equal for the rest of the building, because these bars are not needed in the OpenSees numerical model, furthermore, the shear design is often governed by minimum reinforcement requirements so the same shear solution is used for the whole building.

Table B22. DDBD-3 Web horizontal reinforcement verification.

Story	Spacing (mm)	Total #Bars	#Rebar Type	As,Horiz (mm ²)	Horizontal Ratio (pt)	CHECK As	CHECK Spacing	ϕV_n provided (kN)
Base	300	18	4	2322	0.00287	OK!!	OK!!	1893.20

Table B23. DDBD-6 Web horizontal reinforcement verification.

Story	Spacing (mm)	Total #Bars	#Rebar Type	As,Horiz (mm ²)	Horizontal Ratio (pt)	CHECK As	CHECK Spacing	ϕV_n provided (kN)
Base	240	24	4	3096	0.00358	OK!!	OK!!	2164.10
4th	300	18	4	2322	0.00287	OK!!	OK!!	1893.20

Table B24. DDBD-9 Web horizontal reinforcement verification.

Story	Spacing (mm)	Total #Bars	#Rebar Type	As,Horiz (mm ²)	Horizontal Ratio (ρ_t)	CHECK As	CHECK Spacing	ϕV_n provided (kN)
Base	220	26	4	3354	0.00391	OK!!	OK!!	3430.85
4th	300	18	4	2322	0.00287	OK!!	OK!!	2839.80
6th	300	18	4	2322	0.00287	OK!!	OK!!	2839.80

Table B25. DDBD-3 Web vertical reinforcement verification.

Story	Spacing (mm)	Total #Bars	#Rebar Type	As,Vertical (mm ²)	Vertical Ratio (ρ_l)	CHECK	CHECK Spacing
Base	200	28	4	3612	0.00430	OK!!	OK!!

Table B26. DDBD-6 Web vertical reinforcement verification.

Story	Spacing (mm)	Total #Bars	#Rebar Type	As,Vertical (mm ²)	Vertical Ratio (ρ_l)	CHECK	CHECK Spacing
Base	200	28	5	5600	0.00667	OK!!	OK!!
4th	200	28	4	3612	0.00430	OK!!	OK!!

Table B27. DDBD-9 Web vertical reinforcement verification.

Story	Spacing (mm)	Total #Bars	#Rebar Type	As,Vertical (mm ²)	Vertical Ratio (ρ_l)	CHECK	CHECK Spacing
Base	240	38	5	7600	0.00556	OK!!	OK!!
4th	300	30	5	6000	0.00444	OK!!	OK!!
6th	300	30	4	3870	0.00287	OK!!	OK!!

Boundary elements reinforcement results are shown in Tables B31 to B33, verification of how many storeys need boundary elements was performed but only one example is shown here (Table B34), as boundary elements were extended until roof top in all buildings. Transversal reinforcement is calculated for the boundary elements as presented in Tables B35 to B37. All results correspond to design of a single wall.

Table B28. DDBD-3 Summary design for flexure.

Story	Pu, Max (kN)	Pu, Min (kN)	Mu (kNm)	Mn,CS (kNm)	c (mm)	φMn,CS (kNm)	Shear Magnification*	Rebars Boundary	Rebars Web
3	258.52	117.87	2365.87	6107.76	334.2	6107.76	N/A		
2	569.46	262.53	1593.58	6637.28	367.5	6637.28	N/A		
Base	880.24	407.09	2826.60	7159.01	401.7	7159.01	N/A	12 #4	28 #4

*Does not apply as shear forces have been modified by capacity design envelopes

Table B29. DDBD-6 Summary design for flexure.

Story	Pu, Max (kN)	Pu, Min (kN)	Mu (kNm)	Mn,CS (kNm)	c (mm)	φMn,CS (kNm)	Shear Magnification*	Rebars Boundary	Rebars Web
6	258.52	117.87	2335.12	6107.80	334.2	6107.8	N/A		
5	569.51	262.53	4670.23	6637.40	367.5	6637.4	N/A		
4	880.40	407.16	7005.35	7159.30	401.7	7159.3	N/A	12#4	28 #4
3	1191.32	551.79	6592.41	12790.20	574.5	12790.2	N/A		
2	1502.23	696.42	9215.25	13260.00	605.0	13260.0	N/A		
Base	1813.08	841.04	11940.93	13717.80	635.8	13717.8	N/A	4#7 + 8#6	28 #5

*Does not apply as shear forces have been modified by capacity design envelopes

Table B30. DDBD-9 Summary design for flexure.

Story	Pu, Max (kN)	Pu, Min (kN)	Mu (kNm)	Mn,CS (kNm)	c (mm)	φMn,CS (kNm)	Shear Magnification*	Rebars Boundary	Rebars Web
9	333.40	154.08	3837.15	9906.0	367.8	9906.0	N/A		
8	731.26	341.07	7674.29	10974.0	411.1	10974.0	N/A		
7	1129.05	528.03	11511.44	12024.1	456.0	12024.1	N/A	12#4	30 #4
6	1526.84	715.00	15348.58	23115.3	771.2	23115.3	N/A		
5	1924.64	901.97	19477.25	24044.5	813.4	24044.5	N/A		
4	2322.43	1088.93	23605.92	24959.4	855.9	24959.4	N/A	12#6	30#6
3	2720.22	1275.90	19935.99	31145.1	999.3	31145.1	N/A		
2	3118.00	1462.86	24327.80	31987.3	1039.0	31987.3	N/A		
Base	3515.53	1649.71	28793.53	32812.4	1078.5	32812.4	N/A	12#7	38 #6

*Does not apply as shear forces have been modified by capacity design envelopes

Table B31. DDBD-3 Boundary element vertical reinforcement verification.

Story	Spacing (mm)	Total #Bars	#Rebar	Asb,Vertical (mm ²)	Vertical Ratio (pl,b)	CHECK	CHECK Spacing
Base	90	12	12 #4	1548	0.01032	OK!!	OK!!

Table B32. DDBD-6 Boundary element vertical reinforcement verification.

Story	Spacing (mm)	Total #Bars	#Rebar	Asb,Vertical (mm ²)	Vertical Ratio (pl,b)	CHECK	CHECK Spacing
Base	90	12	4#7 + 8#6	3820	0.0255	OK!!	OK!!
4th	90	12	12#4	1548	0.0103	OK!!	OK!!

Table B33. DDBD-9 Boundary element vertical reinforcement verification.

Story	Spacing (mm)	Total #Bars	#Rebar	Asb,Vertical (mm ²)	Vertical Ratio (pl,b)	CHECK	CHECK Spacing
Base	110	12	12#7	3408	0.0189	OK!!	OK!!
4th	110	12	12#6	3408	0.0189	OK!!	OK!!
7th	110	12	12#4	1548	0.0086	OK!!	OK!!

Table B34. DDBD-6 Boundary element requirement check.

Story	N.A. - c (mm) (For Mn,CS and Pu)	δu (mm) - Design Displacement	lw (mm)	hw(mm)	δu/hw >=0.005	Check Factor	Boundary Element Required?
6	334.2	144.63	4000	18000	0.0080	553.12	NO!
5	367.5	144.63	4000	18000	0.0080	553.12	NO!
4	401.7	144.63	4000	18000	0.0080	553.12	NO!
3	574.5	144.63	4000	18000	0.0080	553.12	YES!
2	605.0	144.63	4000	18000	0.0080	553.12	YES!
Base	635.8	144.63	4000	18000	0.0080	553.12	YES!

Table B35. DDBD-3 Boundary element transversal reinforcement spacing verification.

Requirement	Value	Check
0.3Agf'c (kN)	1260	
Pu vs 0.3Agf'c	0.699	Tie every (hx) Distance (f'c<70)
Dist. Tied bars hx,max 1	200	
Dist. Tied bars hx,max 2	200	
hx,max Limit (mm)	200	
so (mm)	150	
Spacing Limit (mm)	76.2	Use this one!!

Table B36. DDBD-6 Boundary element transversal reinforcement spacing verification.

Requirement	Value	Check
0.3Agfc (kN)	1260	
Pu vs 0.3Agfc	1.439	Must tie all bars, check max spacing
Dist. Tied bars hx,max 1	200	
Dist. Tied bars hx,max 2	200	
hx,max Limit (mm)	200	
so (mm)	150	
Spacing Limit (mm)	100	Use this one!!

Table B37. DDBD-9 Boundary element transversal reinforcement spacing verification.

Requirement	Value	Check
0.3Agfc (kN)	1512	
Pu vs 0.3Agfc	2.325	Must tie all bars, check max spacing
Dist. Tied bars hx,max 1	200	
Dist. Tied bars hx,max 2	200	
hx,max Limit (mm)	200	
so (mm)	150	
Spacing Limit (mm)	100	Use this one!!

The final product of the design process are the cross-sections of the walls, which were presented in Figures 4.18 to 4.20. of Chapter 4.

APPENDIX C. HAZARD CURVES, RECORDS SELECTION AND MAFE CURVES

C.1 Hazard curves and disaggregation

Figure C1 shows the hazard curves for the structural periods considered in this thesis. Figures C2 to C7 show the disaggregation results in terms of M-R- ϵ used for ground motion records selection.

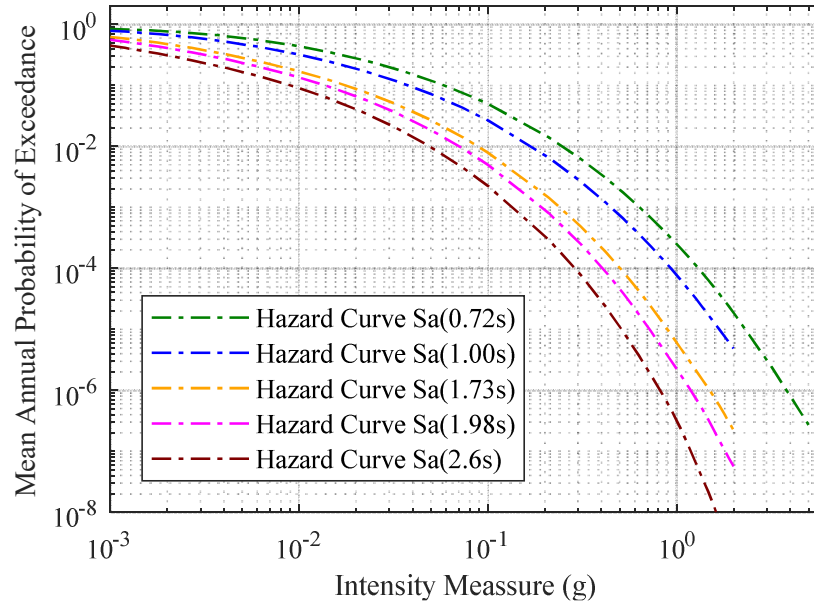


Figure C1. Hazard curves for Sa(T1) of each building.

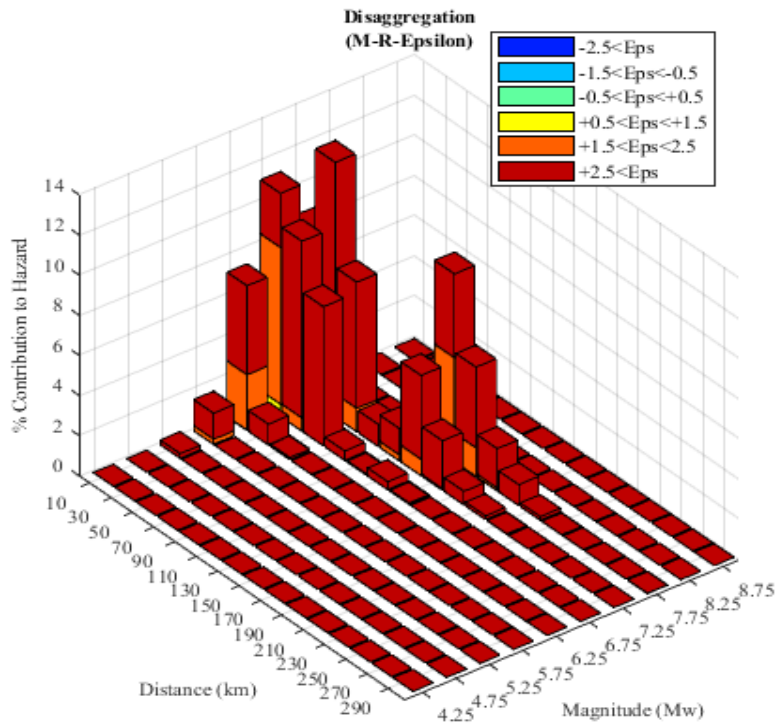


Figure C2. Disaggregation Sa(0.72s) 2475-years return period.

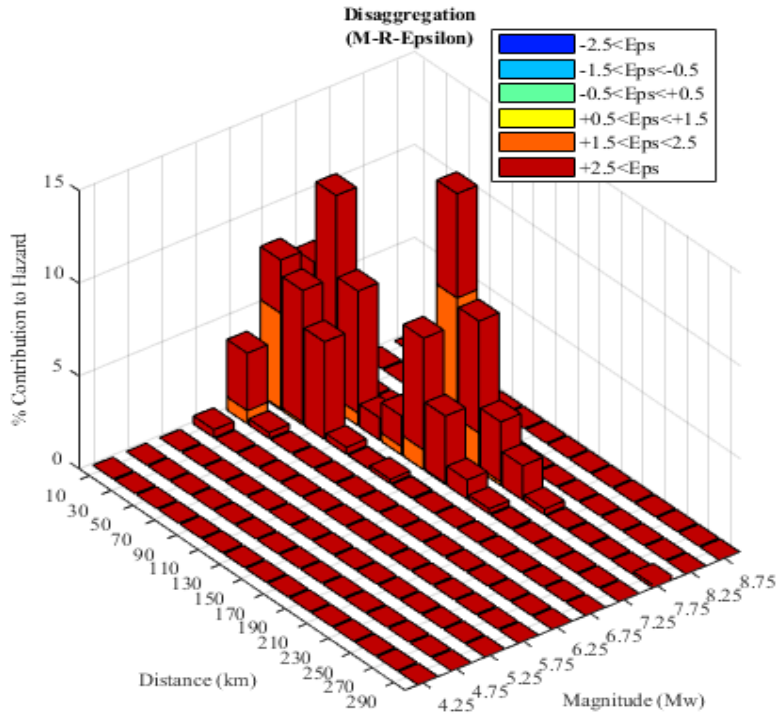


Figure C3. Disaggregation Sa(1.00s) 2475-years return period.

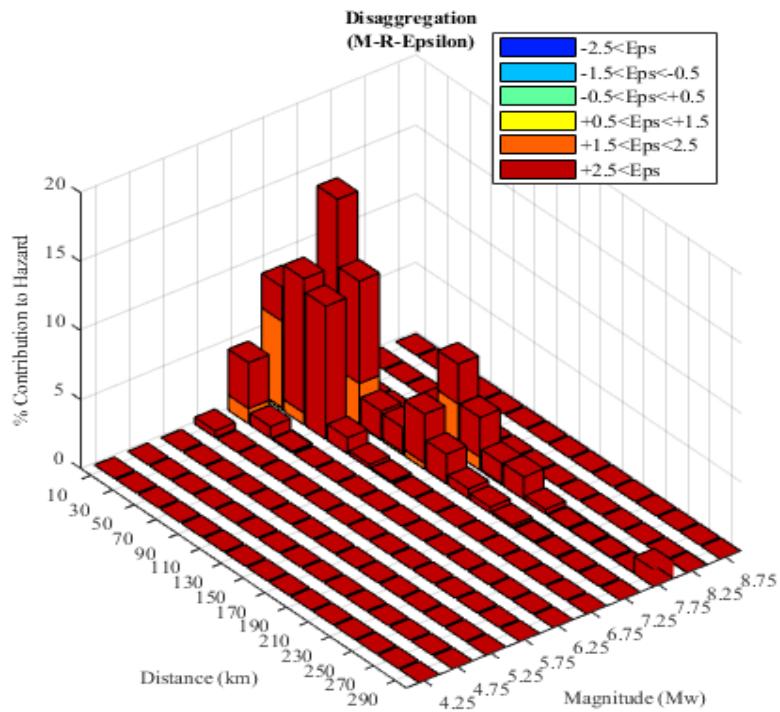


Figure C4. Disaggregation Sa(1.17s) 2475-years return period.

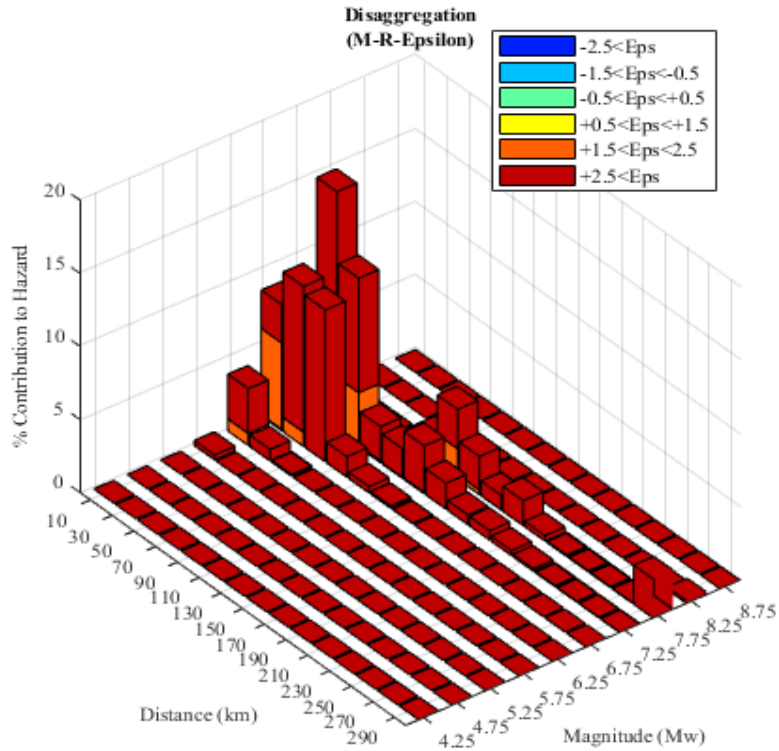


Figure C5. Disaggregation Sa(1.40s) 2475-years return period.

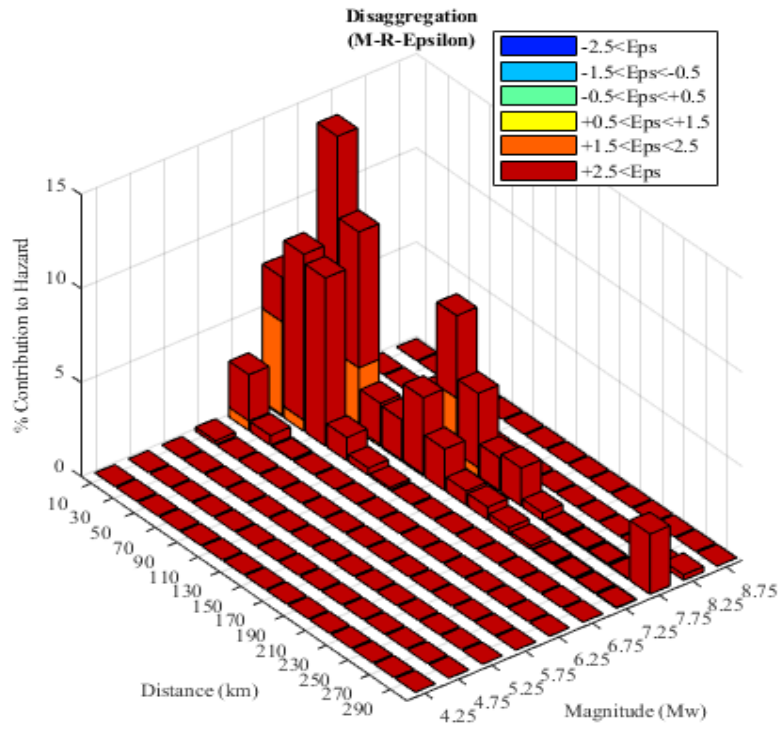


Figure C6. Disaggregation Sa(1.73s) 2475-years return period.

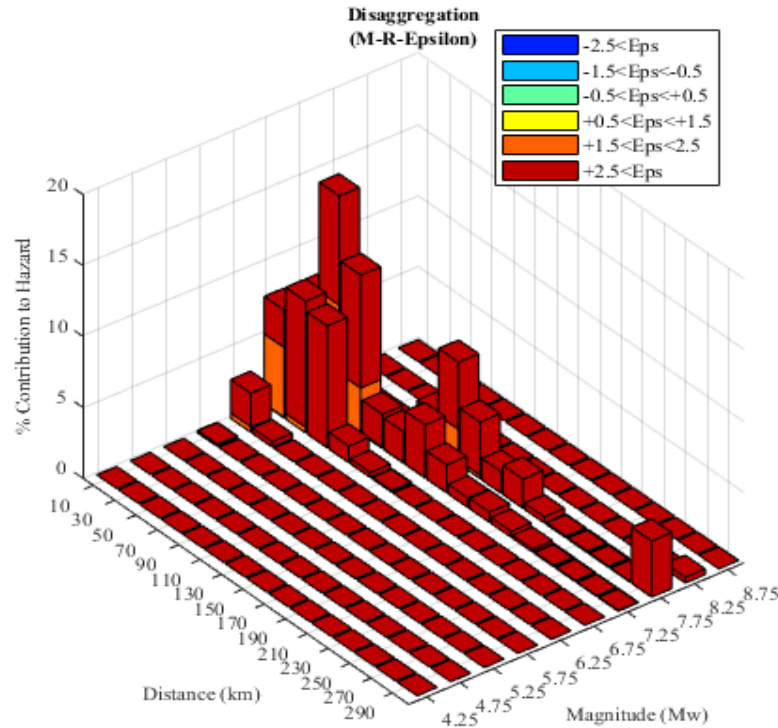


Figure C7. Disaggregation Sa(1.98s) 2475-years return period.

C.2 Conditional spectrum and records selection

Figures C8 to C13 show the conditional spectrum and response spectrum of the ground motion records selected for each case, as described in Section 6.2 of Chapter 6.

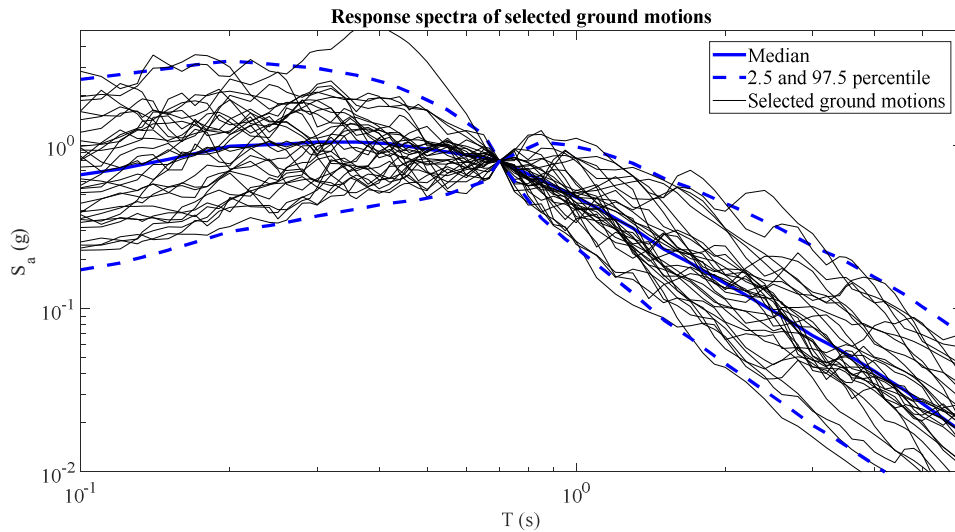


Figure C8. FBD-3: Response spectra of selected ground motion records conditioned on $Sa(T_1=0.72\text{s})$.

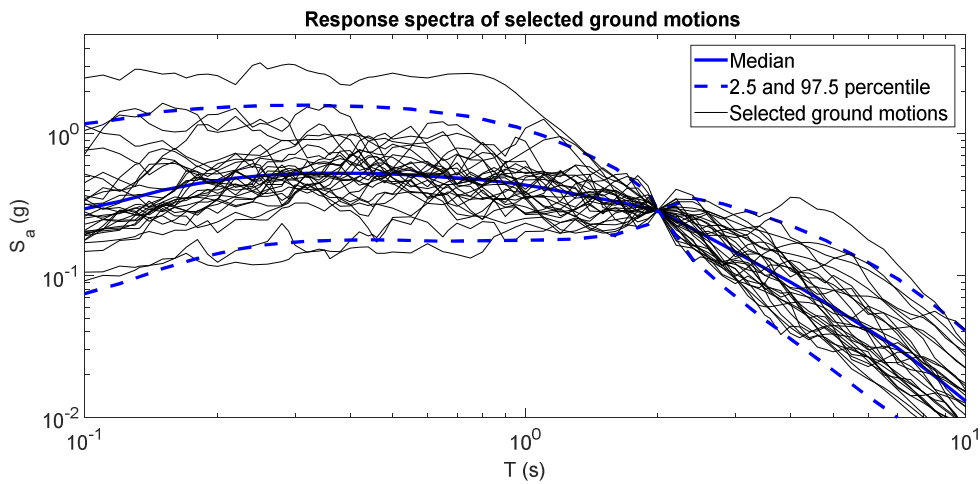


Figure C9. FBD-6: Response spectra of selected ground motion records conditioned on $Sa(T_1=1.94\text{s})$.

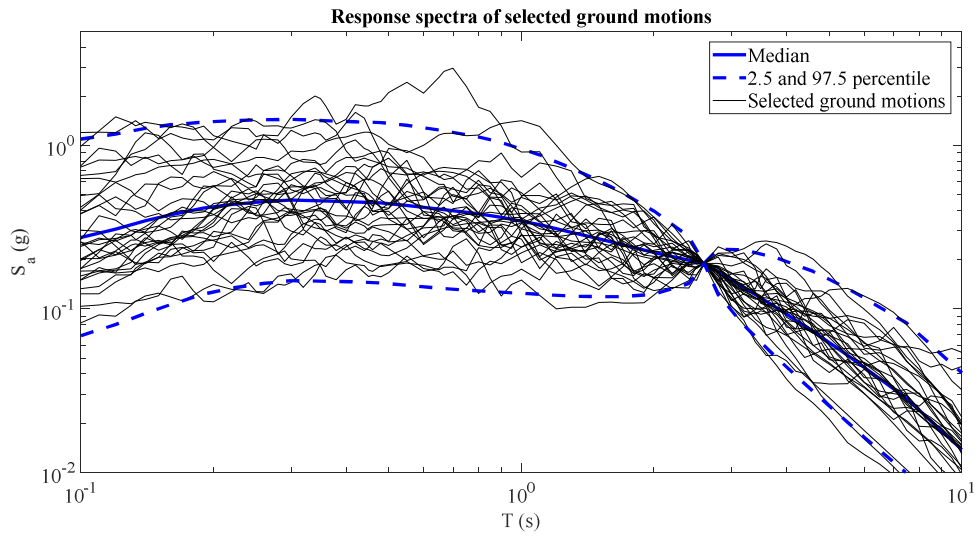


Figure C10. FBD-9: Response spectra of selected ground motion records conditioned on $Sa(T_1=2.60\text{s})$.

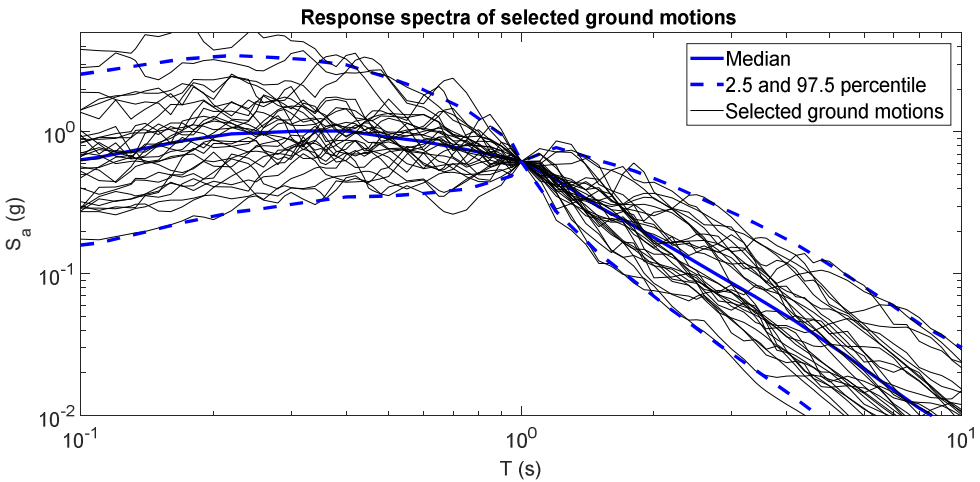


Figure C11. DDDB-3: Response spectra of selected ground motion records conditioned on $Sa(T_1=1.00\text{s})$.

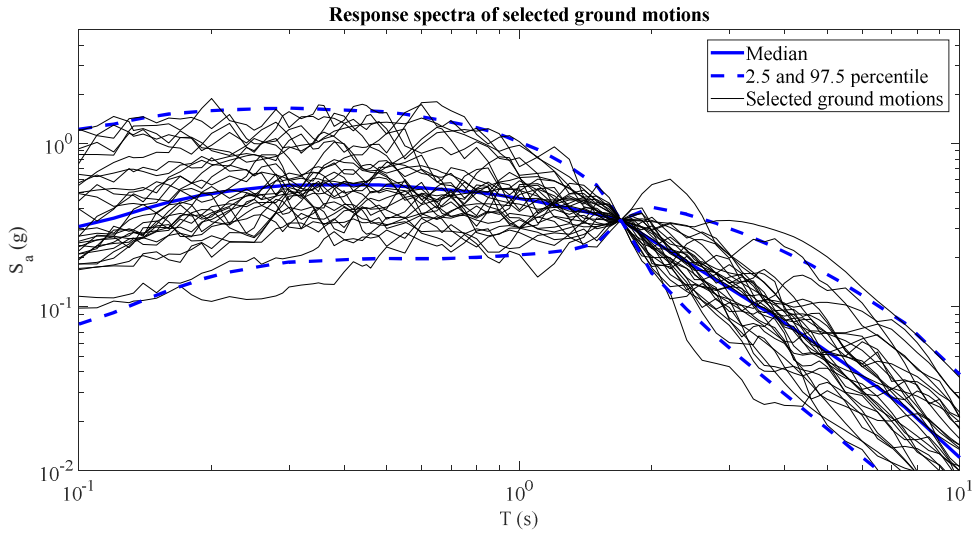


Figure C12. DDBD-6: Response spectra of selected ground motion records conditioned on $Sa(T_1=1.73\text{s})$.

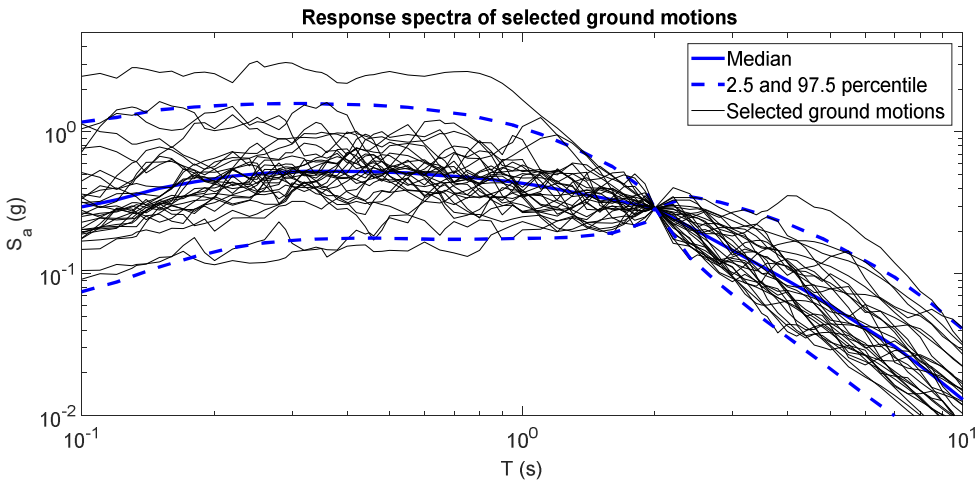


Figure C13. DDBD-9: Response spectra of selected ground motion records conditioned on $Sa(T_1=1.98\text{s})$.

C.3 Hazard fit and individual MAFE curves

Figures C14 to C19 show in green the hazard curves obtained from probabilistic seismic hazard analysis and in red the second-order polynomial fit used for collapse risk computations as described in Sections 6.6 and 6.7 of Chapter 6. Figures C20 to C25 show the MAFE vs maximum peak storey drift (MPSD) ratio obtained for each building studied.

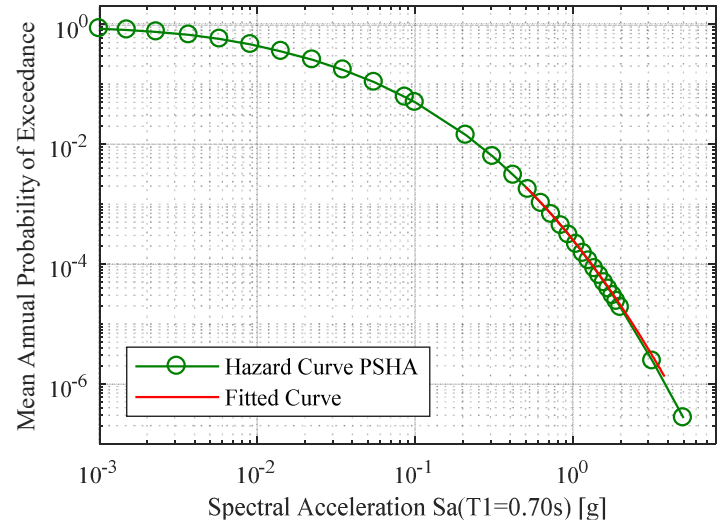


Figure C14. FBD-3 hazard curve polynomial fit.

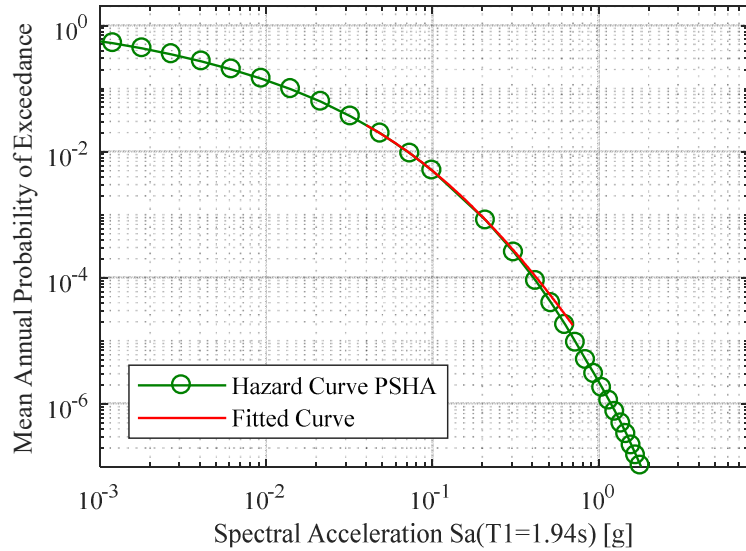


Figure C15. FBD-6 hazard curve polynomial fit.

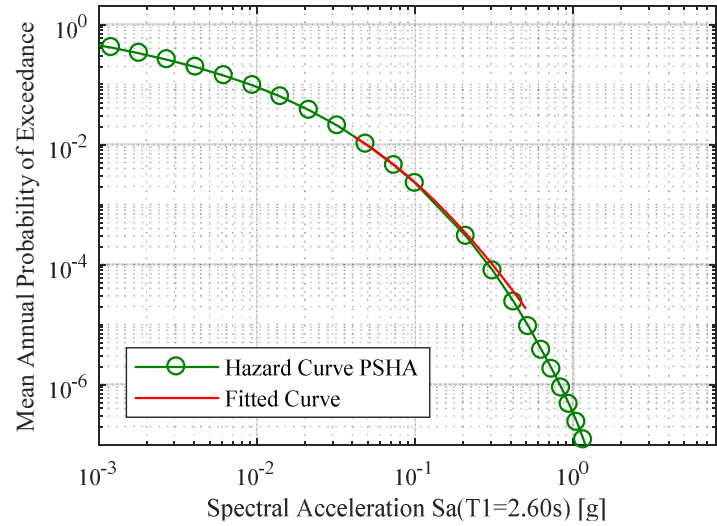


Figure C16. FBD-9 hazard curve polynomial fit.

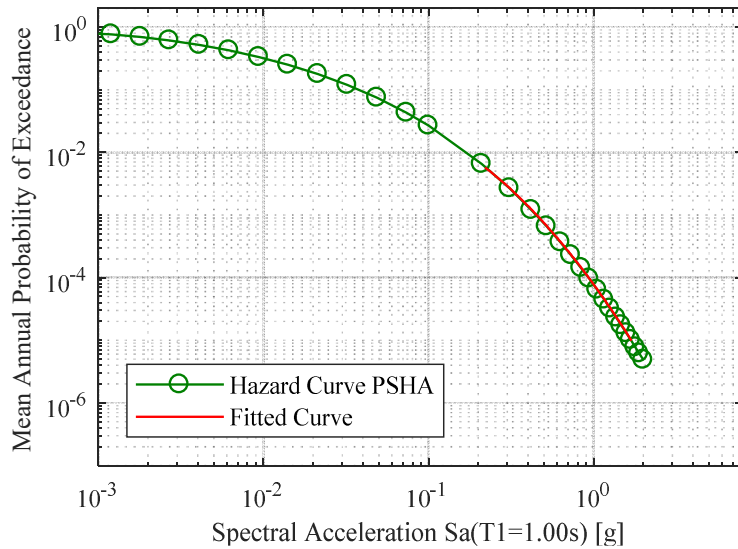


Figure C17. DDBD-3 hazard curve polynomial fit.

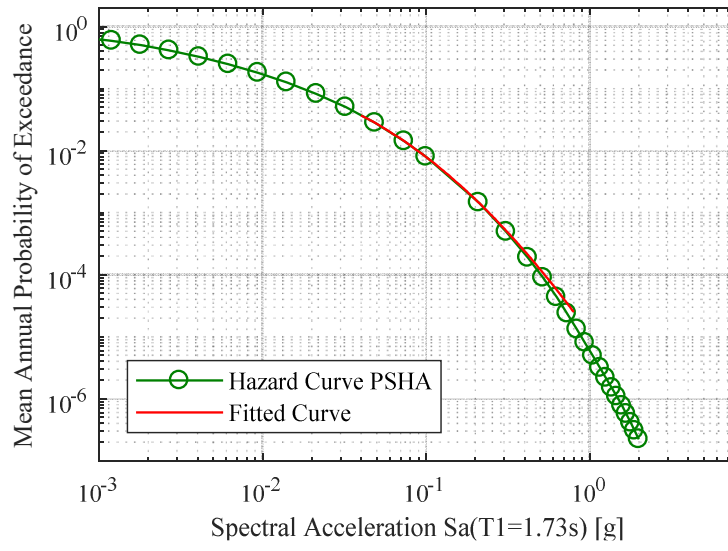


Figure C18. DDBD-6 hazard curve polynomial fit.

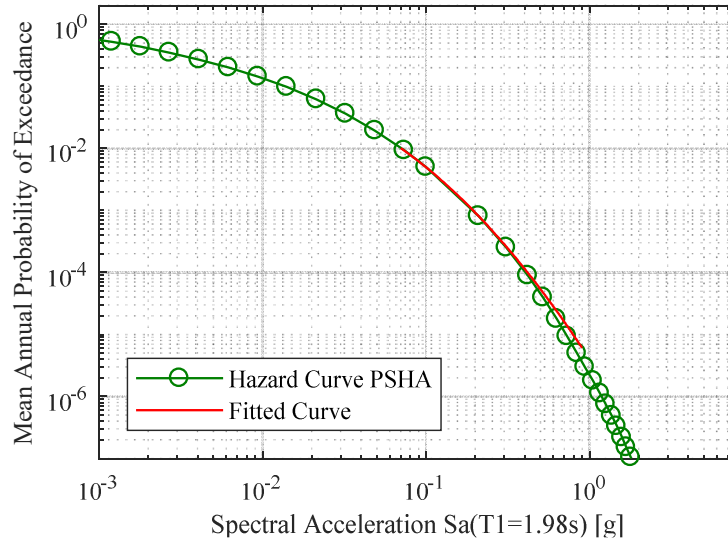


Figure C19. DDBD-9 hazard curve polynomial fit.

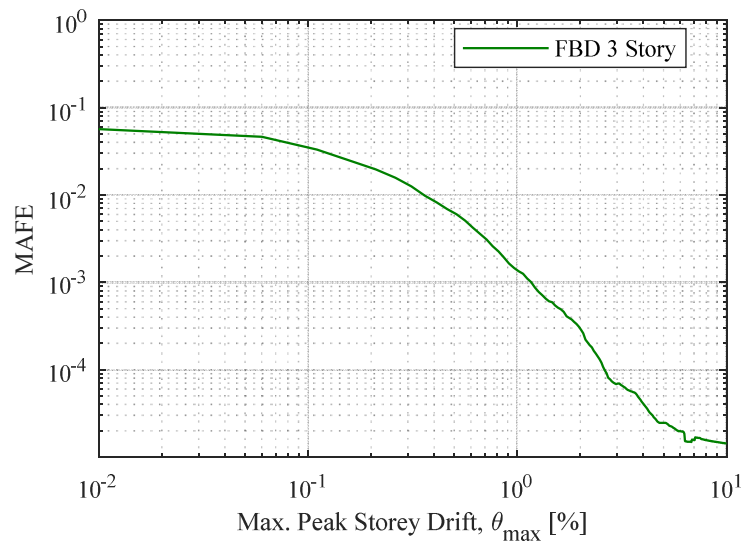


Figure C20. FBD 3-Story building, maximum peak storey drift ratio MAFE curve.

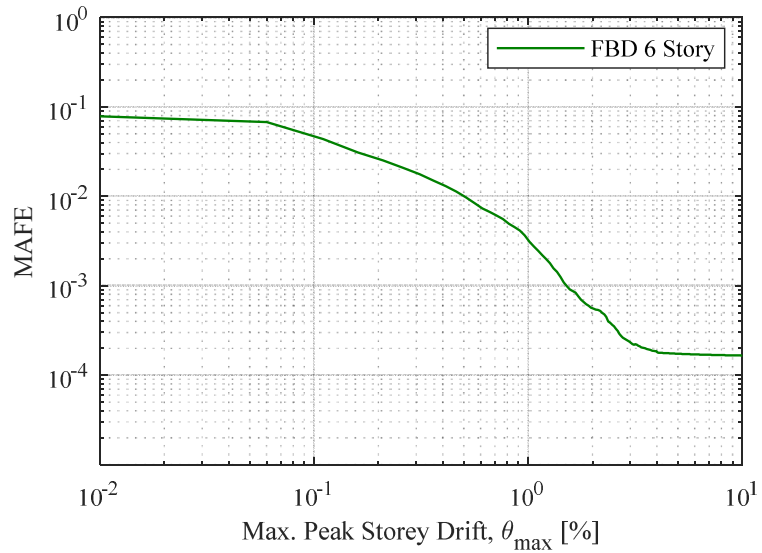


Figure C21. FBD 6-Story building, maximum peak storey drift ratio MAFE curve.

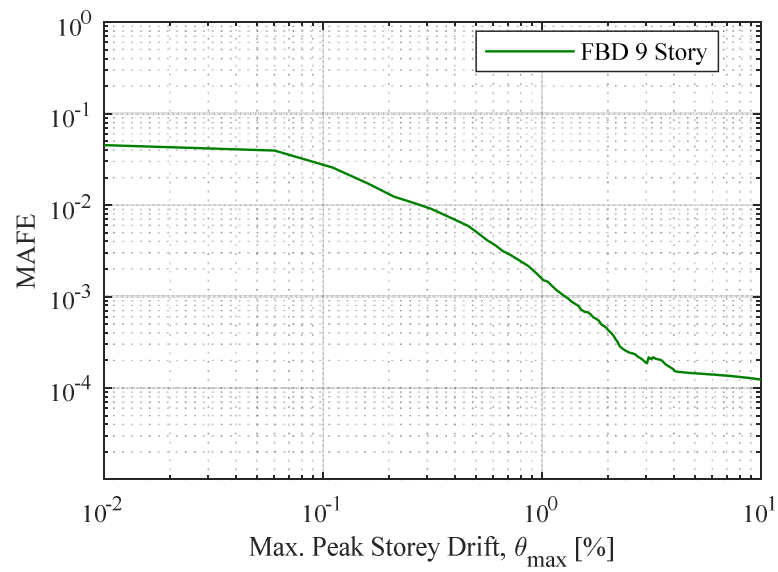


Figure C22. FBD 9-Story building, maximum peak storey drift ratio MAFE curve.

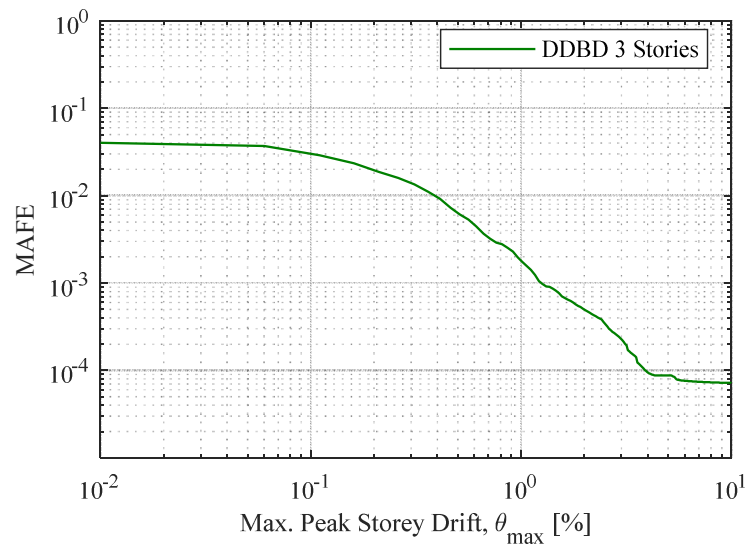


Figure C23. DDBD 3-Story building, maximum peak storey drift ratio MAFE curve.

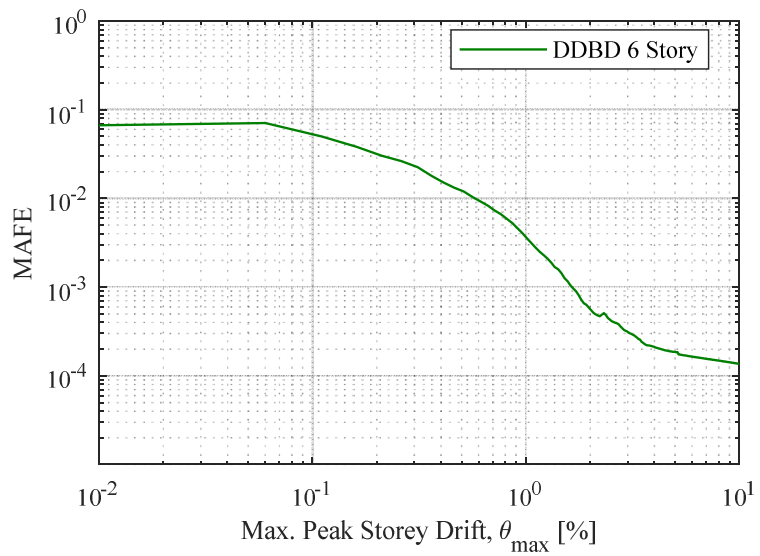


Figure C24. DDBD 6-Story building, maximum peak storey drift ratio MAFE curve.

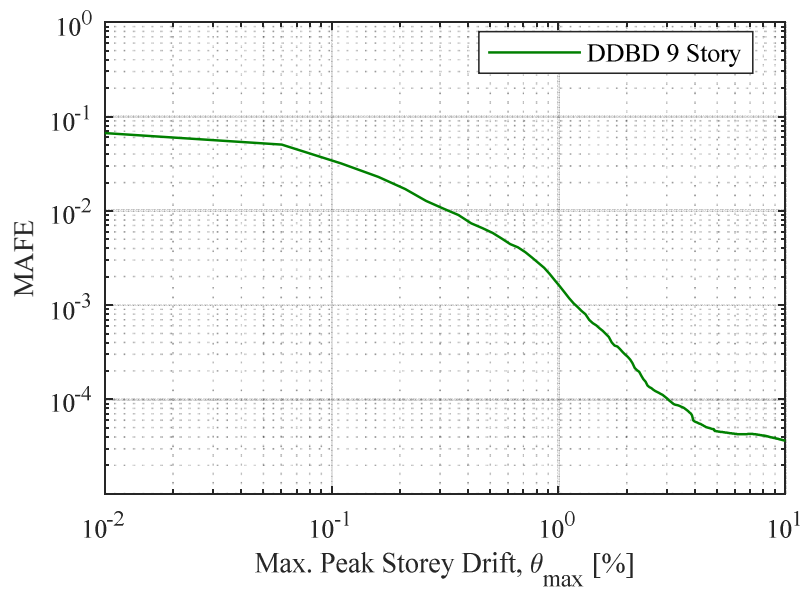


Figure C25. DDBD 9-Story building, maximum peak storey drift ratio MAFE curve